

**Mapping noncompetitive antagonists binding sites in the nicotinic  
acetylcholine receptor**

A thesis presented

by

Megan Benson Pratt

to

The Division of Medical Sciences  
in partial fulfillment of the requirements

for the degree of

Doctor of Philosophy

in the subject of

Neurobiology

Harvard University

Cambridge, Massachusetts

September, 1999

© 1999 by Megan Benson Pratt

All rights reserved.

## Abstract

The nicotinic acetylcholine receptor (nAChR) is a ligand-gated ion channel that is opened upon the binding of agonist to the extracellular surface. Noncompetitive antagonists of the nAChR block the response of the nAChR to agonist without preventing the binding of agonist. While most aromatic amine noncompetitive antagonists appear to bind within the lumen of the ion channel, the binding site of the fluorescent noncompetitive antagonist ethidium has been predicted by fluorescence resonance energy transfer studies to lie at the most extracellular aspect of the receptor. [<sup>3</sup>H]Ethidium diazide, a photoactivatable analog of ethidium, was used to map the binding site of ethidium in the desensitized state. Sequence analysis showed that [<sup>3</sup>H]ethidium diazide photoincorporated into the  $\alpha$  and  $\delta$  M2 segments, which are known to contribute to the lumen of the channel, and particularly into residues which have been shown to line the channel. Additionally, photoincorporation was also evident in the M1 segments of these two subunits, indicating that the M1 segment contributes to the formation of the lumen of the channel.

[<sup>3</sup>H]3-Aziocanol is a photoaffinity probe that is a general anesthetic that inhibits the nAChR. Sequence analysis of nAChR photolabeled with this probe showed that the primary site of [<sup>3</sup>H]3-aziocanol incorporation in the desensitized state of the nAChR was  $\alpha$ Glu-262, at the extracellular end of  $\alpha$ M2, indicating binding within the lumen of the channel. In addition, [<sup>3</sup>H]3-aziocanol incorporated at lower efficiency into residues at the protein-lipid interface, at equal levels in the presence or absence of agonist. In the absence of agonist, [<sup>3</sup>H]3-aziocanol also reacted with low efficiency with  $\alpha$ Tyr-190 and  $\alpha$ Tyr-198, residues contributing to the binding site of agonist.

[<sup>3</sup>H]Progesterin aryl azide is a photoaffinity analog of the steroid anesthetic progesterone. Although most noncompetitive antagonists appear to bind within the lumen of the channel, the high hydrophobicity of steroids suggests that they may interact at the protein-lipid interface. The primary site of [<sup>3</sup>H]progesterin aryl azide incorporation in the  $\alpha$ -subunit was mapped within a large fragment containing  $\alpha$ M4, known to form the protein-lipid interface. However, the instability of the photoadducts to HPLC and sequencing conditions precluded identification of labeled residues.

## TABLE OF CONTENTS

<b>CHAPTER 1 INTRODUCTION TO THE THESIS</b>	<b>1</b>
LIGAND GATED ION CHANNELS AS ALLOSTERIC PROTEINS	4
STRUCTURAL MOTIFS	6
<i>Agonist binding site</i>	6
<i>Transmembrane segments</i>	10
NONCOMPETITIVE ANTAGONISTS	14
<i>Amine NCAs</i>	15
<i>Anesthetics</i>	17
PHOTOAFFINITY LABELING	21
THESIS SYNOPSIS	24
<b>CHAPTER 2 IDENTIFICATION OF THE SITES OF INCORPORATION OF [<sup>3</sup>H]ETHIDIUM DIAZIDE IN THE NACHR</b>	<b>30</b>
ABSTRACT	30
INTRODUCTION	31
MATERIALS AND METHODS	33
<i>Materials</i>	33
<i>Equilibrium Binding Assay</i>	34
<i>Photoaffinity labeling of nAChR-enriched membranes with [<sup>3</sup>H]ethidium diazide</i>	35
<i>Gel Electrophoresis</i>	37
<i>EndoLysC digest</i>	38
<i>HPLC purification</i>	38
<i>Sequence Analysis</i>	39
RESULTS	40
<i>Equilibrium binding of [<sup>3</sup>H]ethidium to nAChR-rich membranes</i>	40
<i>Photoincorporation of [<sup>3</sup>H]ethidium diazide into nAChR-rich membranes</i>	42
<i>Mapping the [<sup>3</sup>H]ethidium diazide incorporation in nAChR <math>\alpha</math>-subunit with <i>S. aureus</i> V8 protease</i>	44
<i>Localization of [<sup>3</sup>H]ethidium diazide incorporation into the <math>\alpha</math>-subunit</i>	44
<i>Localization of [<sup>3</sup>H]ethidium diazide incorporation into the <math>\delta</math>-subunit</i>	47
DISCUSSION	50
<b>CHAPTER 3 IDENTIFICATION OF THE SITES OF INCORPORATION OF [<sup>3</sup>H]3-AZIOCTANOL IN THE NACHR</b>	<b>64</b>
ABSTRACT	64
INTRODUCTION	65
MATERIALS AND METHODS	67
<i>Materials</i>	67
<i>Photoaffinity labeling of nAChR-enriched membranes with [<sup>3</sup>H]3-azioctanol</i>	68
<i>Gel Electrophoresis</i>	69
<i>Proteolytic digestion:</i>	70
<i>HPLC purification</i>	70
<i>Sequence Analysis</i>	71
RESULTS	72
<i>Photoincorporation of [<sup>3</sup>H]3-Azioctanol into nAChR-Rich Membranes.</i>	72

<i>Localization of the sites of incorporation of [<sup>3</sup>H]3-azioctanol in aV8-20 segment</i>	79
<i>Incorporation of [<sup>3</sup>H]3-azioctanol into aV8-18</i>	82
<i>Localization of the sites of incorporation of [<sup>3</sup>H]3-azioctanol in aV8-10</i>	83
DISCUSSION	85
<b>CHAPTER 4 IDENTIFICATION OF THE SITES OF INCORPORATION OF [<sup>3</sup>H]PROGESTIN ARYL AZIDE IN THE NACHR</b>	<b>99</b>
ABSTRACT	99
INTRODUCTION	99
MATERIALS AND METHODS	102
<i>Materials</i>	102
<i>Photoaffinity labeling of nAChR-enriched membranes with [<sup>3</sup>H]progesterin aryl azide</i>	102
<i>Gel Electrophoresis</i>	104
<i>Proteolytic digestion</i>	104
<i>HPLC purification</i>	104
<i>Sequence Analysis</i>	105
RESULTS	106
<i>Photoincorporation of [<sup>3</sup>H]progesterin aryl azide into nAChR-rich membranes</i>	106
<i>Mapping the [<sup>3</sup>H]progesterin aryl azide incorporation in nAChR <b>a</b> subunit with V8 protease</i>	107
<i>Localization of [<sup>3</sup>H]progesterin aryl azide incorporation within aV8-10</i>	107
<i>Localization of [<sup>3</sup>H]progesterin aryl azide incorporation in the nAChR <b>b</b> subunit</i>	109
<i>Localization of [<sup>3</sup>H]progesterin aryl azide incorporation in the nAChR <b>g</b>-subunit</i>	110
<i>Localization of [<sup>3</sup>H]progesterin aryl azide incorporation in the nAChR <b>d</b>-subunit</i>	111
DISCUSSION	111
<b>CHAPTER 5 SUMMARY AND FUTURE DIRECTIONS</b>	<b>121</b>

## TABLE OF FIGURES

Figure 1-1. Proposed subunit topology and receptor oligomerization.	27
Figure 1-2. 9 Å structure of nAChR from electron microscopy	27
Figure 1-3. Agonist and benzodiazepine binding sites of the nAChR family	27
Figure 1-4 M2 and M1 segments of the nAChR	27
Figure 1-5. M3 and M4 segments of the nAChR	28
Figure 1-6. NCAs of the nAChR	28
Figure 1-7. The binding site of ethidium localized by FRET	28
Figure 1-8. Proposed binding sites of alcohols on the nAChR and GABA <sub>A</sub> R <b>Error! Bookmark not defined.</b>	
Figure 1-9. Formation of photoreactive intermediates from aryl azides and diazirines.	29
Figure 1-10. Photoaffinity probes of the nAChR	29
Figure 2-1. Binding of [ <sup>3</sup> H]ethidium in the presence and absence of various cholinergic drugs.	56
Figure 2-2. Photoincorporation of [ <sup>3</sup> H]ethidium diazide into integral and peripheral membrane proteins of nAChR-rich membranes in the presence or absence of carbamylcholine or PCP.	57
Figure 2-3. Photoincorporation of [ <sup>3</sup> H]ethidium diazide into integral and peripheral membrane proteins of nAChR-rich membranes in the presence of oxidized glutathione.	57
Figure 2-4. Photoincorporation of [ <sup>3</sup> H]ethidium diazide into integral and peripheral membrane proteins of nAChR-rich membranes in the presence of various cholinergic drugs.	58
Figure 2-5. Proteolytic mapping of sites of [ <sup>3</sup> H]ethidium diazide incorporation into the nAChR α-subunit using <i>S. aureus</i> V8 protease.	58
Figure 2-6. Reverse-phase HPLC purification of [ <sup>3</sup> H]ethidium diazide labeled fragments from EndoLysC digest of αV8-20.	59
Figure 2-7. <sup>3</sup> H and mass release upon N-terminal sequence analysis of HPLC fractions of EndoLysC-digest of [ <sup>3</sup> H]ethidium diazide labeled αV8-20 .	60
Figure 2-8. Proteolytic mapping of the sites of [ <sup>3</sup> H]ethidium diazide incorporation in the nAChR δ-subunit using V8 protease.	61
Figure 2-9. EndoLysC digest of δV8-14 fragment labeled with [ <sup>3</sup> H]ethidium diazide resolved by Tricine SDS-PAGE.	62
Figure 2-10. Reverse-phase HPLC purification of [ <sup>3</sup> H]ethidium diazide labeled fragments from EndoLysC digest of δV8-20.	62
Figure 2-11 Sequence Analysis of δV8-20 EndoLysC digest fragments.	62
Figure 2-12. Model of ethidium and αM2 helix	63
Figure 3-1. Photoincorporation of [ <sup>3</sup> H]3-azioctanol into integral and peripheral membrane proteins of nAChR-rich membranes in the presence or absence of carbamylcholine.	91
Figure 3-2 Time course of incorporation of [ <sup>3</sup> H]3-azioctanol into integral membrane proteins of nAChR-rich membranes in the presence of carbamylcholine.	91
Figure 3-3. Dependence of [ <sup>3</sup> H]3-azioctanol incorporation into α-subunit on the concentration of carbamylcholine.	92

Figure 3-4. Photoincorporation of [ <sup>3</sup> H]3-azioctanol into nAChR-rich membranes in the presence of various cholinergic agonists and competitive antagonists.	92
Figure 3-5. Photoincorporation of [ <sup>3</sup> H]3-azioctanol into nAChR-rich membranes in the presence and absence of various cholinergic drugs.	93
Figure 3-6. Effect of [ <sup>3</sup> H]3-azioctanol concentration on the incorporation into $\alpha$ -subunit.	93
Figure 3-7. Proteolytic mapping of sites of [ <sup>3</sup> H]3-azioctanol incorporation into the nAChR $\alpha$ -subunit using <i>S. aureus</i> V8 protease.	94
Figure 3-8. Reverse phase HPLC purification of [ <sup>3</sup> H]3-azioctanol labeled fragments from an EndoLysC digest of $\alpha$ V8-20 and sequence analysis of HPLC fractions	94
Figure 3-9. Reverse phase HPLC purification of [ <sup>3</sup> H]3-azioctanol labeled fragments from <i>S. aureus</i> V8 protease digest of $\alpha$ V8-20.	95
Figure 3-10. Reverse phase HPLC purification of [ <sup>3</sup> H]3-azioctanol labeled $\alpha$ V8-18 and sequence analysis of HPLC fraction.	96
Figure 3-11. Reverse phase HPLC purification of [ <sup>3</sup> H]3-azioctanol labeled fragments from trypsin digestion of $\alpha$ V8-10 and sequence analysis of HPLC fractions.	96
Figure 3-12. Model of 3-azioctanol and $\alpha$ M2 helix	97
Figure 4-1. Structure of progesterone and photoaffinity derivatives	115
Figure 4-2. Photoincorporation of [ <sup>3</sup> H]progesterin aryl azide into integral and peripheral membrane proteins of nAChR-rich membranes in the presence or absence of various cholinergic drugs.	115
Figure 4-3. Proteolytic mapping of sites of [ <sup>3</sup> H]progesterin aryl azide incorporation into the nAChR $\alpha$ -subunit using <i>S. aureus</i> V8 protease.	115
Figure 4-4. Reverse phase HPLC purification of [ <sup>3</sup> H]progesterin aryl azide labeled fragments from trypsin digest of $\alpha$ V8-10	116
Figure 4-5. HPLC purification of [ <sup>3</sup> H]progesterin aryl azide labeled fragments from trypsin digest of $\beta$ -subunit	117
Figure 4-6. HPLC purification of [ <sup>3</sup> H]progesterin aryl azide labeled fragments from trypsin digest of $\gamma$ -subunit	117
Figure 4-7. HPLC purification of [ <sup>3</sup> H]progesterin aryl azide labeled fragments from EndoLysC digest of $\delta$ -subunit	118

## Acknowledgements

None of the work presented in this thesis would have been possible without the help of other people. Steen Pedersen, Shaukat Husain, and John Katzenellenbogen provided the photoaffinity compounds with which I worked, to whom I am indebted. While a rotation student in the lab, Aimée Powelka did experiments with the [<sup>3</sup>H]3-azioctanol, and I used some of her data for figures in that chapter.

I have greatly enjoyed my time in the Program in Neuroscience in the Cohen lab. My advisory committee provided valuable input along the way, and I appreciate their time and effort. All of the members of the Cohen lab have contributed in their own way to this work. I would especially like to thank Dr. Larry Dangott who got me started on the protein chemistry experiments. Finally, I would like to thank my advisor, Jonathan Cohen, for letting me join the lab. I can't imagine a better person to have as an advisor and mentor.

## Abbreviation List

ACh	acetylcholine
1-AP	1-azidopyrene
CPZ	chlorpromazine
FRET	fluorescence resonance energy transfer
GluR	glutamate receptor
HTX	histrionicotoxin
HPLC	high-performance liquid chromatography
nAChR	nicotinic acetylcholine receptor
NCA	noncompetitive antagonist
PAGE	polyacrylamide gel electrophoresis
PCP	phencyclidine
PTH	phenylthiohydantoin
SDS	sodium dodecyl sulfate
TFA	trifluoroacetic acid
TID	3-(trifluoromethyl)-3-m-(iodophenyl)diazirine
TPP	triphenylphosphonium
TPS	<i>Torpedo</i> physiological saline
V8	<i>staphylococcus aureus</i> V8 protease

## Chapter 1 Introduction to the Thesis

The nicotinic acetylcholine receptor (nAChR) is one member of the group of transmembrane receptors known as ligand gated ion channels, which are opened upon binding of ligand to the extracellular surface. The three main superfamilies of these receptors are the nicotinic acetylcholine receptor family (for review, see Changeux and Edelstein (1998)), the glutamate receptors (GluR) (reviewed in Paas (1998)), and the P2X receptors (reviewed in Buell *et al.* (1996)). The nAChR family is composed of channels gated by the neurotransmitters acetylcholine (ACh), GABA, glycine, and serotonin (5HT<sub>3</sub>). Although the nAChR and 5HT<sub>3</sub> receptors conduct cations, while GABA<sub>A</sub> and glycine receptors conduct anions, there is still ~25%-60% sequence homology between their subunits. Within the GluR family, with 18-70% sequence identity, all of the channels are gated by glutamate but are further subdivided based on sensitivity to other drugs, AMPA, kainate, and NMDA. The P2X receptors, which have 36-48% sequence identity between subunits, are all gated by ATP.

The proposed topology of these channels was elucidated first by hydropathy plots and further by biochemical and mutational analyses (Figure 1-1). The subunits of the nAChR family have four transmembrane spanning segments, with extracellular N- and C-termini, and the channel is formed by a pentamer of subunits (Karlin and Akabas, 1995). Originally, the GluR subunits were proposed to have four transmembrane segments by analogy to the nAChR. However, subsequent data indicates that the subunits consist of 3 transmembrane spanning segments, with extracellular N-termini and intracellular C-termini. The N-terminal segment and residues between the second and third transmembrane segment contribute to the agonist binding site (Paas, 1998). A hairpin loop between the first and second transmembrane segments contributes to the channel but does not cross the bilayer, similar to K<sup>+</sup> channels (Kuner *et al.*, 1996). Additionally, like

K<sup>+</sup> channels, the GluR family forms tetramers (Laube *et al.*, 1998; Mano and Teichberg, 1998). The trimeric P2X receptors (Nicke *et al.*, 1998) are composed of subunits with only 2 transmembrane segments, with the N- and C-termini on the intracellular side of the membrane (Newbolt *et al.*, 1998; Rassendren *et al.*, 1997).

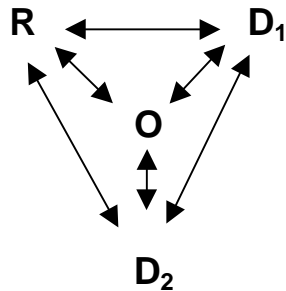
Multiple receptor isoforms can be generated from the variety of homologous subunits available. The composition of subunits of the nAChR varies in the two subtypes, muscle-type and neuronal. In *Torpedo* and embryonic muscle nAChR, the nAChR is composed of  $\alpha_2\beta\gamma\delta$ , while in adult muscle the subunit composition is  $\alpha_2\beta\varepsilon\delta$ . Neuronal nAChR can consist of either  $\alpha$  homomultimers or combinations of  $\alpha$  and  $\beta$  (non- $\alpha$ ) subunits, with 8 known neuronal  $\alpha$  subunits and 3 known neuronal  $\beta$  subunits (Role and Berg, 1996). Within the brain the main receptor isoforms contain either  $\alpha_4$  and  $\beta_2$  or  $\alpha_2$  and  $\beta_4$  subunits, though the ratio of subunits which form the pentamer is unknown. Six  $\alpha$ , 3  $\beta$ , 3  $\gamma$ , 1  $\delta$ , 1  $\varepsilon$ , 1  $\pi$ , and 3  $\rho$  subunits of the GABA<sub>A</sub>R have been identified (Mehta and Ticku, 1999). The GABA<sub>A</sub>R is the primary inhibitory channel of the central nervous system, and the major adult isoform is  $\alpha_1\beta_2\gamma_2$  (McKernan and Whiting, 1996), with a proposed stoichiometry of  $\alpha_1\beta_2\gamma_2$  (Chang *et al.*, 1996). The glycine receptor, the main inhibitory channel of the spinal cord, has 3  $\alpha$  and 1  $\beta$  subunits with which to form channels (Rajendra *et al.*, 1997).

The glutamate receptors, the primary excitatory channels of the brain, can be formed by several subunits. The AMPA receptors are composed of the GluR1-4 subunits, while the KA receptors are composed of the GluR5-7, KA1, and KA2 subunits. The NMDA receptors have two types of subunits, NR1 and NR2A-D (Barnard, 1997). The 7 homologous P2X (Chang *et al.*, 1996) subunits are expressed throughout the nervous system, as well as in immune cells, glands, and muscle (Buell *et al.*, 1996).

The most studied ligand-gated ion channel is the nAChR. This focus is due to the relative ease with which large amounts of the nAChR can be isolated. The *Torpedo* ray fish uses acetylcholine as the neurotransmitter for stimulation of its electric organs. The postsynaptic membrane fragments can easily be isolated from the organ, yielding nAChR as ~50% of the isolated protein. From each fish, ~100 nmoles of nAChR can be isolated from this simple preparation.

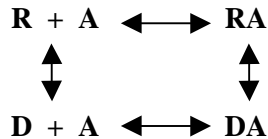
The amount of nAChR that can be isolated has even allowed structural imaging studies (Figure 1-2) (Unwin, 1998). When the isolated post-synaptic membranes are incubated at room temperature, they form a 2-D crystalline array of nAChRs. Electron microscopy of these tubules has resulted in a 9 Å and a 4.6 Å resolution structure (Unwin, 1993; Miyazawa *et al.*, 1999). Viewed from the extracellular face, the pentameric structure is readily identifiable. The nAChR is roughly shaped as a cylinder 110 Å long and 70 Å in diameter. The extracellular portion of the cylinder is approximately 60 Å long, with a 20 Å diameter opening along the central axis. The intracellular portion is only 15 Å long, also including an opening 20 Å in diameter. The portion spanning the lipid bilayer is approximately 30 Å long, with no apparent opening but rather a constriction, indicating that this area may be the gate for the ion channel. The density of each subunit closest to the central axis appears to be  $\alpha$ -helical, indicating a transmembrane segment lining the pore. This helix appears to have a kink near the middle of the bilayer, proposed to form the channel gate. A putative area for the agonist binding site has been proposed, approximately 30 Å above the lipid bilayer. However, full details of the structure are not available because the low resolution of the images does not allow a trace of the protein backbone.

## LIGAND GATED ION CHANNELS AS ALLOSTERIC PROTEINS



The ligand-gated ion channels are each modulated allosterically by several types of drugs. Agonists cause a change in the distribution of states, shifting the equilibrium from the resting state (R) to the open state (O). Prolonged exposure to agonist converts the receptor to a desensitized state, characterized by high agonist affinity but lack of current. Two desensitized states have been observed, one ( $D_1$ ), occurring within a second of agonist exposure, and the second one ( $D_2$ ) occurring after seconds to minutes of exposure. Competitive antagonists block the binding of agonist and thereby prevent agonist from shifting the equilibrium to the open state. Other drugs, known as noncompetitive antagonists, allow agonist to bind but prevent the gating of the ion channel. This reduction in current flow could result from different actions of the drugs. For example, preferential binding in the channel could sterically occlude the channel, blocking the flow of current. Alternatively, a drug may stabilize the desensitized state of the receptor, reducing the amount of receptor in the activatable state. The response to agonist may also be potentiated by drugs, drugs that either stabilize the open state or destabilize the desensitized state.

At equilibrium, the permeability response of the receptor in the presence of agonist is not observed, due to the desensitization of the receptor. The binding of drugs can then be described approximately by a two state model:



where R is the resting state receptor, D is the receptor in the desensitized state, and A is the agonist (or antagonist) (Katz and Thesleff, 1957). This model has been used as a simple scheme with which to characterize the binding of many drugs to the nAChR. The initial ratio of resting to desensitized varies by cell type, with nAChR isolated from the *Torpedo* electric organ being ~10% desensitized (Boyd and Cohen, 1980a) while the nAChR expressed in BC3H-1 cells is ~0.01% desensitized (Sine and Taylor, 1982). nAChR agonists, such as ACh and carbamylcholine, have a higher affinity for the desensitized state than the resting state, causing a shift in the ratio to ~99% desensitized in *Torpedo*. d-Tubocurarine (dTC), a competitive antagonist, has a slight preference for the desensitized state, resulting in ~60% of the *Torpedo* nAChRs desensitized (Neubig and Cohen, 1979).  $\alpha$ -Bungarotoxin ( $\alpha$ BgTx), in contrast, does not cause an allosteric shift in the ratio of the states, but acts primarily to block the binding of agonist to the nAChR.

The binding of other cholinergic drugs, such as the noncompetitive antagonists (NCAs), to the nAChR can also be described using this two-state model. Three of these drugs, phencyclidine (PCP), histrionicotoxin (HTX), and tetracaine, have been shown to bind the nAChR with a stoichiometry of one drug per nAChR (Middleton *et al.*, 1999; Heidmann *et al.*, 1983). Similar to agonists and competitive antagonists, the binding of these drugs is dependent on the state of the nAChR. To determine the affinity of these drugs for the resting vs. desensitized state, agonists or competitive antagonists have been used to fix the conformation of the nAChR. PCP binds preferentially to the desensitized state, with a  $K_D$  of 0.8  $\mu$ M in the presence of carbamylcholine. In the resting state, defined by the binding of PCP in the presence of  $\alpha$ BgTx, PCP has a  $K_D$  of 5  $\mu$ M

(Heidmann *et al.*, 1983). Tetracaine binds the resting state with higher affinity than the desensitized state, with a  $K_D$  of 0.5  $\mu\text{M}$  in the absence and a  $K_D$  of 40  $\mu\text{M}$  in the presence of carbamylcholine (Middleton *et al.*, 1999). At 20 °C, HTX binds both states with similar affinity ( $K_D=0.16 \mu\text{M}$  in the presence of carbamylcholine, 0.25  $\mu\text{M}$  in the presence of  $\alpha\text{BgTx}$ ) (Heidmann *et al.*, 1983). At 4 °C, however, HTX has a higher affinity for the desensitized state ( $K_D=0.4 \mu\text{M}$  in the presence of carbamylcholine, 6  $\mu\text{M}$  in the absence) (Boyd and Cohen, 1984). This model provides a rudimentary system with which to study the interactions of other drugs with the nAChR.

## **STRUCTURAL MOTIFS**

In the absence of high resolution structural information, studies using affinity labeling and mutagenesis have yielded information on the overall structure of the receptors in the nAChR family. The main structural motifs identified are the agonist binding site, pore-forming region, and the protein-lipid interface. These regions appear homologous across the members of the family, at least in basic topology, as expected from their sequence similarities. The agonist binding sites of the receptors are composed of at least 6 loops at the interface of 2 subunits, both of which contribute 3 loops. Each loop contains residues conserved across all subunits, perhaps contributing to the structure of the loops. Of the four transmembrane segments, the M2 segment has been the most extensively studied, and it appears to form most of the ion channel. In the nAChR, evidence indicates that the M1 segment also contributes to the ion channel, while the M3 and M4 segments are present at the protein-lipid interface.

### **Agonist binding site**

The agonist binding site of the nAChR consists of at least 6 loops at the subunit interfaces, with regions contributed by the  $\alpha$  subunit and, in non-homomeric nAChRs, the

non- $\alpha$  subunit (the  $\gamma$  or  $\delta$  subunit in *Torpedo* nAChR or embryonic muscle) (Figure 1-3). In the  $\alpha$  subunit Loop A, Tyr-93 has been implicated in agonist and competitive antagonist binding by both affinity labeling and mutational studies (Sine *et al.*, 1994; Cohen *et al.*, 1991; Galzi *et al.*, 1990). In Loop B, Trp-149 and Tyr-151 are labeled by DDF, a reversible competitive antagonist (Dennis *et al.*, 1988). Mutations of Trp-149 have also implicated it as contributing to the agonist binding site (Zhong *et al.*, 1998). Several residues in Loop C contribute to agonist and competitive antagonist binding. Tyr-190, Cys-192, Cys-193, and Tyr-198 have each been implicated by photoaffinity labeling (Middleton and Cohen, 1991; Abramson *et al.*, 1989; Dennis *et al.*, 1988; Chiara and Cohen, 1997; Kao *et al.*, 1984). Mutations at Tyr-190, Tyr-198, and Asp-200, as well as several other residues in Loop C, affect the binding of a several agonists and antagonists (Tomaselli *et al.*, 1991; Aylwin and White, 1994; Sine *et al.*, 1994; Fu and Sine, 1994; O'Leary *et al.*, 1994; Ackermann and Taylor, 1997; Osaka *et al.*, 1998).

Loops D, E, and F are on the opposite side of the subunit interface, the  $\gamma$  or  $\delta$  subunits in the *Torpedo* or embryonic muscle nAChR. Within Loop D,  $\gamma$ Trp-55 and its homolog in  $\delta$ ,  $\delta$ Trp-57, contribute to agonist and antagonist binding, as shown by both affinity labeling and mutagenesis (Prince and Sine, 1996; Chiara and Cohen, 1997; Chiara *et al.*, 1998; O'Leary *et al.*, 1994; Corringer *et al.*, 1995). Loop E residues at positions  $\gamma$ Tyr-111,  $\gamma$ Met-116, and  $\gamma$ Tyr-117, their homologs in  $\delta$ , and  $\gamma$ Leu-119 all contribute to the agonist binding site (Fu and Sine, 1994; Chiara *et al.*, 1999; Sine, 1993; Sine *et al.*, 1995). In loop F of the *Torpedo*,  $\gamma$ Asp-174 and its homolog in  $\delta$  affect the binding of agonists and antagonists.  $\gamma$ Ser-161 and  $\gamma$ Phe-172 in mouse muscle, as well as their homologs in  $\delta$ , also affect the binding of agonists and antagonists (Martin and Karlin, 1997; Osaka *et al.*, 1998; Czajkowski *et al.*, 1993; Sine, 1993; Sine *et al.*, 1995).

This multi-loop structure is also present in the GABA<sub>A</sub> agonist binding site. In the GABA<sub>A</sub> receptor, however, the agonist site is at the interface of  $\beta$  and  $\alpha$ , where GABA<sub>A</sub>  $\alpha$  plays a role similar to that of the  $\gamma$  or  $\delta$  subunit of the nAChR. So far, Loops B, C, D, and E have been shown to contribute to the binding site. In Loop B, mutation of Tyr-157 or Thr-160 shifts agonist EC<sub>50</sub> rightward (Amin and Weiss, 1993). Similarly, mutations of  $\beta$ Thr-202 or  $\beta$ Tyr-205 in Loop C cause a shift in response to GABA (Amin and Weiss, 1993). In Loop D, on the  $\alpha$  subunit,  $\alpha$ 1 Phe-65 was implicated in agonist binding by both photoaffinity labeling and mutagenesis (Smith and Olsen, 1994; Buhr and Sigel, 1997). Mutation of  $\alpha$ 1Ile-121 in Loop E reduces the binding affinity and potency of agonist (Westh-Hansen *et al.*, 1997).

The glycine and 5HT<sub>3</sub> receptor agonist sites also appear to consist of the multi-loop structure. Residues in loops B and C have been shown to contribute to the glycine site, while residues in Loop D have been shown to contribute to 5HT<sub>3</sub> binding. In the glycine receptor  $\alpha$ 1 Loop B, mutation of Phe-159, Gly-160, or Tyr-161 alters the agonist binding properties of the receptor (Vandenberg *et al.*, 1992; Schmeiden *et al.*, 1993). In Loop C, mutations of residues at  $\alpha$ 1Lys-200 and Tyr-202 affect the binding of antagonists (Vandenberg *et al.*, 1992). In the 5HT<sub>3</sub> receptor, residues Trp-89, Arg-91, and Tyr-93 of Loop E contribute to the binding affinity of agonists and competitive antagonists (Yan *et al.*, 1999).

Surprisingly, the binding site on the GABA<sub>A</sub>R of benzodiazepines also is highly homologous to the agonist binding sites on the nAChR family. Benzodiazepines potentiate the response to GABA but are unable to open the channels in the absence of agonist. The binding site of the benzodiazepines is on the  $\alpha$ - $\gamma$  interface, where  $\alpha$  contributes loops similar to nAChR  $\alpha$ , and  $\gamma$  is equivalent to the nAChR  $\gamma$  or  $\delta$ . So far, all the loops except Loop F have been shown to contribute to this binding site.  $\alpha$ 1His-101

has been implicated in the benzodiazepine binding site on Loop A by both photoaffinity labeling and mutational analysis (Duncalfe *et al.*, 1996; Korpi *et al.*, 1993; Wieland *et al.*, 1992; Wieland and Lüddens, 1994). In Loop B of the GABA<sub>A</sub>  $\alpha$  subunit,  $\alpha$ 1Tyr-159,  $\alpha$ 1Tyr-161, and  $\alpha$ 1Thr-162 affect the binding of benzodiazepines (Amin *et al.*, 1997; Buhr *et al.*, 1996; Wieland and Lüddens, 1994). The benzodiazepine binding site also has a contribution from Loop C, at residues Tyr-209, Thr-206, Ser-204, and Gly-200 (Amin *et al.*, 1997; Buhr *et al.*, 1997a; Buhr *et al.*, 1996; Wieland and Lüddens, 1994; Pritchett and Seeburg, 1991; Renard *et al.*, 1999). On the opposite side of the binding site, the equivalent of the non- $\alpha$  subunit of the nAChR, Loop D and Loop E of the GABA<sub>A</sub>  $\gamma$  subunit contribute to the benzodiazepine site. So far, the only residue in Loop D implicated in benzodiazepine binding is Phe-77, while in Loop E mutations at Met-130 affect the affinities of several benzodiazepines (Wingrove *et al.*, 1997; Buhr *et al.*, 1997b).

From a combination of the multiple mutagenesis and affinity labeling experiments, the basic contributions to the agonist binding sites have been established. However, many questions remain unanswered. For example, the position of the agonist site within the three-dimensional receptor structure is not well described, although some predictions of the location have been made by inspection of the electron micrograph images (Miyazawa *et al.*, 1999) and by fluorescence resonance energy transfer (Herz *et al.*, 1989; Valenzuela *et al.*, 1994). Additionally, a large number of residues have been implicated as contributing to the binding site, but it would be very difficult for so many to interact with all agonists, including one as small as trimethylammonium. Further studies of binding in the agonist site of all these receptors will be necessary to define the agonist sites.

## Transmembrane segments

The subunits of the nAChR family each have four transmembrane segments, M1-M4. An understanding of the functional role and position of each has been elucidated with a variety of experiments, the majority on the nAChR. From the electron microscopy studies, the channel lining appears to be made up of an  $\alpha$  helix contributed by each of the subunits. Based on photoaffinity labeling and electrophysiological data, this helix is the M2 segment. Additional evidence is beginning to show the participation of the M1 segment in channel formation as well. The M3 and M4 segments form the majority of the protein-lipid interface.

## Ion Channel

The binding of agonist to the ligand gated ion channels causes a structural change that opens the ion pore. Although the GABA<sub>A</sub> and glycine receptors are permeant to anions while the nAChR and 5HT<sub>3</sub> receptors are permeant to cations, structurally their pores appear similar. In each, the pore is lined primarily by one face of the M2 segment contributed by each subunit. There is also very strong evidence that common sites of the M2 helices compose the binding sites of at least some noncompetitive antagonists.

Mutagenesis studies with the muscle-type nAChR have illustrated some of the structural features of the M2 segment (Figure 1-4). A multiring structure formed by homologous amino acids contributed by all five subunits is predicted by many of these studies. (The residues in M2 are numbered from a homologous lysine or arginine in the N-terminus, as noted in Figure 1-4). The nature of the side chains in these rings also affects the current flow through the channel. Mutations at the C-terminal end of the M2 segments, position 20', result in an inward rectification, while mutations near the C-terminus, -5', result in an outward rectification. Additionally, mutations in these position

in all 4 subunits show similar, additive effects, suggesting a charge ring structure (Imoto *et al.*, 1988). At position 9', mutation of Leu to Ser decreased ACh EC<sub>50</sub> by 10-fold. For each subsequent mutant subunit present, the shift in EC<sub>50</sub> was additive, such that with 5 mutant subunits, the ACh EC<sub>50</sub> was decreased by 10,000-fold (Labarca *et al.*, 1995). Additionally  $\gamma$ Leu9'Thr showed a decrease in desensitization and stabilization of the open state (Filatov and White, 1995). At the 2' position, conductance is inversely related to the volume of the amino acid. It is possible that this ring forms the narrowest part of the open channel, determining the size of the ions that can flow through the channel (Villarroel *et al.*, 1991; Imoto *et al.*, 1991). Mutations in two other M2 residues, 12' and 15', have been linked to congenital myasthenic syndromes, with the 12' mutation resulting in prolonged openings in the presence of agonist (Ohno *et al.*, 1995; Gomez and Gammack, 1995). Most of the aforementioned residues, when mutated to cysteine, are all modified by water soluble probes, and that modification irreversibly alters the current in response to acetylcholine (Akabas *et al.*, 1994; Zhang and Karlin, 1998). The exposure of every third or fourth residue, along with the structural imaging data (Unwin, 1993), suggests an  $\alpha$ -helical structure for the M2 segment.

The interaction of noncompetitive antagonists (NCAs) with the M2 segments provides additional evidence for its role as the ion pore. In single channel studies, the aromatic amine QX-222 is seen to block the current of the open channel but not allow the channel to close. The residency time of QX-222 is shorter than the open time of the channel, and each time QX-222 unbinds, current flows. This flickering suggests that QX-222 enters and leaves the channel rapidly, and its presence in the channel sterically prevents the transition to a closed or desensitized state (Neher, 1983). Additional evidence that QX-222 binds in the channel comes from mutational analysis. For example, mutations of residues at 6' from polar to nonpolar or residues at 10' from

nonpolar to polar reduces the potency of channel block by QX-222 (Charnet *et al.*, 1990; Leonard *et al.*, 1988). Additionally, QX-222 is capable of protecting cysteines at positions 13', 10', 9', 6', and 2' from reaction with a water soluble probe. Cysteines at the extracellular end of the channel, 16' and 20', however, are not protected (Pascual and Karlin, 1998). Evidence for the binding of several other amine NCAs near the M2 segment comes from affinity labeling studies, discussed later.

Mutations in M2 residues of the neuronal nAChR are also capable of dramatically altering the channel conductance. Mutations at the 13', 9', and 6' positions result in conducting desensitized states (Devillers-Thierry *et al.*, 1992; Revah *et al.*, 1991). In addition, certain mutations at position 9' abolish  $\text{Ca}^{++}$  conductance (Bertrand *et al.*, 1993). Mutation of 2 residues, -1' and 13', of the neuronal nAChR M2 segment to their corresponding residues in the GABA<sub>A</sub> and glycine receptors, along with the addition of a proline present in these receptors, is sufficient to convert the nAChR channel from cation to anion selective (Galzi *et al.*, 1992). NCAs also appear to bind near the M2 segment of neuronal nAChR since mutations at Leu-9' to Ser or Thr in the  $\alpha 7$  nAChR suppresses the block by 20  $\mu\text{M}$  QX-222 (Revah *et al.*, 1991).

In addition to the M2 segment, the N-terminal end of the M1 segment also appears to contribute to pore formation. Cysteine mutations in this region are accessible to modification by water soluble probes (Akabas and Karlin, 1995; Zhang and Karlin, 1997). On the other hand, several residues in the C-terminal end of  $\alpha$  and  $\delta$ , which were inaccessible to probes, are labeled by [<sup>125</sup>I]TID in a manner consistent with exposure near the protein-lipid interface (Blanton and Cohen, 1994; White and Cohen, 1992). The effects of side chain size at position  $\gamma\text{Cys-230}$  indicate that this position also is not exposed to the channel (Lo *et al.*, 1991). Therefore, it is likely that just the N-terminus of M1 contributes to the lumen of the channel, while the C-terminus is further removed.

Although the GABA<sub>A</sub> and glycine receptors are anion channels, they appear to function similarly to the M2 segment of the nAChR. Cysteine scanning mutagenesis of the full M2 segment of GABA<sub>A</sub>  $\alpha$ 1, as well as a portion of the GABA<sub>A</sub>  $\gamma$ M2 segment, has shown that the water exposed residues are located in approximately the same positions as those of the nAChR (Xu and Akabas, 1996). Additionally, noncompetitive antagonists of glycine and GABA<sub>A</sub> receptors are affected by mutations in the M2 segment. For example, picrotoxin is affected by the exchange of the glycine  $\beta$ 1 M2 sequence for the  $\alpha$ 1 M2 sequence at non-homologous residues. Partial block is produced by the exchange of the C-terminal portion, while complete block requires exchange of the entire M2 segment (Pribilla *et al.*, 1992). In the GABA<sub>A</sub> receptor, picrotoxin and cyclodienes no longer block current of a *Drosophila* GABA<sub>A</sub> receptor with an Ala3'Ser mutation (French-Constant *et al.*, 1993). Picrotoxin prevents the modification of GABA<sub>A</sub>  $\alpha$ 1Val2'Cys by cysteine modifying reagents, while  $\alpha$ 1Thr6'Cys is still modified in the presence of picrotoxin (Xu *et al.*, 1995). In agreement with picrotoxin binding near the N-terminal, most intracellular end of the GABA<sub>A</sub> M2 segment, mutations at  $\beta$ 1Thr12'Gln allow wild-type block by both picrotoxin and penicillin (Birner *et al.*, 1997). Another NCA of the GABA<sub>A</sub> receptor, Zn<sup>++</sup> is affected by residues at the C-terminal end of the M2 segment. A mutation of  $\beta$ 1His-17' to Ser, the homologous residue in  $\alpha$ 1, reduces the IC<sub>50</sub> of Zn<sup>++</sup> block by 300 fold, while the converse mutant increases the block by Zn<sup>++</sup> (Horenstein and Akabas, 1998).

### Protein-lipid Interface

The structure and location of the M3 and M4 transmembrane segments have been studied by photoaffinity labeling. Although in the three-dimensional structure determined from electron microscopy of the nAChR the only apparent  $\alpha$ -helical content of the nAChR is the M2 segments, the pattern of photoaffinity labeling of the M3 and M4

segments suggests an  $\alpha$ -helical structure (Figure 1-5). [ $^{125}$ I]TID, as well as [ $^3$ H]DAF, photoaffinity labeled several residues on the M4 segment in approximately an every-third pattern, consistent with an  $\alpha$ -helix (Blanton and Cohen, 1992; Blanton and Cohen, 1994; Blanton *et al.*, 1998a). [ $^{125}$ I]TID labeled M3 in a similar manner (Blanton and Cohen, 1994). The incorporation of these hydrophobic drugs into the M3 and M4 segments was not affected by other cholinergic ligands, and these residues are expected to line the protein-lipid interface.

Although the nAChR is functional when the entire M4 segment is exchanged for a transmembrane segment from other membrane proteins (Tobimatsu *et al.*, 1987), particular residues do have dramatic effects on nAChR function. Mutation of  $\alpha$ Cys-418 to a variety of residues resulted in prolonged open channel lifetime, an increase of ~28-fold when mutated to tryptophan (Li *et al.*, 1992; Bouzat *et al.*, 1998; Lee *et al.*, 1994; Lasalde *et al.*, 1996; Ortiz-Miranda *et al.*, 1997). Similar effects were seen with mutations of  $\alpha$ Thr-422 (Bouzat *et al.*, 1998). Additionally, in the mouse nAChR, the nature of the residues at two positions on the  $\gamma$  subunit, at 440 and 442 (homologous to  $\alpha$ Cys-412 and  $\alpha$ Phe-414 of *Torpedo*), alters the nAChR channel kinetics (Bouzat *et al.*, 1994). The composition of the M3 segment has also been shown to affect the gating of the nAChR (Campos-Caro *et al.*, 1997). These mutation illustrate the highly allosteric nature of the nAChR, indicating that modification as far removed from the channel or agonist binding site as the protein-lipid interface can alter the gating.

## **NONCOMPETITIVE ANTAGONISTS**

The noncompetitive antagonists (NCAs) are a structurally diverse group of compounds that reversibly inhibit current through the channel without blocking the binding of agonist (Figure 1-6). As discussed with regards to the M2 transmembrane segment, a simple view of the binding of certain NCAs is pore occlusion. Most aromatic

amine NCAs appear to bind in the lumen of the channel. Other classes of drugs, such as the general anesthetics, have a currently unknown site or sites of action.

### **Amine NCAs**

Several drugs of the aromatic amine family act as NCAs on the nAChR. Photoaffinity labeling studies with many of these have shown that their primary site of binding is the M2 segment, in the lumen of the channel. Of the compounds known to bind one molecule per nAChR, only the binding site of tetracaine has been determined, while the sites of binding of HTX and PCP remain unclear. [<sup>3</sup>H]Tetracaine, which binds preferentially to the resting state, labels residue 9' in all subunits as well as at 13' in  $\alpha$  and  $\delta$  (Gallagher and Cohen, 1999). In the presence of carbamylcholine, [<sup>3</sup>H]chlorpromazine (CPZ) labels residues in all four subunits, including Ser-6' in each (Giraudat *et al.*, 1986; Giraudat *et al.*, 1987; Giraudat *et al.*, 1989; Revah *et al.*, 1990). [<sup>3</sup>H]Triphenylphosphonium (TPP) also labels this residue in all the subunits except  $\gamma$  (Hucho *et al.*, 1986). The binding site of meproadifen is slightly removed from the binding sites of the others, with affinity incorporation of [<sup>3</sup>H]meproadifen mustard into Glu-20' (Pedersen and Cohen, 1990). These results suggest that these noncompetitive antagonists bind in the pore, which is formed by the M2 segments of all of the subunits, and most access the subunits equally.

Two uncharged aromatic NCAs, [<sup>125</sup>I]TID and [<sup>3</sup>H]DAF, label similar regions to the aforementioned aromatic amine NCAs. However, unlike the labeling of these drugs in M4, the labeling in M2 is inhibitable and affected by cholinergic drugs. In the presence of agonist, [<sup>125</sup>I]TID labels residues at 6', as well as at 2', 9', and 13'. In the absence of agonist, however, [<sup>125</sup>I]TID only labels 9' and 13' (White and Cohen, 1992). A derivative of TID, [<sup>125</sup>I]-TID-BE labels  $\beta$ L9',  $\beta$ V13', and  $\beta$ L16' in the presence of carbamylcholine (Blanton *et al.*, 1998b). [<sup>3</sup>H]DAF labels  $\beta$ V13' and  $\delta$ V13' in the

absence of carbamylcholine, with incorporation inhibitable by tetracaine; in the presence of carbamylcholine, incorporation is present at  $\beta$ L9',  $\beta$ A10',  $\delta$ S6' and  $\delta$ L9', with the incorporation inhibitable by PCP, another NCA (Blanton *et al.*, 1998a).

There is some evidence that not all aromatic amines bind in the M2 domain. Quinacrine binds competitively with [ $^3$ H]PCP, but the photoactivatable probe [ $^3$ H]quinacrine azide incorporates into the N-terminus of the M1 segment in the open state (DiPaola *et al.*, 1990; Karlin, 1991). Additionally, mutations in this region affect the block by quinacrine (Tamamizu *et al.*, 1995). The effect of mutations in the M2 segment on the block by quinacrine has yet to be reported. These M1 residues, when mutated to cysteine, are accessible to a water soluble probe, and most likely contribute to the channel lumen (Akabas and Karlin, 1995; Zhang and Karlin, 1997).

The binding sites of other aromatic amine NCAs have been assumed to be near that identified for the photoaffinity drugs. For example, PCP and HTX, in most cases, competitively inhibit the binding of other aromatic amines, although their sites of binding are unknown. Competitive binding of a given drug with HTX or PCP has been used as a simple approximation of binding in the lumen of the channel. However, in certain cases the results challenge this assumption. For example, in the desensitized state, TID fully inhibits the binding of [ $^3$ H]PCP and allosterically inhibits the binding of [ $^3$ H]HTX. In the resting state, though, TID again allosterically inhibits [ $^3$ H]HTX binding, but does not affect the binding of [ $^3$ H]PCP (White *et al.*, 1991). Additionally, mutations in M1 which affect quinacrine inhibition have no effect on the inhibition by CPZ (Tamamizu *et al.*, 1995).

Ethidium is another aromatic amine NCA that inhibits the binding of PCP and HTX. At equilibrium in the presence of agonist, ethidium inhibits the binding of [ $^3$ H]PCP with a  $K_D$  of 0.4-0.6  $\mu$ M (Herz *et al.*, 1987; Pedersen, 1995). The inherent

fluorescence of ethidium makes it a good tool for studies of the structure of the nAChR. Ethidium has been used as a probe in measurements of channel kinetics, with fewer complications than the more traditional flux assays (Rankin *et al.*, 1997). Initial studies using fluorescence resonance energy transfer (FRET) showed that the distance between the ethidium NCA binding site, which was presumed to be the channel lumen, and the agonist site, using fluorescent agonist and competitive antagonist, was  $\sim 30 \text{ \AA}$  (Herz *et al.*, 1989) (Figure 1-7). However, subsequent FRET experiments measured the distance between the ethidium NCA site and the lipid membranes as  $50 \text{ \AA}$ , placing the binding site of ethidium at the most extracellular end of the nAChR (Johnson and Nuss, 1994). This distinct site of binding was unexpected, due to the structural similarity to other aromatic amine NCA. If the ethidium binding site is removed from the channel, the mechanism of action, as well as many assumptions based on competitive binding of drugs, will need to be reconsidered.

## **Anesthetics**

Anesthetics are another class of drugs which act as NCAs on the nAChR, and they also modulate the GABA<sub>A</sub> and glycine receptors. The wide range of structures that cause anesthesia, from small halogenated hydrocarbons to long-chain alcohols to steroids, led earlier researchers to propose that the drugs act by a nonspecific mechanism, probably disordering of the lipids. This theory has been supported by a comparison of the potency of various general anesthetics to their lipid partition coefficient, the Meyer-Overton correlation. However, accumulating evidence suggests that general anesthetics are likely to exert their effects by direct interactions with receptors and other proteins (Franks and Lieb, 1994). Several studies have been aimed at determining if there are specific binding sites for general anesthetics on the ligand gated ion channels.

## Alcohols

One class of anesthetics that has been shown to affect the nAChR family is the alcohols. Evidence for a specific site/sites of action comes from the effects of varying molecule size as well as from interaction between alcohols inhibiting the nAChR. The alcohols have a size cut-off effect, since alcohols longer than dodecanol have no effect on the nAChR (Alifimoff *et al.*, 1989). Based on additional studies with cycloalkanemethanols, the cut off for inhibition is related to the volume, and not the length, of the molecule (Wood *et al.*, 1993).

The size of the molecule affects not only whether the alcohol has an effect, but also the nature of the effect. In flux assays with the nAChR, ethanol shifts the ACh  $K_A$  (the 50% activating concentration) leftward, apparently increasing the ACh affinity, and speeds the desensitization at low concentrations of agonist (Forman and Miller, 1989; Wood *et al.*, 1991). Larger alcohols, such as octanol and hexanol, reduce the maximum flux through the channels without changing agonist affinity (Wood *et al.*, 1991). At low agonist concentrations, propanol and butanol enhance flux, as does ethanol, while at high concentrations they inhibit flux similarly to octanol. When octanol and ethanol are applied together, the maximum flux is decreased, as with octanol alone, and the  $K_A$  of ACh is shifted, as with ethanol, suggesting that the two compounds act at different sites (Wood *et al.*, 1991). Other flux assays suggest that octanol and heptanol act in a mutually exclusive manner, probably binding to the same site (Wood *et al.*, 1995).

Unlike muscle nAChR, the  $\alpha 7$  nAChR is inhibited by ethanol, and the 5HT<sub>3</sub> receptor is potentiated by ethanol. A chimera between these two receptors, with the N-terminal 200 amino acids from the  $\alpha 7$  nAChR, was inhibited by ethanol, showing that ethanol exerts its effects on the nAChR N-terminal to the M2 segment (Yu *et al.*, 1996). Efforts to map the site of action of the long chain alcohols, however, have implicated the

M2 segment of the nAChR (Figure 1-8). Mutation of  $\alpha$ Ser-10'Ile increases the sensitivity of the nAChR to block by octanol. As this side chain is varied, the more hydrophobic side chains increase sensitivity to hexanol. The double mutant,  $\alpha$ Ser-10'Ile and  $\beta$ Thr-10'Ile, increases the sensitivity to hexanol more than  $\alpha$ Ser-10'Ile alone (Forman *et al.*, 1995). However, the  $\beta$ Thr-10'Ile, has less of an effect on the sensitivity to octanol or hexanol than  $\alpha$ Ser-10'Ile, and both affect the sensitivity more than mutations in  $\gamma$ 10' or  $\delta$ 10'. These mutations do, however, have additive effects on sensitivity to alcohol block (Forman, 1997). At least one mutation in the 6' position,  $\alpha$ Ser-6'Phe, does not affect the sensitivity to alcohols as much as the mutations at the 10' position, suggesting that the alcohols do not bind on the more intracellular side of the channel (Forman *et al.*, 1995).

Unlike their actions on the nAChR, alcohols potentiate the response in the GABA<sub>A</sub> and glycine receptors, at least with some isoforms. Using mutagenesis, several experiments have addressed the location of the alcohol binding site (Ye *et al.*, 1998; Wick *et al.*, 1998; Mihic *et al.*, 1997). These studies have implicated two residues, one in the M2 segment and one in M3. The residue in the M2 segment, 15', is predicted to lie on the face of the  $\alpha$ -helix pointing away from the channel lining. The position of the M3 residue is less well defined, but has been predicted to lie on the face of M3 adjacent to the M2 helix, at approximately the same level as the M2 residue (Wick *et al.*, 1998). The size of the residues at these positions affects the cut-off of the alcohols on these receptors. In addition to alcohols, substitutions at these residues also alter the potentiation by volatile general anesthetics, isoflurane and enflurane, as well as intravenous anesthetics, loreclezole and etomidate (Krasowski *et al.*, 1998; Mihic *et al.*, 1997; Wingrove *et al.*, 1994; McGurk *et al.*, 1998; Moody *et al.*, 1997; Belelli *et al.*, 1997).

The data from the nAChR and GABA<sub>A</sub> and glycine receptor implicate different portions of the M2 segment as the site of action of alcohols. It is possible that the different receptors have distinct binding sites for alcohols. However, either mutation may affect the action of the alcohols allosterically. For example, in the nAChR the  $\alpha$ Ser-10'Ile mutant effectively converts ACh to a partial agonist. This effect alters the observed action of ethanol, although it is not expected that ethanol binds to this site (Forman and Zhou, 1999). An alternative approach, like photoaffinity labeling, could help pinpoint the site of action of the alcohols.

## Steroids

Steroids, another class of anesthetics, also modulate the response of nAChR family receptors. The high lipophilicity of steroids suggests a possible interaction at the protein-lipid interface. However, electrophysiological experiments with the nAChR have provided evidence that the steroids do not act via the protein-lipid interface. Binding to a site accessible only from the extracellular side is supported by a decrease in inhibition when hydrocortisone and 11-deoxycortisone are applied intracellularly (Bouzat and Barrantes, 1993). Experiments with a modified progesterone coupled to bovine serum albumin (BSA) show that even a strongly hydrophilic steroid could still inhibit current, suggesting that the steroid does not need to enter the lipid bilayer to exert its effects (Valera *et al.*, 1992; Ke and Lukas, 1999).

The action of steroids is different from other NCAs, suggesting the existence of a distinct site of binding. When progesterone is applied before agonist, and then washed off, the current is still inhibited (Valera *et al.*, 1992). Hydrocortisone and 11-deoxycortisone cause a decrease in burst duration, indicating that the channel may be able to adopt a closed conformation while still being bound by the steroid (Bouzat and

Barrantes, 1993). Additionally, the application of hydrocortisone with QX-222 alters the single channel properties from those seen with QX-222 alone, suggesting that the two drugs bind different sites (Bouzat and Barrantes, 1996). This data suggests that steroids are not traditional channel-blockers, if they even bind in the channel at all.

As with the nAChR, the site of action of steroids on the GABA<sub>A</sub> receptor is unknown. The site of interaction is not at any of the traditional binding sites, such as the agonist, barbiturate, or benzodiazepine sites. A variety of steroids enhance agonist and benzodiazepine binding to the GABA<sub>A</sub> receptor, and steroids still enhance current in the presence of barbiturates (Paul and Purdy, 1992). Chimeric proteins constructed from the glycine  $\alpha$ 1 subunit and the GABA<sub>A</sub>  $\alpha$ 2 or  $\beta$ 1 subunits indicate the site of action of steroids is N-terminal to the middle of the M2 segment (Rick *et al.*, 1998). Mutations in residues implicated in the binding of alcohols and small molecule anesthetics show no effect on the action of neurosteroids, providing additional evidence that they bind an as-yet undiscovered site (Belelli *et al.*, 1997; McGurk *et al.*, 1998).

Based on photoaffinity labeling studies on the nAChR with [<sup>3</sup>H]promegestone, steroids bind near the protein-lipid interface, at least. [<sup>3</sup>H]Promegestone photoincorporated into residues in M4 previously identified by [<sup>125</sup>I]TID as forming the protein-lipid interface (Blanton *et al.*, 1999). However, lack of labeling in the channel could be explained by poor reactivity of the photoactivatable group with the channel sidechains or the positioning of the group far from any sidechains. Further work is necessary to determine clearly the site of steroid action.

## **PHOTOAFFINITY LABELING**

While much of the data regarding the functional domains of the receptors comes from mutagenesis studies, there are complications in interpreting results from these

experiments. For example, a mutation in one area may cause an allosteric change in a distant area, as with the M4 mutant that alters channel gating (Li *et al.*, 1992). These changes may also affect the binding of drugs. A mutation may cause a structural change undetectable by agonist response, but affecting the response to another drug.

Alternatively, a mutation may alter the response to agonist and thereby alter the effect of another drug. The  $\alpha$ Ser-10'Ile mutation causes such a change in nAChR response to ethanol (Forman and Zhou, 1999).

To complement mutational analyses, photoaffinity labeling potentially provides a means of identifying amino acids contributing to the drug binding site. As described above, this method has been used extensively with the nAChR to map the agonist binding site and also to identify the binding sites of aromatic amines within the ion channel. In these studies, photoaffinity labeling and mutational studies showed complementary results. Photoaffinity labeling, however, also is problematic. Ideally, the photoactivatable compound has a similar structure to the drug of interest, possibly being the drug itself. Additionally, the compound should bind similarly to, and have the same pharmacological effects as, the drug of interest. Photolysis should be carried out at a UV wavelength that does not damage the protein. The photolysis should generate a reactive group that reacts rapidly and efficiently, with no selectivity for the nature of the neighboring side chain. The adduct formed should be robust to conditions used in analysis, such as HPLC and sequencing. In reality, most photoaffinity probes do not meet all of these criteria.

The aryl azides are the most commonly used photoaffinity probes, due to their ease of synthesis. However, they can display selective reactivity, and the adducts formed are often not stable. When aryl azides are photolyzed, they form reactive singlet nitrenes, which, unfortunately, readily rearrange to ketenimine azepines (Figure 1-9). The nitrenes have a broad reactivity while the azepine reacts preferentially with nucleophiles such as

cysteines. Although cysteines have been labeled predominantly by aryl azide ligands, other, less nucleophilic amino acids have also been shown to react with aryl azides (Fleming, 1995; Kotzyba-Hibert *et al.*, 1995). One other disadvantage of the aryl azide photochemistry is that the photoadducts formed between the ketenimine azepines and glutamic and aspartic acids are very sensitive to hydrolysis, and adducts with some other amino acids are also slightly sensitive (Bayley, 1983). In addition, aryl azides must be photolyzed at 254 nm, a wavelength that can damage protein.

Aryl azide derivatives of several nAChR NCAs have been synthesized (Figure 1-10). For example, progestin aryl azide was synthesized as a probe of the progesterone receptor (Kym *et al.*, 1995). This compound binds the progesterone receptor with high affinity, and shows high photoincorporation efficiency, with approximately 60% of the receptor labeled with high specificity. Since progesterone acts as a NCA on the nAChR, this compound could be useful in localizing the site of steroid binding on the nAChR. [<sup>3</sup>H]Quinacrine azide, which has been used as a photoaffinity probe of the nAChR, is also an aryl azide (DiPaola *et al.*, 1990). A photoactivatable derivative of ethidium, ethidium diazide, has also been synthesized for studying the nAChR (Witzemann and Raftery, 1978; Pedersen, 1995). This drug binds the nAChR similarly to ethidium and photoincorporates into several subunits. Further studies with this compound will help localize the site of ethidium binding on the nAChR.

Another photoactivatable group, the diazirine, shows less selectivity and higher reactivity than the aryl azides. One aromatic diazirine, (trifluoromethyl)phenyldiazirine, for example, shows broad reactivity to side chains, and is photolyzed at 365 nm, a wavelength that is not expected to cause changes in the protein. This group has been used successfully with the nAChR as [<sup>125</sup>I]TID. [<sup>125</sup>I]TID labeled a wide variety of side

chains, including some with which it is expected to have low reactivity (Blanton and Cohen, 1992; Blanton and Cohen, 1994; White and Cohen, 1992). Aromatic diazirines, however, are not used as frequently as the aryl azides, due to difficulties of synthesis of the diazine.

An alternative to the aromatic diazine is the aliphatic diazine. Although the aliphatic carbene generated upon photolysis is not as well stabilized as the aromatic carbene, aliphatic diazirines have been useful in photoaffinity studies. Examples of aliphatic diazirines include several oligosaccharides as well as a fatty acid (Schmider *et al.*, 1996; Liessem *et al.*, 1995). However, most reports have not been able to clearly identify the labeled amino acids by sequence analysis, though one report has determined the labeled residue by alternative methods (Liessem *et al.*, 1995). Another aliphatic diazine that has been developed is 3-azidoctanol (Husain *et al.*, 1999). This compound has been shown to have similar pharmacological properties to octanol. In tadpoles it induces anesthesia with an  $EC_{50}$  of  $\sim 160 \mu\text{M}$ , between the potency of heptanol and octanol. Additionally, 3-azidoctanol potentiates the current in  $\text{GABA}_A$  receptors, while inhibiting the current in nAChR, similarly to octanol. This compound will be useful in localizing the site of action of long chain alcohols on the nAChR and, potentially, on the  $\text{GABA}_A$  receptor.

### **THESIS SYNOPSIS**

This dissertation consists of experimental work with three different nAChR NCAs, each presented in a separate chapter. The localization of the binding site of [ $^3\text{H}$ ]ethidium diazide is presented in Chapter 2. Based on homology to other aromatic amines, the binding site of ethidium might be expected to be in the nAChR pore. However, as described above, experiments with fluorescence resonance energy transfer indicated a binding site near the most extracellular region of the nAChR. [ $^3\text{H}$ ]Ethidium

diazide has been previously shown to photoincorporate into nAChR (Witzemann and Raftery, 1978; Pedersen, 1995) and was used it here to map the site of ethidium binding. nAChR subunits labeled with [<sup>3</sup>H]ethidium diazide were isolated by SDS-PAGE and subjected to proteolytic digestion and Edman degradation to identify the sites of incorporation. The experiments showed that the high affinity binding site of ethidium in the nAChR in the desensitized state is within the lumen of the channel, with contributions from both the M2 and M1 segments.

In Chapter 3, the results of photoincorporation of [<sup>3</sup>H]3-azioctanol are presented. Evidence from mutational studies with the nAChR and GABA<sub>A</sub>R has implicated the M2 segment as contributing to the sites of action of long chain alcohols on these receptors. However, the regions identified in the two receptors are on different faces of the M2 helix. Here, the photoactivatable alcohol [<sup>3</sup>H]3-azioctanol was photoincorporated into the nAChR. The sites of incorporation were mapped using proteolytic digestion and Edman degradation in an attempt to clarify the site of binding of long chain alcohols on the nAChR. The primary site of [<sup>3</sup>H]3-azioctanol incorporation in the nAChR in the desensitized state was αGlu-262, at the extracellular end of M2, indicating binding within the lumen of the channel.

Preliminary studies using the photoactivatable steroid [<sup>3</sup>H]progesterin aryl azide as a probe of the steroid binding site on the nAChR are presented in Chapter 4. Previous reports on the incorporation of a photoactivatable steroid, [<sup>3</sup>H]promegestone, showed incorporation in the M4 segment. To extend this analysis, I used a structurally related steroid, [<sup>3</sup>H]progesterin aryl azide, which contained a different photoactivatable group, to determine if another steroid labeled M4 or other regions of the nAChR. Labeled subunits were subjected to proteolytic digestion and Edman degradation to determine labeled regions. Although the instability of the photoadducts to HPLC and sequencing conditions,

as well as the poor recovery of peptide fragments, precluded the identification of labeled residues, the primary site of [<sup>3</sup>H]progesterin aryl azide incorporation in the  $\alpha$ -subunit was within  $\alpha$ M4.

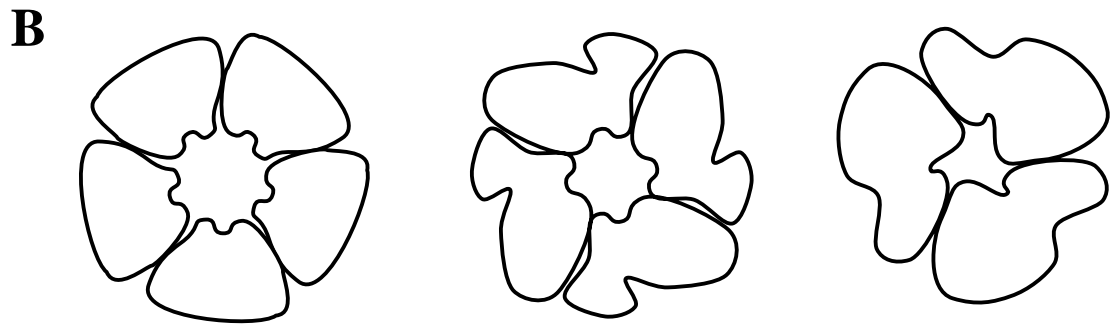
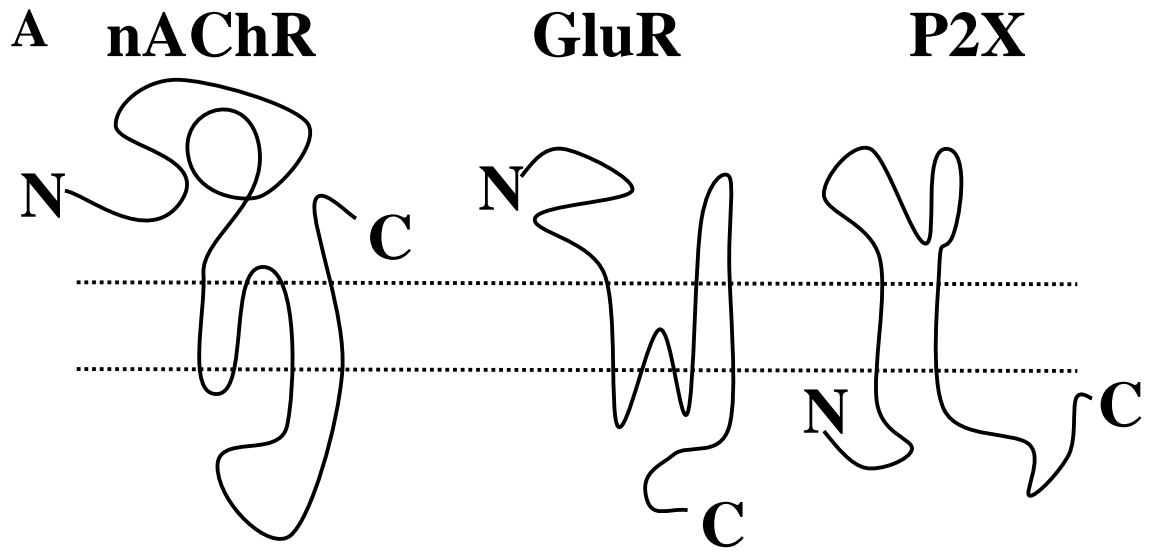


**Figure 1-1. Proposed subunit topology and receptor oligomerization.**

A. Proposed subunit membrane topology of the nAChR, GluR, and P2X receptor families.

B. Proposed oligomerization of the nAChR, GluR, and P2X receptor families.

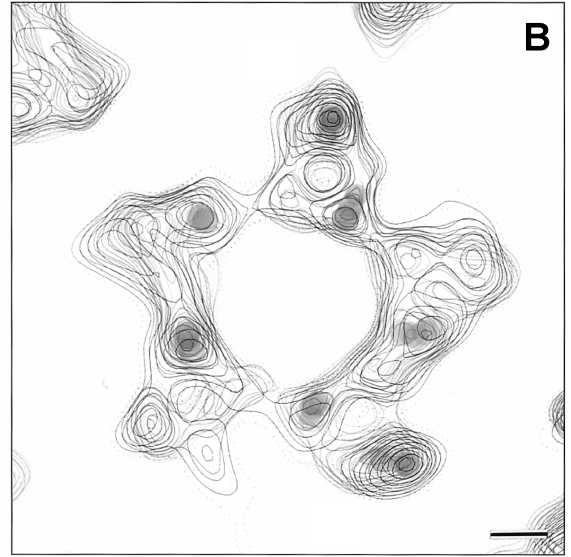
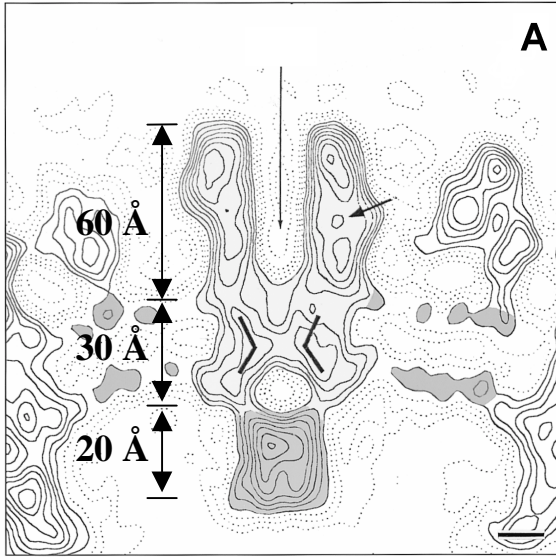
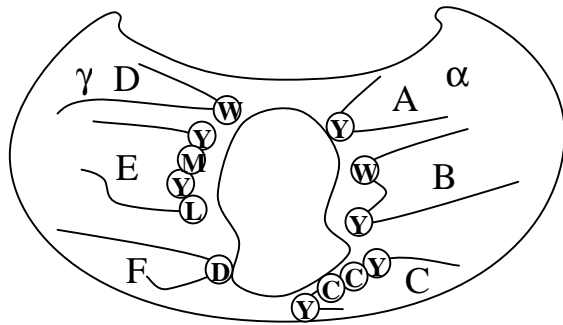


**Figure 1-2. 9 Å structure of nAChR from electron microscopy**

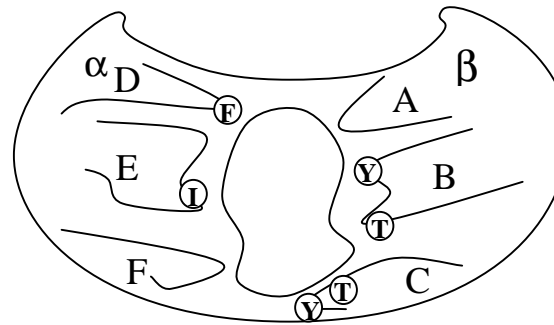
A. View of nAChR from side, showing ion pore and predicted agonist binding site.

Approximate dimensions are indicated (adapted from Unwin (1998)).

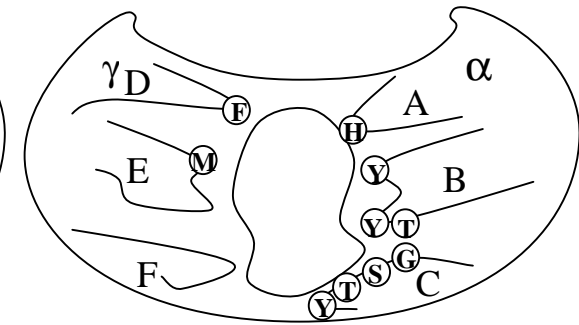
B. View from the extracellular side, showing the five  $\alpha$ -helical segments.



**nAChR agonist site**



**GABA<sub>A</sub> agonist site**

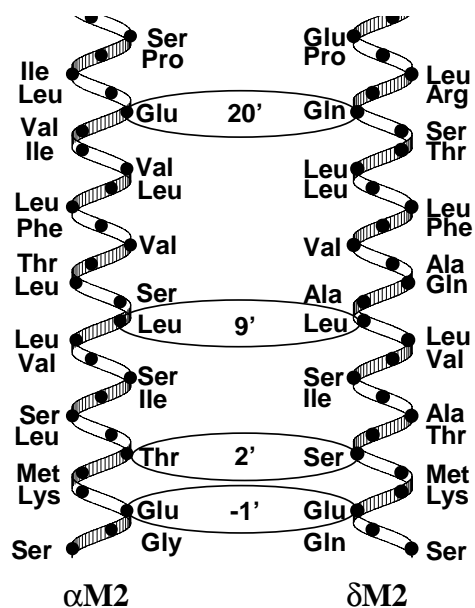


**GABA<sub>A</sub> benzodiazepine site**

	Loop A		Loop B		Loop C			Loop D			Loop E			Loop F																																			
	8	9	1	1	1	1	1	9	5	6	1	1	1	1	1	1																																	
	8	4	4	6	2	9	8	3	0	7	9	6	0	9	6	0																																	
nAChR α	P	D	L	V	L	Y	N	L	G	I	W	T	Y	D	Y	Y	T	C	C	P	D	T	P	Y	N	V	R	L	R	Q	Q	W	K	L	L	L	D	Y	T	G	K	I	M	W	T	D	L	S	T
nAChR γ	P	D	V	V	L	F	N	F	R	S	Q	T	Y	D	W	Q	L	T	K	D	D	T	D	F	N	V	W	I	F	I	Q	W	N	V	L	V	Y	N	D	G	S	M	Y	W	L	D	P	E	D
nAChR δ	P	D	I	V	L	Q	N	F	T	A	L	N	Y	D	P	D	K	F	P	N	G	T	N	Y	N	V	W	M	D	H	A	W	N	V	L	V	R	P	N	G	Y	V	T	W	L	D	P	E	A
GABA <sub>A</sub> R α1	P	D	T	F	F	H	N	F	G	S	Y	A	Y	T	G	I	V	Q	S	S	T	G	E	Y	D	V	F	F	R	Q	S	W	L	L	R	I	T	E	D	G	T	L	L	Y	T	D	G	S	R
GABA <sub>A</sub> R β2	P	D	T	Y	P	L	N	I	E	S	Y	G	Y	T	K	K	V	V	F	S	T	G	S	Y	T	M	Y	F	Q	Q	S	W	M	I	R	L	H	P	D	G	T	V	L	Y	G	D	N	A	V
GABA <sub>A</sub> R γ2	P	D	T	F	F	R	N	F	S	S	Y	G	Y	P	E	V	V	K	T	T	S	G	D	Y	D	I	F	F	A	Q	T	W	M	L	R	I	W	N	D	G	R	V	L	Y	T	D	T	R	S
gly α1	P	D	L	F	F	A	N	L	E	S	F	G	Y	T	C	T	K	H	Y	N	T	G	K	F	N	I	F	L	R	Q	Q	W	L	L	R	I	S	R	N	G	N	V	L	Y	S	D	V	Q	T
gly β1	P	D	L	F	F	A	N	L	E	S	F	G	Y	T	T	K	Y	Y	K	G	T	G	Y	Y	N	I	F	L	R	Q	K	W	L	L	F	I	F	R	D	G	D	V	L	V	S	D	T	Q	R
5HT <sub>3</sub> R	P	D	I	L	I	-	N	F	T	S	W	L	H	T	E	F	S	M	E	S	S	N	Y	Y	Y	I	W	Y	R	Q	Y	W	Y	V	Y	I	R	H	Q	G	E	V	Q	N	Y	D	V	Q	N

**Figure 1-3. Agonist and benzodiazepine binding sites of the nAChR family**

1. Model of the agonist sites of nAChR and GABA<sub>A</sub>R and the benzodiazepine site on the GABA<sub>A</sub>R showing the amino acids identified by either photoaffinity labeling or site-directed mutagenesis and their corresponding loops.
2. Sequence of the nAChR family subunits in the loop regions. Amino acids identified as contributing to the binding sites of agonist (○ ACh, □ GABA, △ glycine, ◇ serotonin) or benzodiazepine (■) are marked, as are conserved residues (■). The numbering of the *Torpedo* α subunit is shown above.



## M2 segment

	-5'	-3'	-1'	0	2'	6'	9'	13'	17'	20'																			
nAChR $\alpha$	238-D	S	G	-	E	K	M	T	L	S	I	S	V	L	L	S	L	T	V	F	L	L	V	I	V	E	L	I	P
nAChR $\beta$	244-D	A	G	-	E	K	M	S	L	S	I	S	A	L	L	A	V	T	V	F	L	L	L	L	A	D	K	V	P
nAChR $\gamma$	246-Q	A	G	G	Q	K	C	T	L	S	I	S	V	L	L	A	Q	T	I	F	L	F	L	I	A	Q	K	V	P
nAChR $\delta$	252-E	S	G	-	E	K	M	S	T	A	I	S	V	L	L	A	Q	A	V	F	L	L	L	T	S	Q	R	L	P
GABA <sub>A</sub> $\alpha$ 1	250-E	S	V	P	A	R	T	V	F	G	V	T	T	V	L	T	M	T	T	L	S	I	S	A	R	N	S	L	P
GABA <sub>A</sub> $\beta$ 1	245-D	A	S	A	A	R	V	A	L	G	I	T	T	V	L	T	M	T	T	I	S	T	H	L	R	E	T	L	P
GABA <sub>A</sub> $\gamma$	260-D	A	V	P	A	R	T	S	L	G	I	T	T	V	L	T	M	T	T	L	S	T	I	A	R	K	S	L	P
gly $\alpha$ 1	214-D	A	S	A	A	R	V	G	L	G	I	T	T	V	L	T	M	T	T	Q	S	S	G	S	R	A	S	L	P
gly $\beta$ 1	271-D	A	S	A	A	R	V	P	L	G	I	F	S	V	L	S	L	A	S	E	C	T	T	L	A	A	E	L	P
nAChR $\alpha$ 7	234-D	S	G	-	E	K	I	S	L	G	I	T	V	L	L	S	L	T	V	F	M	L	L	V	A	E	I	M	P

■ Water accessible, based on Cys modification

## M1 segment

nAChR $\alpha$	211-P	L	Y	F	I	V	N	V	I	I	P	C	L	L	F	S	F	L	T	G	L	V	F	Y	L	P
nAChR $\beta$	217-P	L	F	Y	L	V	N	V	I	A	P	C	I	L	I	T	L	L	A	I	F	V	F	Y	L	P
nAChR $\gamma$	219-P	L	F	Y	I	I	N	I	I	A	P	C	V	L	I	S	S	L	V	V	L	V	Y	F	L	P
nAChR $\delta$	225-P	L	F	Y	V	I	N	F	L	T	P	C	V	L	I	S	F	L	A	S	L	A	F	Y	L	P

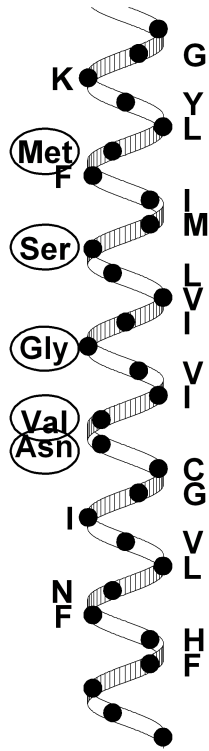
○ Labeled by [<sup>125</sup>I]TID as protein lipid interface

■ Water accessible, based on Cys modification

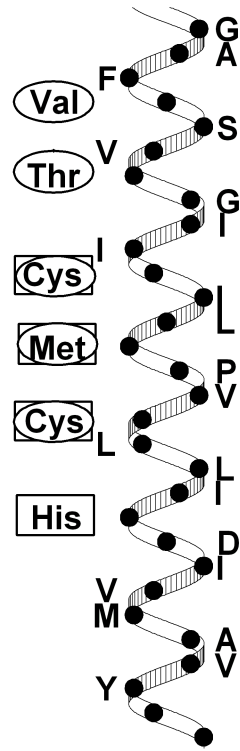
**Figure 1-4 M2 and M1 segments of the nAChR**

A. Helical model of the M2 segment showing rings known to affect channel function and QX-222 interactions

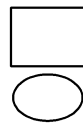
B. Sequences of M1 and M2 segments of LGICs showing residues which were modified by water soluble probes (■) as well as those residues in M1 which were labeled by [<sup>125</sup>I]TID as protein-lipid interface (○).



$\delta$ M3



$\alpha$ M4

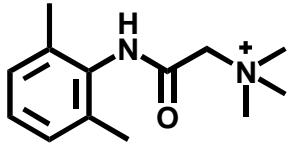


Residues labeled by  $[^3\text{H}]\text{DAF}$

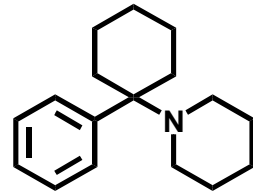
Residues labeled by  $[^{125}\text{I}]\text{TID}$

**Figure 1-5. M3 and M4 segments of the nAChR**

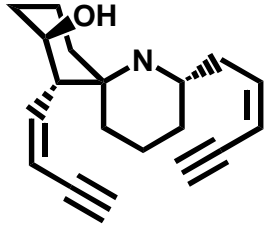
Helical model of the nAChR  $\delta$ M3 and  $\alpha$ M4 segments showing those residues labeled by [ $^{125}$ I]TID ( $\circ$ ) and [ $^3$ H]DAF ( $\square$ ).



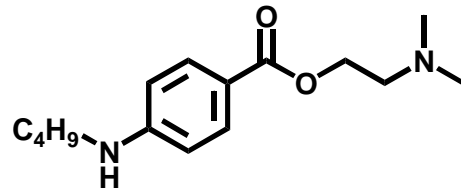
**QX-222**



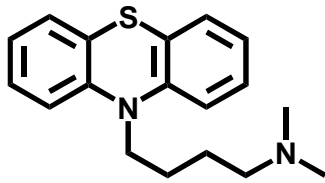
**Phencyclidine (PCP)**



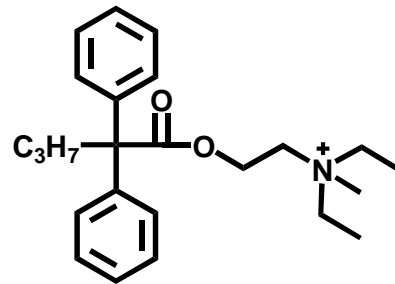
**Histronicotoxin (HTX)**



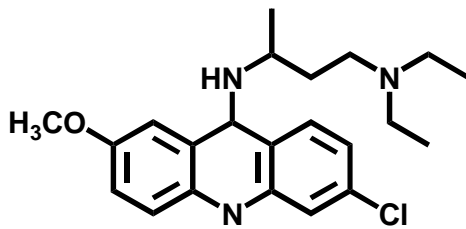
**Tetracaine**



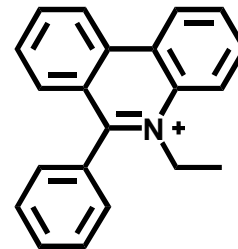
**Chlorpromazine (CPZ)**



**Meproadifen**



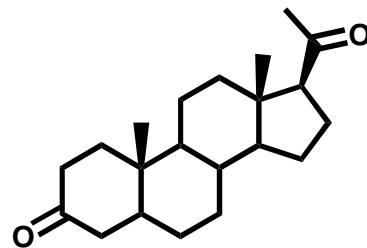
**Quinacrine**



**Ethidium**



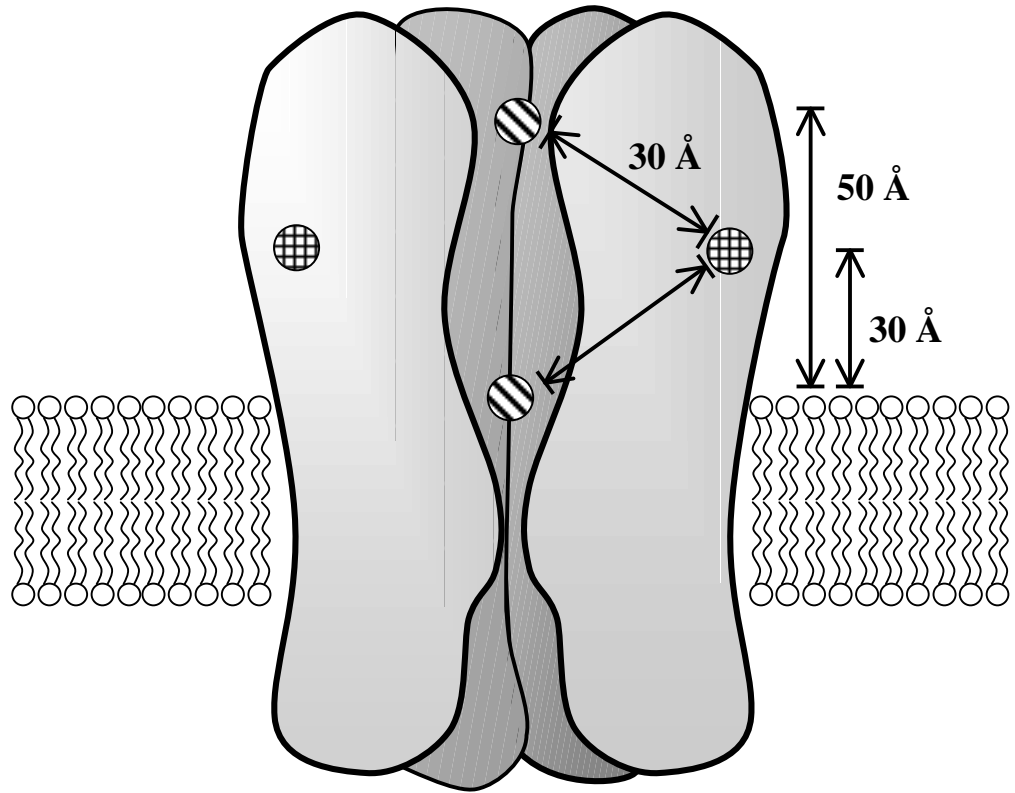
**Octanol**



**Progesterone**

**Figure 1-6. NCAs of the nAChR**

Structure of various compounds which act as NCA on the nAChR.

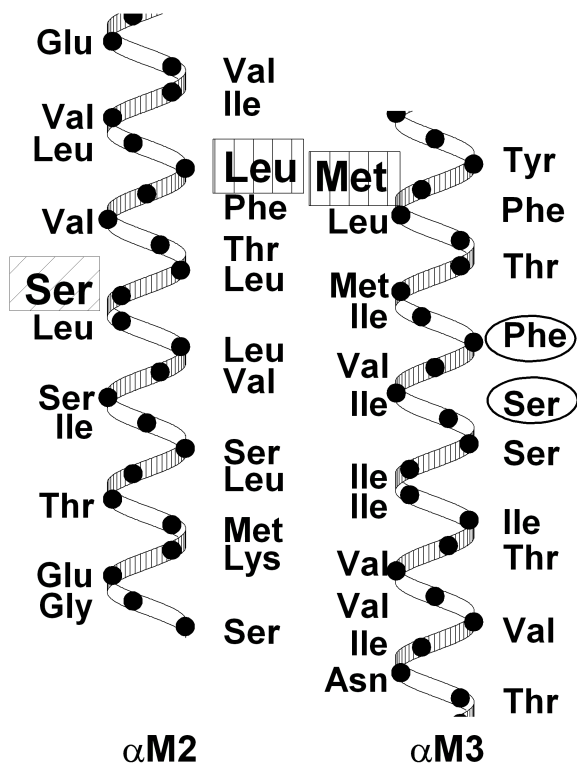


 **Agonist binding sites**

 **Ethidium binding sites**

**Figure 1-7. The binding site of ethidium localized by FRET**

The proposed distance between the agonist site and the ethidium NCA binding site is ~30 Å (Herz *et al.*, 1989), while the distance between the agonist site and the lipid is ~30 Å (Valenzuela *et al.*, 1994; Unwin, 1993). The two possible ethidium binding sites based on these measurements are indicated. Measurement of the distance between the ethidium binding site and the lipid (~50 Å) favors the binding site at the extracellular end of the channel (Johnson and Nuss, 1994).



-  Position affecting alcohol potency on nAChR inhibition
-  Position affecting alcohol modulation of GABA<sub>A</sub> and glycine receptors
-  Residues labeled by [<sup>125</sup>I]TID as lipid-protein interface

**Figure 1-8 Proposed binding sites of alcohols on the nAChR and GABA<sub>A</sub>R**

Mutations at position 10' of nAChR alter the effects of alcohols on this receptor (  ). Also shown are the nAChR M2 and M3 residues homologous to those implicated in the action of alcohols in the GABA<sub>A</sub> and glycine receptors (  ) (positioning on M3 residue similar to that of Wick *et al.* (1998). Residues in  $\alpha$ M3 that were labeled by [<sup>125</sup>I]TID as protein-lipid interface are indicated (  ).

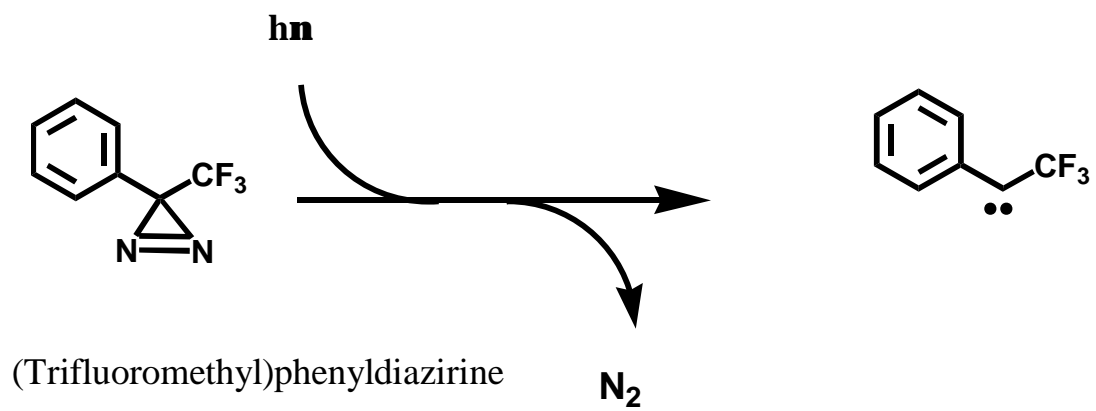
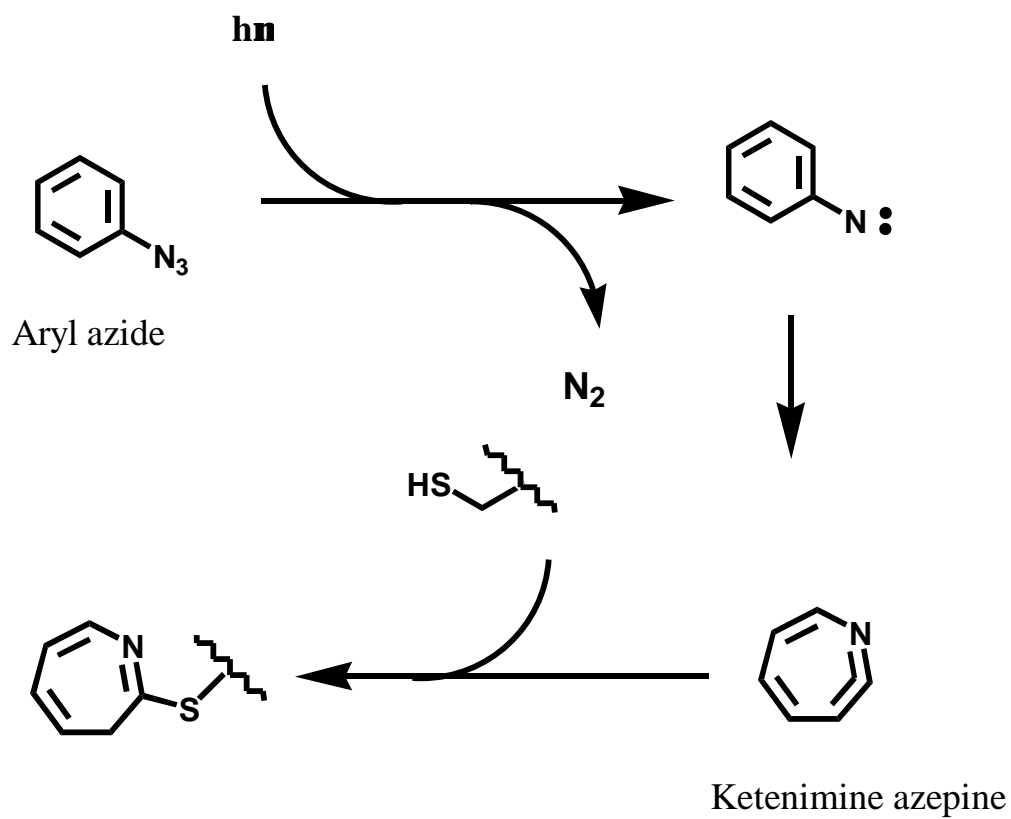
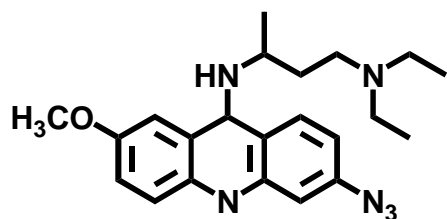


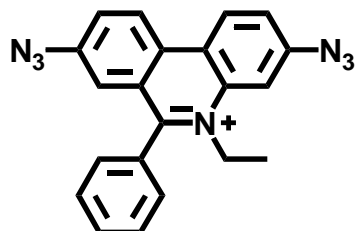
**Figure 1-9. Formation of photoreactive intermediates from aryl azides and diazirines.**

A, Formation of singlet nitrene and subsequent rearrangement to ketenimine azepine by aryl azides.

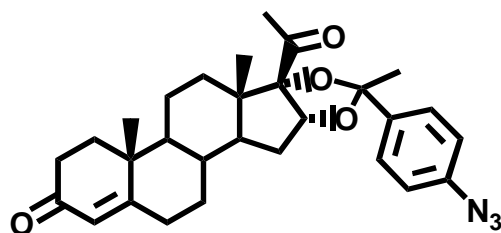
B, Formation of carbene by (trifluoromethyl)phenyldiazirine.



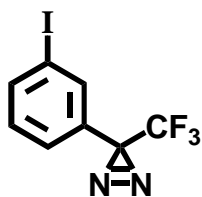
**Quinacrine Azide**



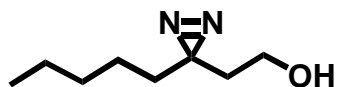
**Ethidium Diazide**



**Progestin Aryl Azide**



**TID**



**3-Aziocetanol**

**Figure 1-10. Photoaffinity probes of the nAChR**

Compounds which have previously been used as photoaffinity probes of the nAChR or which were used in this thesis.

## Chapter 2 Identification of the Sites of Incorporation of [<sup>3</sup>H]Ethidium Diazide in the nAChR

### ABSTRACT

The binding sites of ethidium, a noncompetitive antagonist of the nAChR, have been localized in the *Torpedo* nAChR in the desensitized state by use of a photoactivatable derivative, [<sup>3</sup>H]ethidium diazide. At 10 μM [<sup>3</sup>H]ethidium diazide, the incorporation into the α, β, and δ subunit was inhibited by the presence of PCP. Within the α-subunit, the incorporation was mapped to a 20 kD fragment beginning at Ser-173 and containing the first three transmembrane segments, αM1, αM2, and αM3. Further digestion of this fragment generated two fragments with PCP-inhibitable incorporation, one containing αM1 and one containing both αM2 and αM3. Within αM2, specific incorporation was present in αLeu-251 and αSer-252, residues that have been previously shown to line the lumen of the ion channel. Digestion of δ-subunit with *S. aureus* V8 protease generated a 14 kD and a 20 kD fragment, both of which began at Ile-192 and contained PCP-inhibitable labeling. The 14 kD fragment, containing δM1 and δM2, was further digested to generate a 3 kD fragment, containing δM2 alone, with PCP-inhibitable incorporation. Digestion of the 20 kD fragment, which contained δM1, δM2, and δM3, generated two fragments with incorporation, one containing the δM1 segment, and the other containing δM2 and δM3. These results establish that in the desensitized state of the nAChR, the high affinity binding site of ethidium is within the lumen of the ion channel, and that the bound drug is in contact with amino acids from both the M1 and M2 hydrophobic segments.

## RESULTS

### Equilibrium binding of [<sup>3</sup>H]ethidium to nAChR-rich membranes

To characterize the reversible interactions of ethidium with the nAChR, equilibrium binding of [<sup>3</sup>H]ethidium to *Torpedo* nAChR-rich membranes was measured in the presence of cholinergic agonists, competitive antagonists, and noncompetitive antagonists. To quantify binding in the desensitized state, [<sup>3</sup>H]ethidium binding was measured in the presence of 2 mM carbamylcholine in the presence and absence of 100 μM PCP (Figure 2-1A). The binding in the desensitized state was characterized by binding to a high affinity site ( $K_{eq} \sim 0.6 \mu\text{M}$ ) as well as a nonspecific component defined by the binding in the presence of PCP, a line with a slope of  $\sim 0.08$ . This high affinity binding was similar to literature values, measured both by the inhibition of [<sup>3</sup>H]PCP binding ( $K_{eq} \sim 0.4\text{-}0.6 \mu\text{M}$  (Herz *et al.*, 1987; Pedersen, 1995)) as well as by the fluorescence of bound ethidium ( $K_{eq} \sim 0.3\text{-}0.8 \mu\text{M}$  (Herz *et al.*, 1987; Lurtz *et al.*, 1997)). In the presence of d-tubocurarine, [<sup>3</sup>H]ethidium was bound with a similar high affinity to the same number of sites. There was no evidence of high affinity [<sup>3</sup>H]ethidium binding in the presence of  $\alpha\text{BgTx}$ , as the binding in the presence of  $\alpha\text{BgTx}$  was approximately linear with a slope of  $\sim 0.09$ , similar to the slope in the presence of carbamylcholine and PCP. Since high affinity binding of [<sup>3</sup>H]ethidium was seen when the agonist site was occupied either by agonist or competitive antagonist, [<sup>3</sup>H]ethidium must bind to a site distinct from the ACh site. The binding at this site was inhibited by the presence of PCP, indicating that this site was a noncompetitive antagonist site.

[<sup>3</sup>H]Ethidium bound with an apparent lower affinity and to a greater number of sites in the absence of carbamylcholine than in the presence of carbamylcholine (Figure 2-1B). The binding of [<sup>3</sup>H]ethidium in the absence of other drugs is expected to be

complex since [<sup>3</sup>H]ethidium was expected to bind both the two agonist sites as well as the NCA site. The reported affinity for the  $\alpha$ - $\gamma$  agonist site is  $\sim 5 \mu\text{M}$  (Pedersen, 1995), while it is  $\sim 100 \mu\text{M}$  for the  $\alpha$ - $\delta$  agonist site. Based on the binding reported above, [<sup>3</sup>H]ethidium binds with low affinity in the resting state. Since [<sup>3</sup>H]ethidium bound with high affinity in the presence of dTC, which shifts the nAChR state equilibrium toward the desensitized state even when bound to just the  $\alpha$ - $\gamma$  site, the high affinity binding of [<sup>3</sup>H]ethidium to the NCA site should occur following binding of [<sup>3</sup>H]ethidium to the  $\alpha$ - $\gamma$  site. Therefore, the binding of [<sup>3</sup>H]ethidium at the low concentrations was modeled as two-interdependent sites using Equation 2 (see Methods). This model assumed an equal number of available binding sites for the two sites but that the binding to a second site only occurs following binding to the first site. When the binding of [<sup>3</sup>H]ethidium at low concentrations was fit to the two-interdependent-sites model, the measured  $K_{eqs}$  were  $24 \pm 8 \mu\text{M}$  and  $4.2 \pm 2.3 \mu\text{M}$ . [<sup>3</sup>H]Ethidium, therefore is predicted to bind the  $\alpha$ - $\gamma$  site with a  $K_{eq1}$  of  $24 \mu\text{M}$  (compared to the reported value of  $\sim 5 \mu\text{M}$ ), which would then lead to nAChR desensitization. Once the nAChR was desensitized, [<sup>3</sup>H]ethidium would bind the NCA site with a  $K_{eq2}$  of  $5 \mu\text{M}$ . The number of binding sites for each site was  $\sim 280 \text{ nM}$ , near that predicted by the binding to the high affinity site in the presence of carbamylcholine ( $B_{max}=214 \text{ nM}$ ). When the data was fit to a single site model, the  $K_{eq}$  was  $100 \pm 92 \mu\text{M}$ , higher than expected for binding to at least the first agonist site, and the  $B_{max}$  was  $\sim 2800 \text{ nM}$ , not a realistic prediction. If  $B_{max}$  was set to  $200 \mu\text{M}$ , near that predicted by the binding in the presence of carbamylcholine, the  $K_{eq}$  was  $1.7 \pm 2.0 \text{e-}6$ . However, the curve was not well fit to the data (Figure 2-1B, dashed line). Alternatively, if the binding was expected to be a two independent sites with different affinities (Equation 3), when  $B_{max}$  was set to  $200 \mu\text{M}$ , the two  $K_{eqs}$  were not similar to those expected from literature values ( $K_{eq1}=7.8 \pm 0.2 \text{ mM}$ ,  $K_{eq2}=8.7 \pm 0.9 \text{ M}$ ), while the curve appeared to fit the data well (not

shown). Shown in Figure 2-1C are the binding curves calculated without the nonspecific binding, including the single and two-interdependent site model fits for the binding in the absence of other drugs. Although these two lines appear similar, the calculated values for  $B_{\max}$  and  $K_{\text{eq}}$  for the single site model are not physically realistic.

### **Photoincorporation of [<sup>3</sup>H]ethidium diazide into nAChR-rich membranes**

Initial photoincorporation experiments were designed to determine the general aspects of [<sup>3</sup>H]ethidium photoincorporation as well as the effects of agonists and NCAs on the incorporation. nAChR-rich membranes (2 mg/ml) were equilibrated with 10  $\mu\text{M}$  [<sup>3</sup>H]ethidium diazide in the presence and absence of 2 mM carbamylcholine or 100  $\mu\text{M}$  PCP. These experiments were carried out in the presence of 10 mM oxidized glutathione (GSSG) as a scavenger (Gallagher and Cohen, 1999). Initially, incorporation of <sup>3</sup>H was determined following SDS-PAGE by fluorography. In the presence of carbamylcholine, [<sup>3</sup>H]ethidium diazide incorporated into all subunits of the nAChR as well as into rapsyn, a 43 kD protein associated with the cytoplasmic aspect of the nAChR, and the  $\alpha$ -subunit of  $\text{Na}^+/\text{K}^+$  ATPase, a 90 kD polypeptide from a contaminating membrane fraction (Figure 2-2). The incorporation in the  $\alpha$ ,  $\beta$ , and  $\delta$  subunits was reduced in nAChR equilibrated with PCP.

The effect of oxidized glutathione (GSSG) as a scavenger was tested over a range of concentrations. In the presence of carbamylcholine, increasing GSSG concentrations reduced the incorporation in all polypeptides, both in the presence and absence of PCP (Figure 2-3). The incorporation in non-nAChR polypeptides, those running at 37 and 90 kD (corresponding to calectrin and the  $\alpha$ -subunit of  $\text{Na}^+/\text{K}^+$  ATPase, respectively), was similar in the two conditions at all concentrations of GSSG. The absolute amount of PCP-inhibitable labeling in the  $\alpha$ ,  $\beta$ , and  $\delta$  subunits was constant across the range of

GSSG conditions tested, indicating that GSSG reduced the nonspecific, but not the specific, incorporation into the polypeptides.

In further experiments in the presence of 10 mM GSSG, the effects of carbamylcholine and PCP as well as several other drugs were studied by quantification of  $^3\text{H}$  from bands excised from a gel (Figure 2-4). Bands containing the nAChR subunits, as well as non-nAChR polypeptides were excised. The presence of cholinergic agonists and antagonists did not affect the incorporation into two bands containing non-nAChR polypeptides, a band at 43 kD, containing the protein rapsyn, as well as one at 58 kD, which contained syntrophin, a protein of the dystrophin complex (Carr *et al.*, 1989). For membranes equilibrated with carbamylcholine, the incorporation of [ $^3\text{H}$ ]ethidium diazide in the  $\alpha$  and  $\delta$  subunits was reduced by 40% by the presence of PCP, while in the  $\beta$ -subunit, the incorporation was reduced 20%. As was seen for [ $^3\text{H}$ ]ethidium binding to *Torpedo* nAChR membranes, nAChR subunit labeling by [ $^3\text{H}$ ]ethidium diazide in the presence of  $\alpha\text{BgTx}$  was similar to that in the presence of carbamylcholine and PCP in all subunits. The incorporation in the presence of dTC was similar to that seen with carbamylcholine, consistent with the binding affinity of [ $^3\text{H}$ ]ethidium in the presence of these drugs. For the nAChR  $\beta$  and  $\delta$  subunits, the incorporation in the absence of other drugs was less than that in the presence of carbamylcholine, while the incorporation in  $\alpha$  was similar in both conditions. Based upon the total pmols of nAChR loaded in each gel lane and the observed  $^3\text{H}$  in the subunit gel slice, the total  $^3\text{H}$  incorporation in  $\alpha$  and  $\delta$  in the presence of carbamylcholine was approximately 0.04 mol [ $^3\text{H}$ ]ethidium diazide/mol subunit, while the incorporation in the presence of both carbamylcholine and PCP was approximately 0.02 mol/mol.

### **Mapping the [<sup>3</sup>H]ethidium diazide incorporation in nAChR $\alpha$ -subunit with *S. aureus* V8 protease**

To further characterize the site of incorporation, the  $\alpha$ -subunit was subjected to proteolysis with *S. aureus* V8 protease in a mapping gel (Figure 2-5). V8 protease cleavage in the gel generates 4 large fragments,  $\alpha$ V8-20,  $\alpha$ V8-18,  $\alpha$ V8-10, and  $\alpha$ V8-4, named according to their apparent molecular weights (Pedersen *et al.*, 1986).  $\alpha$ V8-20 (Ser-173–Glu-338) contains the  $\alpha$ M1,  $\alpha$ M2 and  $\alpha$ M3 transmembrane segments, as well as a portion of the N-terminal extracellular segment. The  $\alpha$ M4 transmembrane segment is within  $\alpha$ V8-10 (Asn-339– $\alpha$ Gly-437).  $\alpha$ V8-18 (Val-46–Glu-172) contains a glycosylation sensitive to EndoglycosidaseH, and when membranes are treated with EndoglycosidaseH, the deglycosylated fragment now runs at ~12 kD ( $\alpha$ V8-12). The autoradiogram shows that the major site of incorporation was in the  $\alpha$ V8-20 fragment, and that incorporation was inhibited by PCP. Based on counting excised gel fragments, ~75% of the <sup>3</sup>H incorporated into the  $\alpha$ -subunit labeled in the absence of PCP was in  $\alpha$ V8-20, and that incorporation was reduced by ~60% in fragments from nAChR equilibrated with PCP.

### **Localization of [<sup>3</sup>H]ethidium diazide incorporation into the $\alpha$ -subunit**

To further characterize the incorporation in the  $\alpha$ -subunit, 10 mg of nAChR membranes were labeled in the presence of 10 mM GSSG and 2 mM carbamylcholine and the absence (denoted as +/-) or presence (+/+) of PCP. These membranes were also labeled with 1-azidopyrene (1-AP) (Blanton and Cohen, 1994) for ease of identifying subunits and fragments following SDS-PAGE, as described in Methods. Following separation of subunits by SDS-PAGE, the  $\alpha$ -subunit was transferred to the well of a

mapping gel for digestion with V8 protease. Proteolytic fragments were identified after electrophoresis by illumination at 365 nm to detect 1-AP incorporation.  $\alpha$ V8-20 was identified by fluorescence and mobility, excised, eluted, and concentrated.

In order to localize the incorporation of [ $^3$ H]ethidium diazide in  $\alpha$ V8-20,  $\alpha$ V8-20 was further digested with EndoLysC, which is known to generate a ~10 kD fragment which begins at  $\alpha$ Met-243, the N-terminus of the  $\alpha$ M2 segment, and presumed to continue through  $\alpha$ M3 (Pedersen *et al.*, 1992). There are only three other lysines in  $\alpha$ V8-20, two lysines near the beginning of  $\alpha$ V8-20 ( $\alpha$ Lys-185 and  $\alpha$ Lys-179) and one prior to  $\alpha$ M3 ( $\alpha$ Lys-276). No cleavage has been reported at  $\alpha$ Lys-276 (Pedersen *et al.*, 1992; Gallagher and Cohen, 1999), and Figure 2-6A shows the expected cleavage products. When the digest was fractionated by HPLC, two hydrophobic peaks, one centered at fraction 29 (~69% organic) and one at fraction 34 (~93% organic), were present (Figure 2-6B). Additional  $^3$ H was not retained on the column, accounting for ~20% of the total  $^3$ H eluted from the column. Since similar levels of  $^3$ H were present in the flow-through when intact  $\alpha$ V8-20 was purified by HPLC (Figure 2-6B, inset), this  $^3$ H was not associated with a hydrophilic digestion fragment, but rather resulted from covalent adducts which were unstable to HPLC conditions or  $^3$ H noncovalently associated with  $\alpha$ V8-20.

Sequence analysis of fraction 34 of the EndoLysC digest of  $\alpha$ V8-20 labeled both in the absence and presence of PCP showed a single sequence beginning at  $\alpha$ Met-243 (+/- :  $I_0=109$  pmol; +/+ :  $I_0=159$  pmol) (Figure 2-7A). No other sequences were detected with more than 5% of the mass of that sequence. Based on the loaded  $^3$ H and the mass present, ~40 cpm were incorporated per pmol fragment labeled with [ $^3$ H]ethidium diazide in the absence of PCP. This incorporation was reduced by ~50% for samples labeled in the presence of PCP. While only low levels of  $^3$ H release were seen, the fragment labeled

in the absence of PCP showed  $^3\text{H}$  release reproducibly in cycles 9 and 10, corresponding to  $\alpha\text{Leu-251}$  and  $\alpha\text{Ser-252}$ . Additionally, release in cycle 15 was seen, though not reproducibly (compare upper and lower panels of Figure 2-7A). [ $^3\text{H}$ ]Ethidium diazide incorporated into  $\alpha\text{Leu-251}$  at 0.5 cpm/pmol ( $\sim 0.0009$  mol [ $^3\text{H}$ ]ethidium diazide/mol  $\alpha\text{Leu-251}$ ).  $^3\text{H}$  was also released in the first cycles, accounting for  $\sim 2\%$  of the loaded  $^3\text{H}$ ; this release was likely due either to the removal of peptide poorly absorbed onto the glass filter or instability of the covalent adduct to sequencing conditions and was similar to that seen during sequence analysis of fragments photolabeled by a different probe (Blanton *et al.*, 1999).

Sequence analysis of fraction 29 (Figure 2-7B) revealed the presence of two  $\alpha$ -subunit fragments, one beginning at  $\alpha\text{His-186}$  (+/-:  $I_0=128$  pmol; +/+ :  $I_0=208$  pmol), and a secondary sequence beginning at  $\alpha\text{Asp-180}$  (+/-:  $I_0=18$  pmol; +/+ :  $I_0=39$  pmol). Both of these fragments must have contained the  $\alpha\text{M1}$  segment since there is no other lysine between  $\alpha\text{His-186}$  and  $\alpha\text{Lys-242}$ , prior to  $\alpha\text{M2}$ . No additional sequences with more than 5% of the mass of the primary sequence were seen. Based on the  $^3\text{H}$  loaded and the mass levels of the two fragments,  $\sim 40$  cpm of  $^3\text{H}$ /pmol was incorporated into the fragments in the absence of PCP. This incorporation was reduced by  $\sim 60\%$  by the presence of PCP during photolysis. Sequence analysis of this fraction from both labeling conditions showed no release of  $^3\text{H}$  after 25 cycles of Edman degradation, except for the progressively declining release in the first three cycles. The region sequenced contained part of the ACh site ( $\alpha 190\text{-}200$ ) but ends prior to M1. The lack of release could either be due to instability of the covalent adduct or labeling at a residue further than 25 amino acids from the N-terminus. For example, if the incorporation were in the  $\alpha\text{M1}$  segment, which begins at  $\alpha 211$ , 25 residues from the N-terminus of this fragment, no release would have been seen.

### Localization of [<sup>3</sup>H]ethidium diazide incorporation into the $\delta$ -subunit

In gel digestion of nAChR  $\delta$ -subunit with V8 protease is known to create two fragments with N-termini of  $\delta$ Ile-192. One fragment, of approximately 20 kD ( $\delta$ V8-20), contains the  $\delta$ M1,  $\delta$ M2, and  $\delta$ M3 segments (Blanton and Cohen, 1994). The second fragment, of ~14 kD ( $\delta$ V8-14), ends at  $\delta$ Glu-262 (Blanton *et al.*, 1994) and, therefore, contains the  $\delta$ M1 and  $\delta$ M2 segments, but not  $\delta$ M3. When the sites of [<sup>3</sup>H]ethidium diazide incorporation in the  $\delta$ -subunit were mapped on an analytical scale by in gel digestion with V8 protease, PCP inhibitable labeling was seen in bands centered at ~ 20 kD and ~12 kD (Figure 2-8A).

To identify the sites of incorporation of [<sup>3</sup>H]ethidium diazide in the nAChR  $\delta$ -subunit, 10 mg of nAChR-rich membranes were photolabeled with [<sup>3</sup>H]ethidium diazide in the absence or presence of PCP followed by labeling with 1-AP. The subunits were separated by SDS-PAGE, and the  $\delta$ -subunit was excised and digested with *S. aureus* V8 protease in a mapping gel. After digestion of  $\delta$ -subunit by V8 protease in the mapping gel, the mobility of digestion products was identified by 1-AP fluorescence. Two fluorescent bands, with estimated mobility near 14 kD ( $\delta$ V8-14) and 20 kD ( $\delta$ V8-20) were excised, eluted, and resuspended, as were other fluorescent bands and non-fluorescent regions of the gel. The two noted fluorescent bands contained ~20% and ~30% of the total eluted <sup>3</sup>H, respectively, as well as the greatest PCP-inhibitable incorporation. Aliquots from these two bands were run on a mapping gel without V8 protease to clearly determine the molecular weight (Figure 2-8B). While all lanes contained similar <sup>3</sup>H in the dye front, the specifically labeled material from the  $\delta$ V8-14 band ran near 14 kD and that from the  $\delta$ V8-20 band ran near 20 kD. The material in these two bands was used in subsequent digestions.

Digestion of nAChR  $\delta$ -subunit with EndoLysC generates a 10 kD fragment beginning at  $\delta$ Met-257, the N-terminus of M2, and containing the M3 segment, with no cleavage observed after  $\delta$ Lys-290, at the N-terminus of M3 (Gallagher and Cohen, 1999). We used EndoLysC digestion of  $\delta$ V8-14 and  $\delta$ V8-20 to map the site(s) of [ $^3$ H]ethidium diazide incorporation into the  $\delta$ -subunit. Within  $\delta$ V8-14 there are two sites of possible EndoLysC cleavage,  $\delta$ Lys-205 and  $\delta$ Lys-256. An additional lysine, at  $\delta$ Lys-224, precedes a proline, so no cleavage is expected at this site. Therefore, three fragments can be generated by EndoLysC digestion of  $\delta$ V8-14 (Figure 2-9A), one beginning at  $\delta$ Ile-192, with a mobility of  $\sim$ 1.5 kD; one beginning at  $\delta$ Phe-206, containing a glycosylation site, with a mobility of  $\sim$ 10 kD; and one beginning at  $\delta$ Met-257 and continuing through  $\delta$ Glu-280, with a mobility of  $\sim$ 3 kD. Sequence analysis of aliquots of the digest of  $\delta$ V8-14 labeled with [ $^3$ H]ethidium diazide revealed the presence of two fragments, one beginning at  $\delta$ Met-257 (+/-:  $I_0=3$  pmol; +/+ :  $I_0=14$  pmol) and one beginning at  $\delta$ Phe-206 (+/-:  $I_0=15$  pmol; +/+ :  $I_0=9$  pmol). Additionally, a fragment beginning at  $\delta$ Ile-192 was expected but was not visible, possibly from loss during sequencing due to the small size of the fragment. The total digest, as well as undigested  $\delta$ V8-14, was separated by a Tricine SDS-PAGE gel. As shown in Figure 2-9B, for the digest of  $\delta$ V8-14 labeled in the absence of PCP, the primary peak of  $^3$ H was present in a band at  $\sim$ 3 kD, and this band contained PCP-inhibitable incorporation. The presence of PCP-inhibitable incorporation in the  $\sim$ 3 kD band indicated that [ $^3$ H]ethidium diazide photoincorporated into the  $\delta$ M2 segment in a PCP-dependent manner. In addition, the broad band of  $^3$ H between 10 kD and 14 kD, also containing PCP-inhibitable incorporation, is shifted relative to undigested  $\delta$ V8-14 (lower panel) consistent with the presence of the  $\sim$ 10 kD fragment beginning at  $\delta$ Phe-206 and ending prior to  $\delta$ M2, as well as possible partially digested products.

Digestion of  $\delta$ V8-20 with EndoLysC is expected to generate 3 fragments, with N-termini similar to those generated by digestion of  $\delta$ V8-14 with EndoLysC. Cleavage of the lysine at position  $\delta$ Lys-290, between the  $\delta$ M2 and  $\delta$ M3 segments, has not been reported. Therefore, the fragments generated should be similar to those created by EndoLysC digestion of  $\delta$ V8-14, with the fragment beginning at  $\delta$ Met-257 containing both the  $\delta$ M2 and  $\delta$ M3 segments (Figure 2-10A). The  $\delta$ V8-20 fragment labeled with [ $^3$ H]ethidium diazide was digested with EndoLysC and fractionated by HPLC. PCP-inhibitable incorporation was present in hydrophobic fractions centered at fraction 27 (62% organic) and fraction 31 (78% organic) as well as in the flow through. Since  $^3$ H was also present in the flow through when intact  $\delta$ V8-20 was repurified by HPLC (Figure 2-10, inset), as seen with  $\alpha$ V8-20, that  $^3$ H probably corresponded to incorporation unstable to the acidic HPLC conditions, and accounted for ~20% of the eluted  $^3$ H.

Sequencing of fraction 31 from the HPLC of both the sample labeled in the absence of PCP as well as that labeled in the presence of PCP showed the presence of two sequences, one beginning at  $\delta$ Met-257 (+/-:  $I_0=19$  pmol; +/+ :  $I_0=6$  pmol) as well as one beginning at  $\delta$ Phe-206 (+/-:  $I_0=27$  pmol; +/+ :  $I_0=15$  pmol) (Figure 2-11). No  $^3$ H release was detected in 25 cycles of Edman degradation, other than the release in the first cycles, accounting for ~3% of the loaded  $^3$ H.

Sequence analysis of fraction 27 of the HPLC of EndoLysC-digested  $\delta$ V8-20 labeled with [ $^3$ H]ethidium diazide in the absence of PCP showed a primary sequence beginning at  $\delta$ Phe-206 ( $I_0=53$  pmol) with a minor sequence beginning at  $\delta$ Met-257 ( $I_0=4$  pmol), present at less than 10% the mass level of the sequence beginning at  $\delta$ Phe-206. As with fraction 31, no release of  $^3$ H above background was seen during 25 cycles of sequence analysis (not shown). Since undigested  $\delta$ V8-20 eluted in fraction 31, the sequence beginning at  $\delta$ Phe-206 in fraction 31 of the HPLC of EndoLysC-digested  $\delta$ V8-

20 should contain the M1, M2, and M3 segments. The sequence beginning at  $\delta$ Phe-206 in fraction 27, however, must have been cleaved at the Lys-256, prior to M2. While the  $^3\text{H}$  release profile provided no information about the site of [ $^3\text{H}$ ]ethidium diazide incorporation in the labeled fragments, the presence of PCP-inhibitable incorporation in this HPLC peak indicated that specific incorporation was present within the fragment beginning at  $\delta$ Phe-206, containing M1 without M2.

## DISCUSSION

The data presented in this chapter localized the specific photoincorporation of [ $^3\text{H}$ ]ethidium diazide in the nAChR  $\alpha$  and  $\delta$  subunit to both the M2 segment and a fragment containing M1. Previous studies of the incorporation of aromatic amine NCAs into the *Torpedo* nAChR in the desensitized state have shown incorporation into only the M2 segment (Giraudat *et al.*, 1986; Giraudat *et al.*, 1987; Revah *et al.*, 1990; Hucho *et al.*, 1986). Additionally, the results reported here have established that, within the  $\alpha$ -subunit,  $\alpha$ Leu-252 ( $\alpha$ Leu-9') and  $\alpha$ Ser-253 ( $\alpha$ Ser-10'), specifically, were labeled by the [ $^3\text{H}$ ]ethidium diazide. These residues line the lumen of the ion channel (Akabas *et al.*, 1994), demonstrating that the high affinity binding site of ethidium is within the nAChR ion channel.

The pharmacology of the photoincorporation of [ $^3\text{H}$ ]ethidium diazide well reflects the pharmacology of binding, and was similar to that reported by Witzemann and Raftery (1978). Their data also indicated that, in the desensitized state, the photoincorporation in the  $\alpha$  and  $\delta$  subunits was inhibited by the presence of an aromatic amine noncompetitive antagonist. The dependence of subunit photoincorporation on cholinergic ligands reported here, however, was in apparent contrast to that reported by Pedersen (1995) using fluorescence to detect levels of incorporation in subunits after SDS-PAGE. In that

report, the incorporation of ethidium diazide in  $\alpha$  and  $\gamma$  subunits was reduced by ~80% by the presence of carbamylcholine, while the addition of PCP produced little or no further change. A likely explanation for that result is that, surprisingly, in subunits resolved by SDS-PAGE the covalent adduct formed within the ACh binding site remains fluorescent, while the adduct formed in the channel in the  $\alpha$  and  $\delta$  subunits is nonfluorescent.

To localize the incorporation in the nAChR to specific fragments of the protein, the  $\alpha$  and  $\delta$  subunits were digested first with V8 protease to generate a fragment containing the first three transmembrane segments, and that fragment was then isolated and digested with EndoLysC. In both subunits, two fragments were generated that contained PCP-inhibitable incorporation, one spanning a portion of the extracellular domain through the M1 segment, the other containing the M2 and M3 domains. In the  $\alpha$ -subunit, sequence analysis of the fragment containing M2 and M3 established PCP-inhibitable incorporation of [ $^3\text{H}$ ]ethidium diazide in  $\alpha\text{Leu-252}$  ( $\alpha\text{Leu-9}'$ ) and  $\alpha\text{Ser-253}$  ( $\alpha\text{Ser-10}'$ ). Thus, in the desensitized nAChR, the high affinity binding site of ethidium is contained at least in part within the M2 ion channel domain.

Since the site of [ $^3\text{H}$ ]ethidium diazide incorporation in the  $\delta$  fragment containing  $\delta\text{M2}$  and  $\delta\text{M3}$  was not evident by sequence analysis, the presence of incorporation into the  $\delta\text{M2}$  fragment was determined by alternative means. The  $\delta\text{V8-14}$  fragment, spanning from  $\delta\text{Ile-192}$  to  $\delta\text{Glu-280}$ , contained a portion of the extracellular segment as well as the  $\delta\text{M1}$  and  $\delta\text{M2}$  segments, but not the  $\delta\text{M3}$  segment. Digestion of this fragment by EndoLysC was expected to generate a 3 kD fragment consisting solely of the  $\delta\text{M2}$  segment. Separation of the digestion products on an SDS-PAGE gel resulted in a 3 kD band with associated  $^3\text{H}$ . Therefore, the M2 segment of  $\delta$ -subunit was labeled with [ $^3\text{H}$ ]ethidium diazide in a PCP-dependent manner. Unfortunately, the specific residues in  $\delta\text{M2}$  labeled with [ $^3\text{H}$ ]ethidium diazide could not be determined by sequence analysis.

Although many other NCAs which have incorporated into the M2 segments label homologous positions in several subunits (White and Cohen, 1992; Giraudat *et al.*, 1986; Giraudat *et al.*, 1987; Revah *et al.*, 1990; Hucho *et al.*, 1986; Gallagher and Cohen, 1999), sequence analysis failed to provide any evidence of reaction of [<sup>3</sup>H]ethidium diazide with either δLeu-266 or δSer-267, the homologs to the positions labeled by [<sup>3</sup>H]ethidium diazide in α. However, due to the low mass levels of the δ-subunit fragment observed during sequencing (19 pmol in fraction 31) (Figure 2-11), incorporation at δLeu-266 at similar levels to αLeu-252 would only have resulted in 6 cpm of release, well below the detection limits of this method.

αLeu-252 and αSer-253 are not necessarily the primary or only sites of labeling in αM2. Approximately 20% of the <sup>3</sup>H incorporated into αV8-20 was not stably incorporated under the acidic HPLC conditions. Additionally, some of the <sup>3</sup>H incorporation was labile to the acid treatment during sequence analysis, as seen by the <sup>3</sup>H release detected in the first cycles of sequence analysis. Acid sensitivity was clearly demonstrated when samples were pretreated with TFA for 4 minutes, followed by a wash with ethyl acetate for 5 minutes to remove excess SDS from the filter prior to sequence analysis. During this treatment, between 10-50% of the <sup>3</sup>H loaded with a fragment labeled with [<sup>3</sup>H]ethidium diazide was released (this prewash was not used in any of the sequences reported here). While as much as 0.15 mol [<sup>3</sup>H]ethidium diazide was incorporated/mol of sequence beginning at αMet-243, based on loaded <sup>3</sup>H and the mass present, αLeu-252 was only labeled at ~0.0008 mol [<sup>3</sup>H]ethidium diazide/mol residue. Therefore the discrepancy between the <sup>3</sup>H incorporated in the fragment and that detected in αLeu-252 was due to either greater incorporation originally at αLeu-252 and αSer-253 or at another site, but this incorporation was labile to the conditions of sequence analysis. This discrepancy is even more evident with the δ-subunit. Although clear evidence of

incorporation of [<sup>3</sup>H]ethidium diazide within the  $\delta$ M2 segment was shown, no <sup>3</sup>H release was seen in any cycles of sequence analysis through this segment. The adducts formed between the [<sup>3</sup>H]ethidium diazide and the  $\delta$ M2 residues, therefore, must have been labile to the HPLC and sequencing conditions.

This difficulty in localization of the incorporation in the subunits resulted from the sensitivity of the incorporation to the HPLC and sequencing conditions. This sensitivity could be due to the formation of acid-labile adducts upon photolysis. The photoactivatable group used in these experiments, the aryl azide, can undergo an intermolecular rearrangement after photolysis to a ketenimine azepine (Bayley, 1983). The adducts formed with the azepine are predicted to be sensitive to acid and may account for the loss of <sup>3</sup>H during HPLC and sequencing.

Another problem with the rearrangement product of the aryl azide is that it is more stable than the initial nitrene. This compound is expected to react preferentially with nucleophiles, such as cysteine. This selective reactivity may pose a problem when the binding site contains no cysteines, as was the case for the M2 segments. However, [<sup>3</sup>H]ethidium diazide successfully photoincorporated into the M2 segments of  $\alpha$  and  $\delta$ , and, particularly, into  $\alpha$ Leu-252 and  $\alpha$ Ser-253.

The binding of ethidium within the M2 channel domain is inconsistent with the site of ethidium binding predicted for the *Torpedo* nAChR from the results of fluorescence resonance energy transfer (FRET). The results of FRET have been interpreted to indicate that, within the desensitized state, the high affinity ethidium binding site is  $\sim 50$  Å from the lipid head groups, within the extracellular domain, well above the transmembrane domain of the nAChR. The discrepancy is likely to reflect the complexity of distance determination by FRET. In order to calculate distances using FRET, either the donor or acceptor molecules must be able to rotate freely (Clegg, 1995).

However, ethidium, when bound to the noncompetitive antagonist site, is likely to be highly constrained, as evidenced by the enhanced fluorescence lifetime of bound ethidium as well as the polarization values, showing a lack of rotational mobility (Herz *et al.*, 1987). Additionally, the lipid environment near the channel has restricted mobility (Marsh and Barrantes, 1978; Marsh *et al.*, 1981) and shows selectivity for the nature of the lipid in the inner annulus (Ellena *et al.*, 1983). Thus it is likely that the lipid probe used in the distance determination is unable to rotate freely or that it may not be localized to the inner annulus of lipids surrounding the nAChR.

Although originally proposed to bind far from the other aromatic amine NCAs, [<sup>3</sup>H]ethidium diazide incorporated into both the M1 and M2 segments, near the other aromatic amine NCAs. In the desensitized state, other aromatic amine NCA, such as [<sup>3</sup>H]CPZ and [<sup>3</sup>H]TPP, labeled residues at the 6' ring (Giraudat *et al.*, 1986; Hucho *et al.*, 1986), while [<sup>3</sup>H]meproadifen mustard incorporated into 20' (Pedersen and Cohen, 1990). [<sup>3</sup>H]Quinacrine azide, on the other hand, labeled the M1 segment in the open state (DiPaola *et al.*, 1990). The structural relation between the M1 and M2 segments is not currently known, but the proximity of these segments to the ethidium binding site indicates that both contribute to the channel pore.

Can the sites of incorporation in the  $\alpha$ M2 segment tell us anything about the possible sites of incorporation into the M1 segment? The photoreactive probe used in this study, [<sup>3</sup>H]ethidium diazide, has two reactive groups,  $\sim 9$  Å apart (Figure 2-12). If [<sup>3</sup>H]ethidium diazide labeled M1 and M2 from a single binding site, then the site of labeling in M1 should be  $\sim 9$  Å from the sites in M2,  $\alpha$ Leu-252 and  $\alpha$ Ser-253.  $\alpha$ Leu-252 and  $\alpha$ Ser-253 are predicted to be near the center of the bilayer, facing the channel pore. The diameter of an  $\alpha$ -helix is 5 Å, and the distance between two residues on the same face of a helix is  $\sim 5$  Å. Therefore, it is unlikely that [<sup>3</sup>H]ethidium diazide

photoincorporated into the residues implicated in the binding of quinacrine, residues at the most extracellular region of the M1 segment. However, if the M1 segment is  $\alpha$  helical, it is possible that the site of incorporation is approximately mid-way down the length of the segment, possibly at  $\alpha$ Val-218, which has been shown to contribute to channel formation by modification of this position by a water-soluble probe (Akabas and Karlin, 1995). Knowledge of the sites of incorporation of [ $^3$ H]ethidium diazide into the M1 segments will clarify the contribution of the M1 segments to the nAChR ion channel.

## INTRODUCTION

The aromatic amines are the most studied structural class of the diverse group of compounds that act as noncompetitive antagonists (NCAs) on the nAChR. Affinity labeling and electrophysiology experiments show that many of these drugs bind in the ion pore, which is lined by the  $\alpha$ -helical M2 segments from each subunit. In the desensitized state, chlorpromazine (CPZ) and triphenylphosphonium (TPP) label amino acids at position 6' (based on numbering the residues of the M2 segment from a conserved lysine at the intracellular end of the helix) in all of the subunits, and mutagenesis of these positions in both *Torpedo* and mouse nAChR has also shown that these residues affect the block by QX-222 (Giraudat *et al.*, 1986; Giraudat *et al.*, 1987; Revah *et al.*, 1990; Hucho *et al.*, 1986; Charnet *et al.*, 1990; Leonard *et al.*, 1988). In the desensitized state, [<sup>3</sup>H]meproadifen mustard incorporates into the most extracellular end of  $\alpha$ M2, position 20' (Pedersen and Cohen, 1990). In the open state, [<sup>3</sup>H]quinacrine azide labels the extracellular end of  $\alpha$ M1 (DiPaola *et al.*, 1990; Karlin, 1991), and mutational studies have also shown that substitutions in this region affect the potency of quinacrine as a NCA (Tamamizu *et al.*, 1995). All of the residues that have been labeled by these NCAs are accessible to water soluble modification agents, consistent with these residues forming a portion of the channel (Akabas and Karlin, 1995). Additionally, all of these compounds bind competitively with [<sup>3</sup>H]phencyclidine (PCP) or [<sup>3</sup>H]histrionicotoxin (HTX), two other aromatic amine NCAs, consistent with a common site of action.

Although known primarily for its ability to intercalate into DNA, the fluorescent compound ethidium is another aromatic amine NCA of the nAChR, which binds competitively with PCP and HTX. The affinity of ethidium for the nAChR in the desensitized state has been determined, with a  $K_I$  of 0.4-0.6  $\mu$ M based on inhibition of [<sup>3</sup>H]PCP binding (Herz *et al.*, 1987; Pedersen, 1995), or a  $K_I$  of 0.3-0.8  $\mu$ M based on

inhibition by PCP of the fluorescence of bound ethidium (Herz *et al.*, 1987; Herz *et al.*, 1989; Lurtz *et al.*, 1997). In contrast to the high affinity binding to the nAChR in the desensitized state, in the presence of  $\alpha$ -bungarotoxin ( $\alpha$ BgTx), ethidium inhibits [ $^3$ H]PCP binding with a  $K_i$  of 1 mM (Herz *et al.*, 1987). Ethidium also binds the agonist site, with an affinity for the  $\alpha$ - $\gamma$  site of  $\sim 5 \mu\text{M}$  and for the  $\alpha$ - $\delta$  site of  $\sim 100 \mu\text{M}$  (Pedersen, 1995).

The fluorescence of ethidium has made it an attractive probe in fluorescence quench and fluorescence resonance energy transfer (FRET) studies of the dimensions of the *Torpedo* nAChR. Initial reports, such as the measured distance between the agonist site and the ethidium NCA site, were consistent with the binding site of ethidium in the channel (Herz *et al.*, 1989). However, subsequent work using a fluorescent membrane probe, C<sub>12</sub>-Texas Red, to measure the distance between the membrane surface and the HTX-sensitive ethidium binding site placed ethidium  $\sim 50 \text{ \AA}$  from the lipid head groups. This result suggests that the high affinity ethidium binding site in the *Torpedo* nAChR in the desensitized state is near the most extracellular portion of the nAChR (Johnson and Nuss, 1994).

Another experimental approach to localizing the binding site of ethidium, using photoaffinity probes, has also been attempted. Early work by Witzemann and Raferty (1978) showed that photoincorporation of [ $^3$ H]ethidium diazide, a photoactivatable derivative of ethidium, into the  $\alpha$  and  $\delta$  subunits of the *Torpedo* nAChR in the desensitized state was inhibitable by HTX. Later, Pedersen (1995) assayed the incorporation of nonradioactive ethidium diazide, as well as two ethidium monoazides, into nAChR by the fluorescence of subunits in the SDS-PAGE gel. In the absence of agonist, the most prominent incorporation into the nAChR was in the  $\alpha$  and  $\gamma$  subunits. This incorporation was reduced by  $\sim 80\%$  by the presence of carbamylcholine, but the addition of NCAs in the presence of carbamylcholine decreased the photoincorporation

little, if at all. The lack of NCA inhibitable labeling is unexpected since the ethidium analogs competitively inhibit the binding of [<sup>3</sup>H]PCP similarly to ethidium. Therefore, the derivatives either can not photoincorporate into the NCA site or, once incorporated, their fluorescence is not detectable. Based on the work by Witzemann and Raferty (1978), it is most likely that the ethidium azides incorporate into the NCA, but the adducts are no longer fluorescent.

Here we utilize [<sup>3</sup>H]ethidium diazide to localize the NCA binding site of ethidium. The photoincorporation of [<sup>3</sup>H]ethidium diazide into the subunits of the *Torpedo* nAChR reflected the general pharmacology of [<sup>3</sup>H]ethidium binding. For nAChR equilibrated with carbamylcholine, in the desensitized state, the addition of PCP reduced the incorporation into the  $\alpha$  and  $\delta$  subunits. [<sup>3</sup>H]Ethidium diazide photoincorporated into the M2 segments of the  $\alpha$  and  $\delta$  subunits, as well as into fragments containing the M1 segment of the  $\alpha$  and  $\delta$  subunits, indicating a binding site in the channel pore. These results lead us to conclude that the high affinity ethidium binding site in the nAChR in the desensitized state is within the channel domain of the nAChR and not in the extracellular domain.

## **MATERIALS AND METHODS**

### **Materials**

nAChR-enriched membranes were isolated from *Torpedo californica* electric organ according to the method described by Sobel *et al.* (1977), modified as described by Pedersen *et al.* (1992). The final membrane suspensions were stored in 38% sucrose at -80 °C under argon. The membranes used here contained 0.5-2.0 nmol acetylcholine binding sites per milligram of protein. [<sup>3</sup>H]Ethidium (specific activity: 1.15 Ci/mmol) and [<sup>3</sup>H]ethidium diazide (specific activity: 0.61 Ci/mmol) were a kind gift from Dr.

Steen Pedersen, synthesized according to the methods described in Pedersen (1995) and Lurtz *et al.* (1997). Azidopyrene (1-AP) was from Molecular Probes. Oxidized glutathione, carbamylcholine, nonradioactive ethidium, and Tricine were from Sigma. *S. aureus* V8 protease was from ICN Biomedical, and Endoproteinase-Lys-C (EndoLysC) was from Boeringher Mannheim. Phencyclidine (PCP) was purchased from Alltech Associates. d-Tubocurare was from Sigma, and  $\alpha$ -bungarotoxin ( $\alpha$ BgTx) was from Biotoxins. EndoglycosidaseH was from Genzyme.

### **Equilibrium Binding Assay**

nAChR-rich membranes (~900 nM sites, not determined simultaneously with [<sup>3</sup>H]ethidium binding assays) in *Torpedo* physiological saline (250 mM NaCl, 5 mM KCl, 3 mM CaCl<sub>2</sub>, 2 mM MgCl<sub>2</sub>, 5 mM sodium phosphate, pH 7.0; TPS) were incubated for two hours at room temperature with varying concentrations of [<sup>3</sup>H]ethidium in the presence or absence of other cholinergic drugs. After incubation, the membrane suspensions (90  $\mu$ l) were filtered through 13 mm glass fiber filters (Schleicher & Schuell #32) which were pretreated with 1% Prosil (Lancaster) to reduce nonspecific binding. The filters were washed with 2 ml TPS and dried under heat lamps. The free concentration (F) was determined by scintillation counting of an aliquot of the filtrate, while the bound concentration (B) was determined from the filters. The data were fit to Equation 1, where  $B_{max}$  is the maximum number of binding sites,  $K_{eq}$  is the concentration of [<sup>3</sup>H]ethidium at which half of the available sites are bound, and  $B_{ns}$  is the nonspecific binding.  $B_{ns}$  was determined from a linear fit of the binding in the presence of carbamylcholine and PCP. The fit was calculated using SigmaPlot from duplicate samples.

**Equation 1.** 
$$B = \frac{B_{\max} \times F}{K_{\text{eq}} + F} + B_{\text{ns}} \times F$$

The binding in the absence of other drugs was also fit to a two-interdependent site model



where the binding to the receptor (R) of the first drug,  $D_1$ , is determined by  $K_{\text{eq}1}$ , while the second drug,  $D_2$ , binds the receptor with  $K_{\text{eq}2}$ , but only after the binding of the first drug. In this case, the two drugs were assumed to be the same compound, and they were assumed to bind to an equal number of sites on the receptor. The two-interdependent site model was fit to Equation 2, where  $K_{\text{eq}1}$  and  $K_{\text{eq}2}$  were the concentration of [ $^3\text{H}$ ]ethidium at which half of each site is bound by [ $^3\text{H}$ ]ethidium. The number of available binding sites for each site was assumed to be equivalent.

**Equation 2.** 
$$B = B_{\max} \times F \times \frac{K_{\text{eq}1} + 2F}{K_{\text{eq}1}K_{\text{eq}2} + K_{\text{eq}2}F + F^2} + B_{\text{ns}} \times F$$

A third model, of two independent sites, was also used to fit the binding of [ $^3\text{H}$ ]ethidium in the absence of other ligands. This model utilized the same variables as Equation 2.

**Equation 3** 
$$B = B_{\max} \times F \times \left( \frac{1}{K_{\text{eq}1} + F} + \frac{1}{K_{\text{eq}2} + F} \right)$$

### **Photoaffinity labeling of nAChR-enriched membranes with [ $^3\text{H}$ ]ethidium diazide**

For analytical labeling experiments, freshly thawed *Torpedo* membranes (100  $\mu\text{g}$  per condition) were diluted with TPS and pelleted (15000xg) for 30 minutes. The pellets were resuspended in TPS, and [ $^3\text{H}$ ]ethidium diazide was added. The membranes were split into aliquots, and additional ligands were added to the final concentrations indicated

in the figure legends. The final concentration of membranes was approximately 2 mg/ml (~1  $\mu$ M nAChR), and the [ $^3$ H]ethidium diazide was present at 10  $\mu$ M. After a 1 hour incubation at room temperature, oxidized glutathione (GSSG) was typically added to a final concentration of 10 mM. The suspensions were irradiated at 254 nm (Spectroline EF-16) for 30 seconds in a plastic 96-well plate on ice. Photolysis for an additional 90 seconds did not increase the incorporation appreciably. The suspensions were diluted with sample loading buffer and directly submitted to SDS-PAGE.

For proteolytic mapping of [ $^3$ H]ethidium diazide labeled  $\alpha$ -subunit with *S. aureus* V8 protease (Cleveland *et al.*, 1977; White and Cohen, 1992), labeling was carried out with 800  $\mu$ g (analytical mapping) or 10 mg (preparative) nAChR-rich membranes. For analytical mapping, samples were photolyzed in a 24-well plate while, for preparative mapping, the samples were photolyzed in two glass crystallization dishes per condition (3 mm inner diameter). Following photolysis, the membrane suspensions were pelleted. For analytical mapping, samples were resuspended in 80  $\mu$ l 50 mM sodium phosphate, pH 7, 1% SDS. Samples were divided in half, and 40  $\mu$ l of 50 mM sodium phosphate, pH 6, with or without 5 mU endoglycosidase H was added to each. After an overnight incubation, samples were diluted with sample buffer and submitted to SDS-PAGE. For preparative mapping, samples were resuspended in TPS (2 mg/ml) following photolysis and pelleting. The samples were labeled further with 1-azidopyrene (1-AP) (Blanton and Cohen, 1994) to ease identification and isolation of subunits and fragments from gels. 1-AP (62.5 mM in DMSO) was added to a final concentration of 500  $\mu$ M. After a 90 minute incubation, the samples were photolyzed for 15 minutes on ice using a 365 nm lamp (Spectroline EN-16). Membranes were pelleted (15000xg) for 30 minutes, resuspended in sample buffer, and submitted to SDS-PAGE.

## Gel Electrophoresis

SDS-PAGE was performed as described by Laemmli (1970), modified as described by Pedersen *et al.* (1986). For analytical gels, the polypeptides were resolved on a 1 mm thick 8% acrylamide gel, visualized by staining with Coomassie Blue (0.25% w/v in 45% methanol and 10% acetic acid). For autoradiography, the gels were impregnated with fluor (Amplify, Amersham), dried, and exposed at -80 °C to Kodak X-OMAT film for various times (6-8 weeks). Additionally, incorporation of  $^3\text{H}$  into individual polypeptides was quantified by scintillation counting of excised gel slices, as described in Middleton and Cohen (1991). For analytical V8 mapping gels, following electrophoresis, the gel was briefly stained with Coomassie Blue and destained to allow visualization of the subunits. The subunits were then excised and placed directly into individual wells of a 1.5 mm mapping gel, composed of a 5 cm, 4.5% acrylamide stacking gel, and a 15 cm, 15% acrylamide separating gel. Into each well was added 1:1 gram subunit:gram *S. aureus* V8 protease in overlay buffer (5% sucrose, 125 mM Tris-HCl, 0.1% SDS, pH 6.8). The gel was run at 150V for two hours, then the current was turned off for one hour. The gel was then run at constant current overnight until the dye front reached the end of the gel. The gel was stained, and the  $^3\text{H}$  was quantified by liquid scintillation. For preparative labelings, the polypeptides were resolved on a 1.5 mm thick, 8% acrylamide gel. The  $\alpha$  and  $\delta$  subunits were identified in the 8% gels by 1-AP fluorescence, excised, and loaded directly onto the 1.5 mm mapping gels. The  $\alpha$ -subunit proteolytic fragment of ~20 kD ( $\alpha\text{V8-20}$ ) was identified by fluorescence and excised. Fluorescent bands near ~14 kD ( $\delta\text{V8-14}$ ) and ~20 kD ( $\delta\text{V8-20}$ ), as well as areas containing no fluorescence, were excised from the V8 mapping gel of  $\delta$ -subunit. The excised proteolytic fragments were isolated by passive elution into 0.1 M  $\text{Na}_2\text{CO}_4$ , 0.1% SDS (Blanton and Cohen, 1994; Hager and Burgess, 1980). The eluate was filtered (Whatman No.1) and concentrated

using Millipore 5K concentrators. To remove excess SDS, acetone was added to the concentrate, and, following incubation at  $-20\text{ }^{\circ}\text{C}$  overnight, the peptides were pelleted.

### **EndoLysC digest**

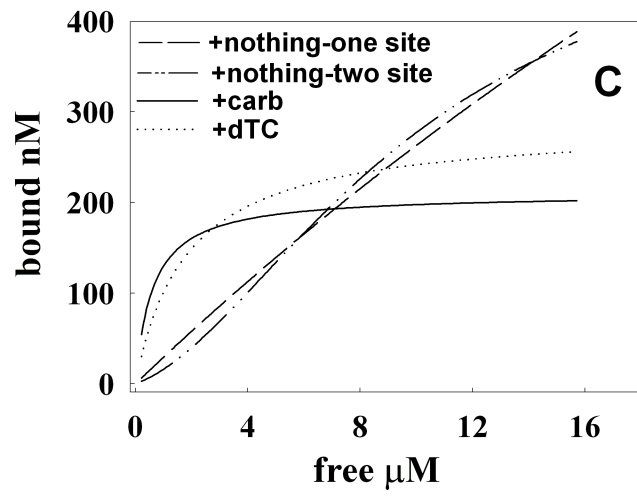
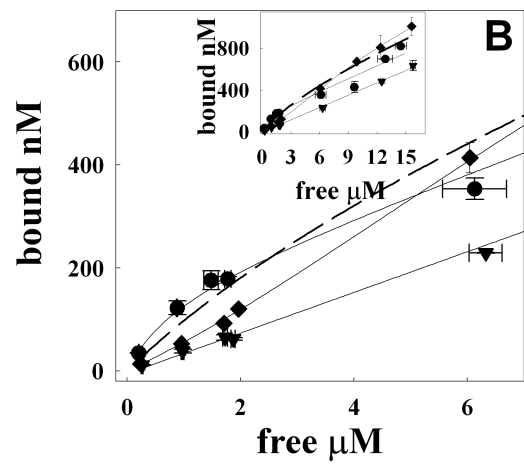
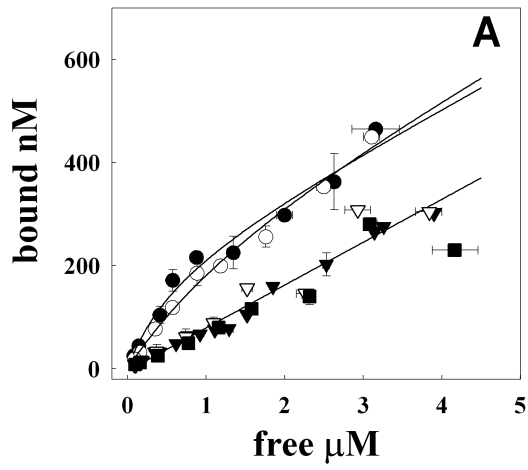
For EndoLysC digestion, acetone precipitated peptides isolated from the mapping gels were resuspended in 15 mM Tris, pH 8.1, 0.1% SDS. EndoLysC (1.5 mU resuspension buffer) was added to a final volume of 100  $\mu\text{l}$ . The digestion was allowed to proceed for 7-9 days before either purification of fragments by HPLC or separation of fragments by Tricine SDS-PAGE (Schagger and von Jagow, 1987).  $^3\text{H}$  in the Tricine gel was quantified by cutting the gel into 2 mm sections throughout the length of the gel. The gel pieces were solubilized, and the  $^3\text{H}$  was counted as described for SDS-PAGE gels.

### **HPLC purification**

Proteolytic fragments from enzymatic digestion of [ $^3\text{H}$ ]ethidium diazide labeled subunits were further purified by reverse-phase HPLC, as described by Blanton and Cohen (1994), using a Brownlee C4 Aquapore column (100 x 2.1 mm; 7  $\mu\text{m}$  particle size). Solvent A was 0.08% TFA in water, and solvent B was 0.05% TFA in 60% acetonitrile/40% 2-propanol. A nonlinear gradient (Waters Model 680 gradient controller, curve No. 7) from 25% to 100% solvent B in 80 minutes was used. The rate of flow was 0.2 ml/min, and 0.5 ml fractions were collected. The elution of peptides was monitored by absorbance at 215 nm, and the fluorescence from 1-AP was detected by fluorescence emission (357 nm excitation, 432 nm emission). Additionally, aliquots from the fractions were taken to determine the presence of radiation by liquid scintillation counting.

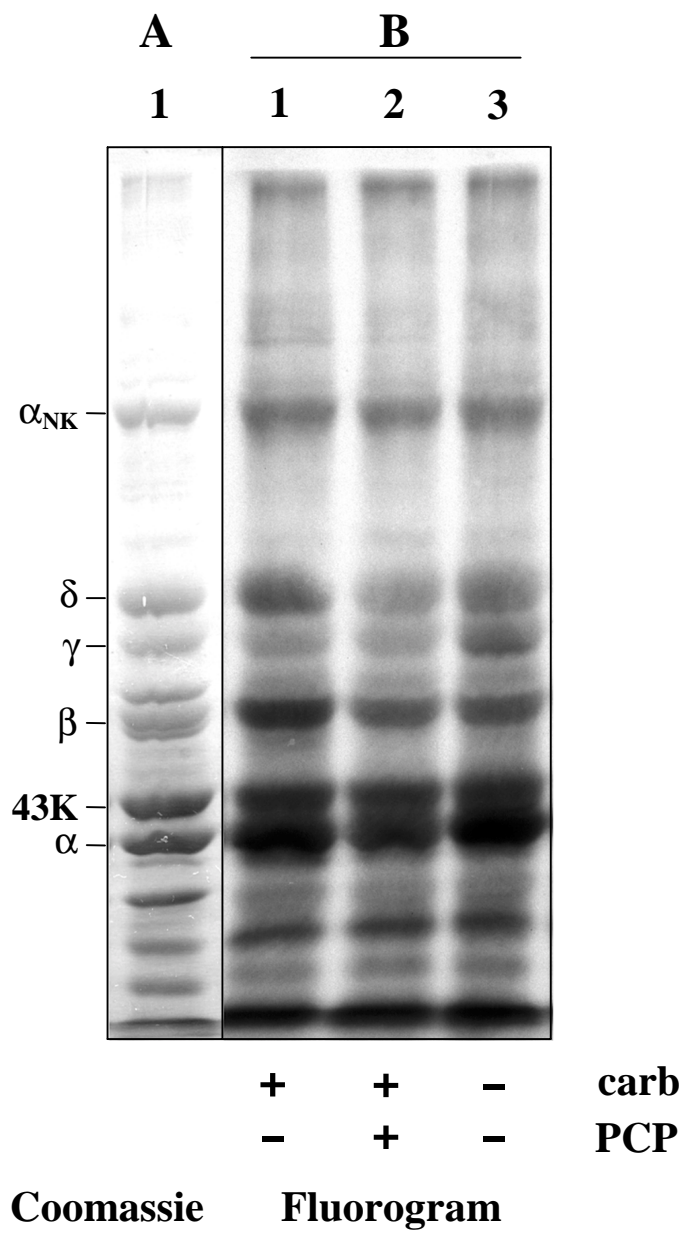
## Sequence Analysis

Automated amino terminal sequence analysis was performed on an Applied Biosystems Model 477A protein sequencer with an in-line 120A PTH analyzer. HPLC samples (450  $\mu$ l) were directly loaded onto chemically modified glass fiber disks (Beckman) in 20  $\mu$ l aliquots, allowing the solvent to evaporate at 40 °C between loads. Samples were loaded directly, as opposed to removing solvent by vacuum centrifugation and resuspending in buffer containing SDS, to avoid the pre-wash step necessary when samples containing SDS are loaded onto the sequencer. The pre-wash step consisted of a four minute treatment with gas-phase TFA followed by a five minute wash with ethyl acetate. When samples labeled with [<sup>3</sup>H]ethidium diazide were subjected to this treatment, up to 50% of the loaded <sup>3</sup>H was removed during this wash step. Sequencing was performed using gas-phase TFA to minimize possible hydrolysis. After conversion of the released amino acids to PTH amino acids, the suspension was divided into two parts. One portion, approximately one-third, went to the PTH analyzer while the remaining two-thirds was collected for scintillation counting. The samples were counted for five minutes, in triplicate at least, and the results were averaged to generate reported errors. Yield of PTH amino acids, along with background-subtracted levels, was calculated from peak height compared with standards using the program Model 610A Data Analysis Program Version 1.2.1. Initial yield and repetitive yield were calculated by a nonlinear least squares regression to the equation  $M=I_0 \cdot R^n$ , where M is the observed release,  $I_0$  is the initial yield, R is the repetitive yield, and n is the cycle number using SigmaPlot. Derivatives known to have poor recovery (Ser, Arg, Cys, and His) were omitted from the fit.



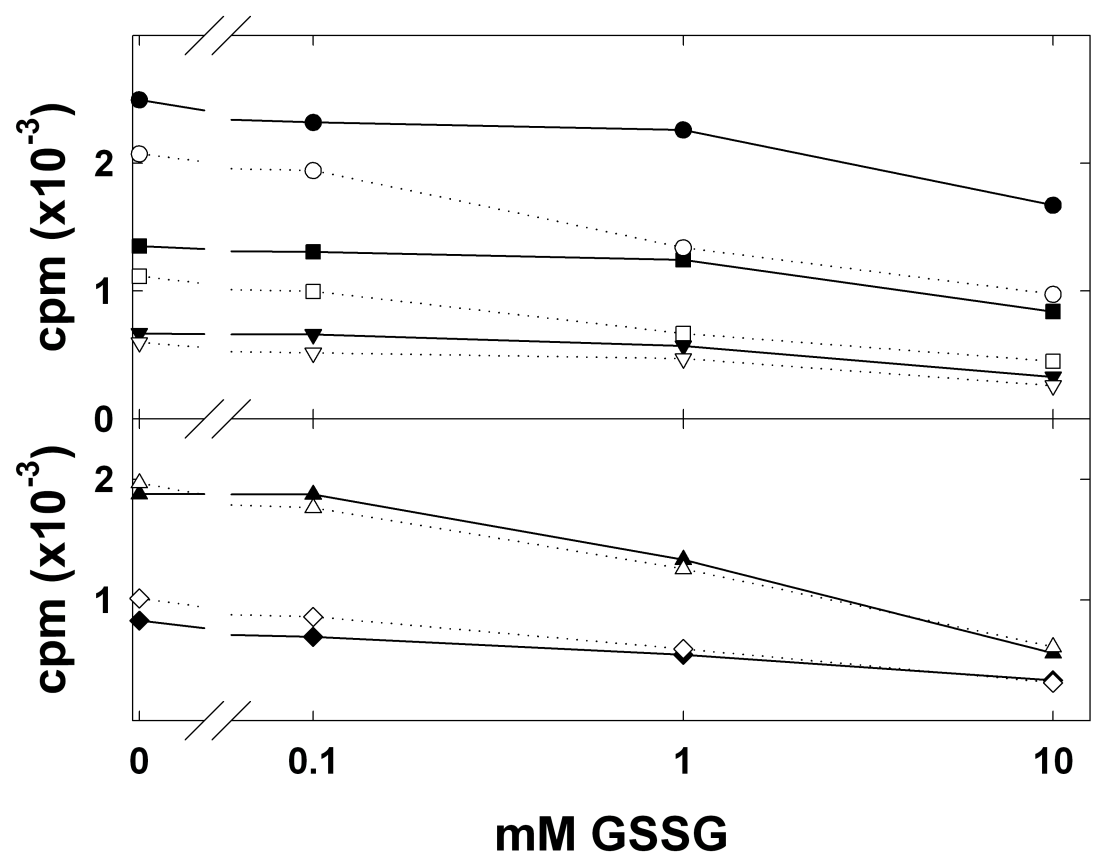
**Figure 2-1. Binding of [<sup>3</sup>H]ethidium in the presence and absence of various cholinergic drugs.**

A, B, nAChR-rich membranes (2 mg/ml with ~900 nM ACh binding sites) were equilibrated with various cholinergic drugs (2 mM carbamylcholine (●), 100 μM dTC (○), 2 mM carbamylcholine with 100 μM PCP (▼), 10 μM αBgTx (▽), 125 μM ethidium (■), and no other drug (◆)) with increasing concentrations of [<sup>3</sup>H]ethidium. After a two hour incubation, the concentration of bound and free [<sup>3</sup>H]ethidium was determined by filtration. The points plotted are the averages of duplicate samples. The observed binding in the presence of αBgTx, ethidium, or carbamylcholine with PCP was fit to a line to determine the nonspecific binding ( $B_{ns}$ ). The specific binding in the presence of carbamylcholine or dTC was determined according to Equation 1 in Methods. Both the  $B_{max}$  and the  $K_{eq}$  were variables, and  $B_{ns}$  was determined from the slope of the binding in the presence of carbamylcholine and PCP. The specific binding in the absence of other drugs was determined either as described for the binding in the presence of carbamylcholine or dTC or by a fit to Equation 2 in Methods. For Equation 2, both  $K_{eq}$ s were variables, as was  $B_{max}$ . However, in this model the  $B_{max}$  was assumed to be equal for the two binding sites. A. +carb:  $K_{eq}=0.6 \pm 0.3 \mu\text{M}$ ,  $B_{max}=200 \pm 30 \text{ nM}$ ; +dTC:  $K_{eq}=1.7 \pm 0.3 \mu\text{M}$ ,  $B_{max}=270 \pm 50 \text{ nM}$ . If [<sup>3</sup>H]ethidium is constrained to a common value of  $B_{max}$ , 220 nM, then  $K_{eq}$  (+carb)= $0.7 \pm 0.1$ ;  $K_{eq}$  (+dTC)= $1.1 \pm 0.1$ . +carb/+PCP: slope= $0.083 \pm 0.004$ ; +ethidium: slope= $0.065 \pm 0.008$ ; +αBgTx:  $0.085 \pm 0.004$  B. +carb:  $K_{eq}=1.6 \pm 0.9 \mu\text{M}$ ;  $B_{max}=210 \pm 30 \text{ nM}$ ; +nothing: Equation 1 with  $B_{max}=200 \mu\text{M}$ :  $K_{eq}=1.7 \pm 2.0 \mu\text{M}$  (dashed line); Equation 2:  $K_{eq1}=25 \pm 8 \mu\text{M}$ ;  $K_{eq2}=4.2 \pm 2.3 \mu\text{M}$ ;  $B_{max}=280 \pm 30 \text{ nM}$  C, The specific binding in each condition was calculated from Equation 1 or Equation 2 (for the binding in the presence of no other drug). When the binding data in the absence of other drugs was determined by a fit to Equation 1,  $K_{eq}=100 \pm 90 \mu\text{M}$ ,  $B_{max}=2800 \pm 2300 \text{ nM}$ .



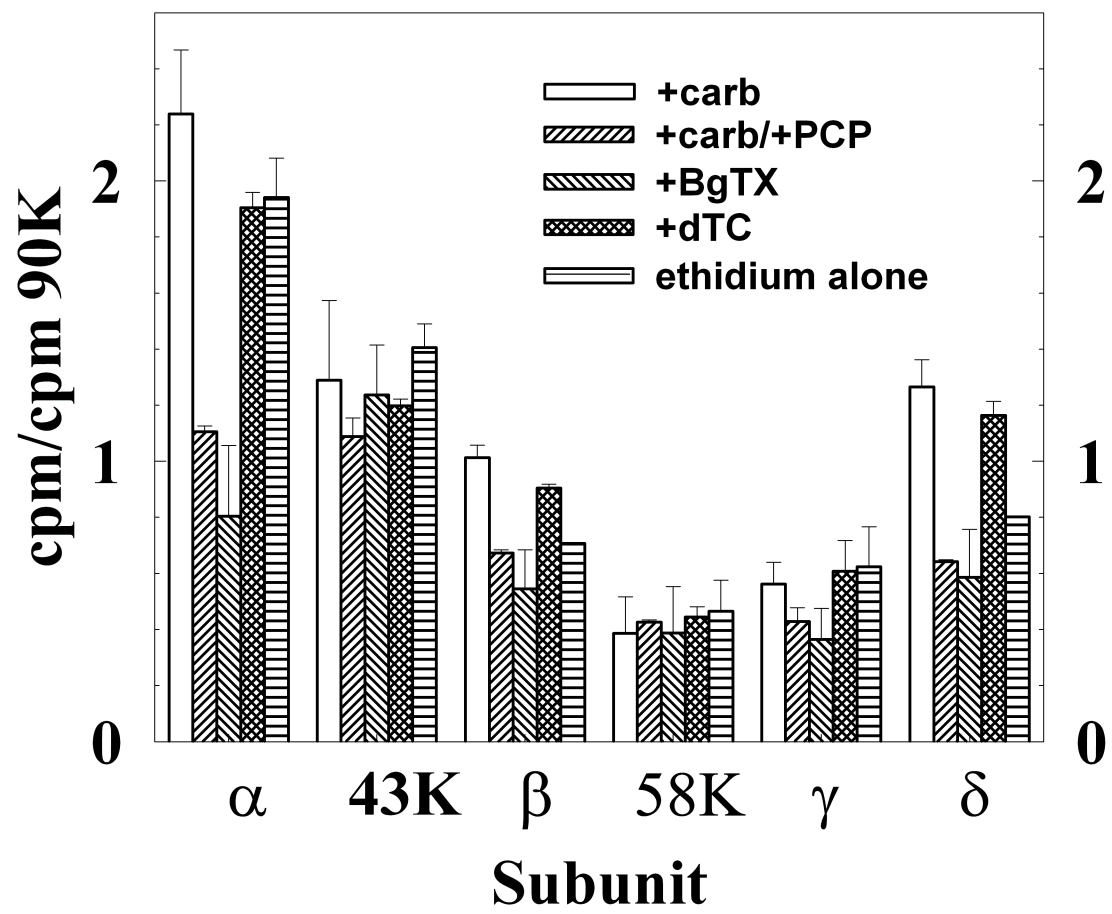
**Figure 2-2. Photoincorporation of [<sup>3</sup>H]ethidium diazide into integral and peripheral membrane proteins of nAChR-rich membranes in the presence or absence of carbamylcholine or PCP.**

nAChR-rich membranes (100 μg) were equilibrated with [<sup>3</sup>H]ethidium diazide in TPS (2 mg/ml) in the presence of 10 mM oxidized glutathione in the presence (lanes 1 & 2) or absence (lane 3) of 2 mM carbamylcholine and the absence (lanes 1 & 3) or presence (lane 2) of 100 μM PCP. After photolysis at 265 nm for 30 seconds, the samples were subjected to SDS-PAGE, visualized by Coomassie Blue (Panel A), processed for fluorography, and exposed to film for 6 weeks (Panel B). Indicated on the left are the mobilities of the nAChR subunits, rapsyn (43K), and the α-subunit of the Na<sup>+</sup>/K<sup>+</sup> ATPase (αNK).



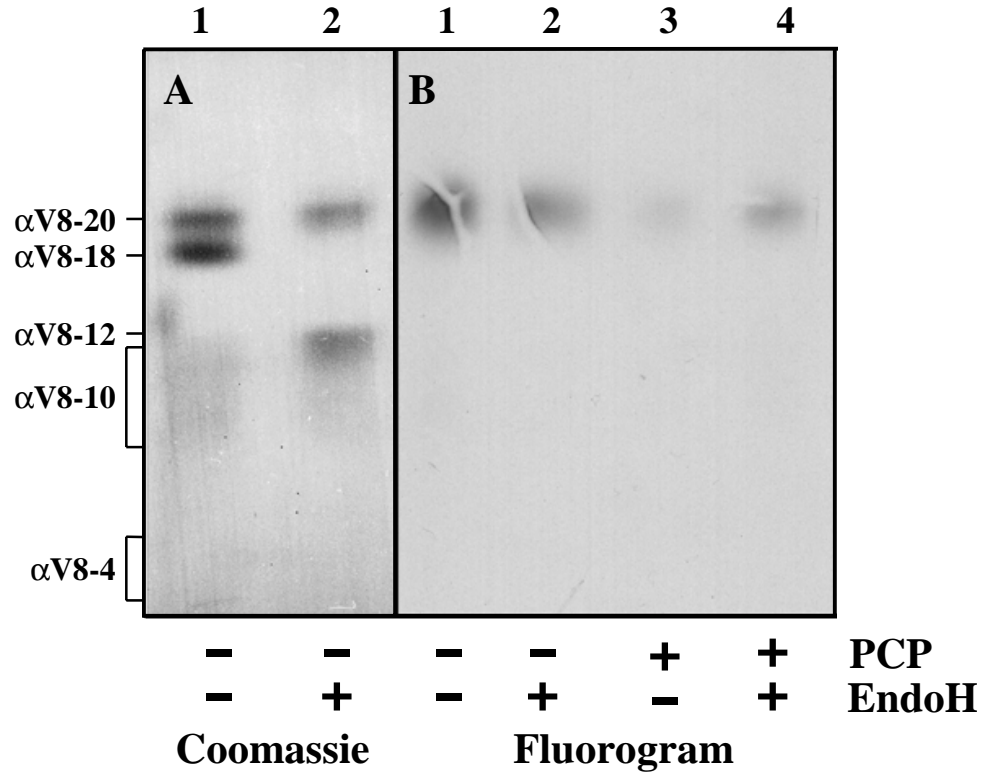
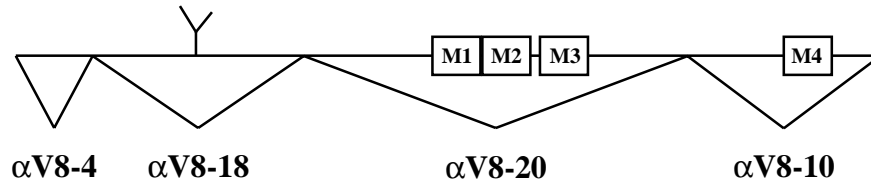
**Figure 2-3. Photoincorporation of [<sup>3</sup>H]ethidium diazide into integral and peripheral membrane proteins of nAChR-rich membranes in the presence of oxidized glutathione.**

nAChR-rich membranes (100 μg) were equilibrated with [<sup>3</sup>H]ethidium diazide in TPS (2 mg/ml) in the presence of 2 mM carbamylcholine without (solid symbols) or with (open symbols) 100 μM PCP. After photolysis at 265 nm for 30 seconds, samples were subjected to SDS-PAGE and visualized by Coomassie Blue. The nAChR α (●,○), γ (▼,▽), and δ (■,□) subunits as well as bands of 37 kD (calectrin, ◆,◇) and 90 kD (α-subunit of Na<sup>+</sup>/K<sup>+</sup> ATPase, ▲,△) were excised. <sup>3</sup>H was quantified by scintillation counting.



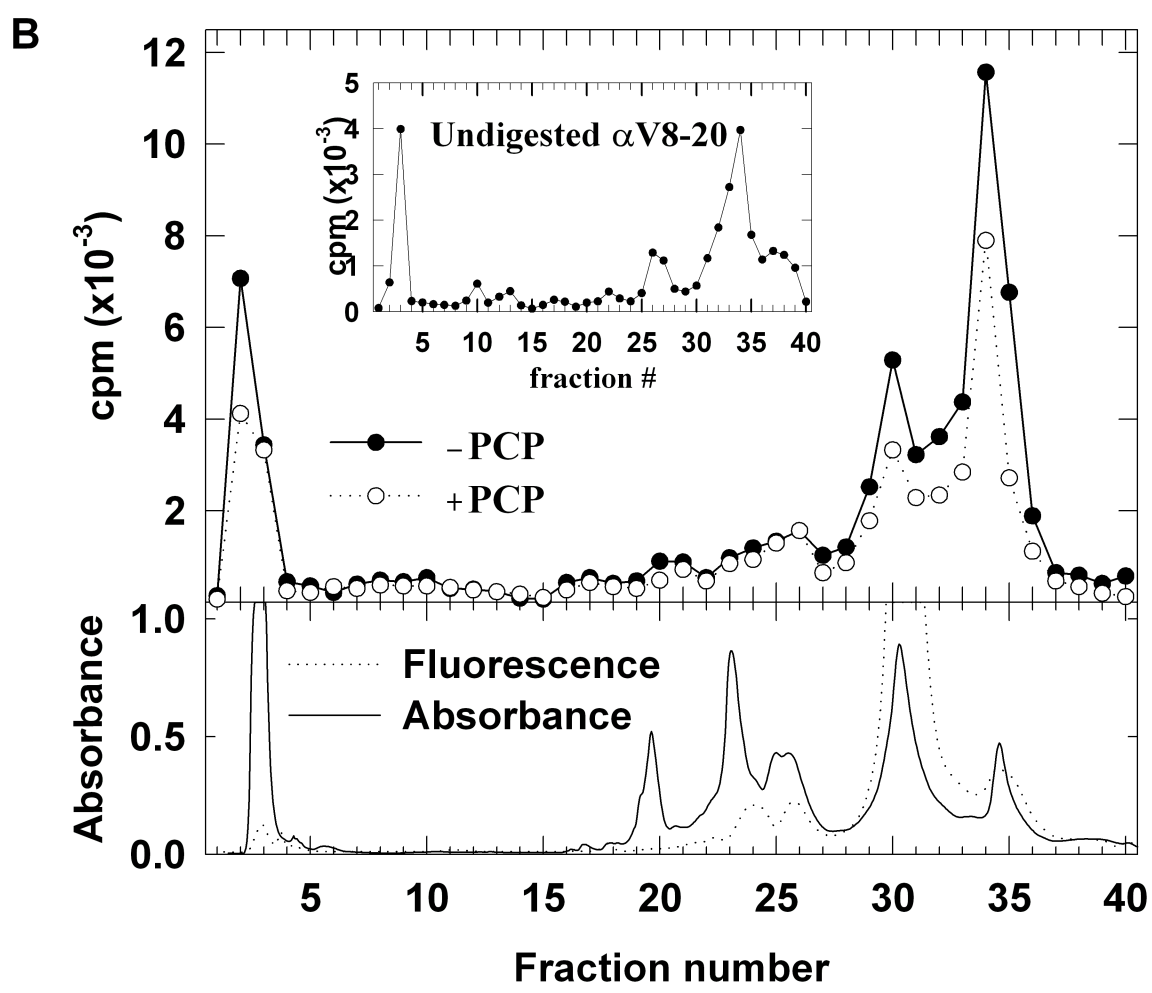
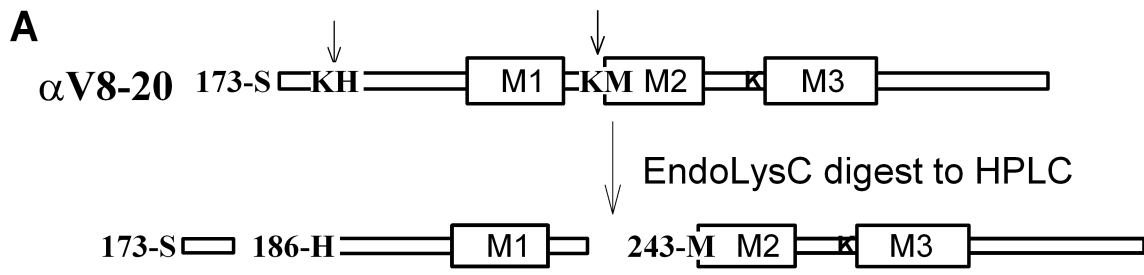
**Figure 2-4. Photoincorporation of [<sup>3</sup>H]ethidium diazide into integral and peripheral membrane proteins of nAChR-rich membranes in the presence of various cholinergic drugs.**

nAChR-rich membranes (100 µg) were equilibrated with [<sup>3</sup>H]ethidium diazide in TPS (2 mg/ml) in the presence of 10 mM oxidized glutathione in the presence of 2 mM carbamylcholine, 2 mM carbamylcholine and 100 µM PCP, 10 µM αBgTx, 100 µM d-tubocurarine, or no other drug. After photolysis at 265 nm for 30 seconds, samples were subjected to SDS-PAGE and visualized by Coomassie Blue. Bands corresponding to indicated polypeptides, as well as a 90 kD band, containing the α-subunit of Na<sup>+</sup>/K<sup>+</sup> ATPase, were excised. <sup>3</sup>H was quantified by scintillation counting. Values are the average from duplicate lanes for each condition, with the <sup>3</sup>H normalized with respect to that in the 90 kD band, to reduce variability between lanes. Average incorporation in polypeptides labeled in the presence of carbamylcholine (+/-) or the presence of carbamylcholine and PCP (+/+): α-subunit: +/-: 2098 ± 27 cpm; +/+ : 1278 ± 310 cpm. δ-subunit: +/-: 1186 ± 15 cpm; +/+ : 740 ± 159 cpm. β-subunit: +/-: 952 ± 44; +/+ : 775 ± 161. For αNK: +/-: 942 ± 84; +/+ : 1154 ± 256.



**Figure 2-5. Proteolytic mapping of sites of [<sup>3</sup>H]ethidium diazide incorporation into the nAChR  $\alpha$ -subunit using *S. aureus* V8 protease.**

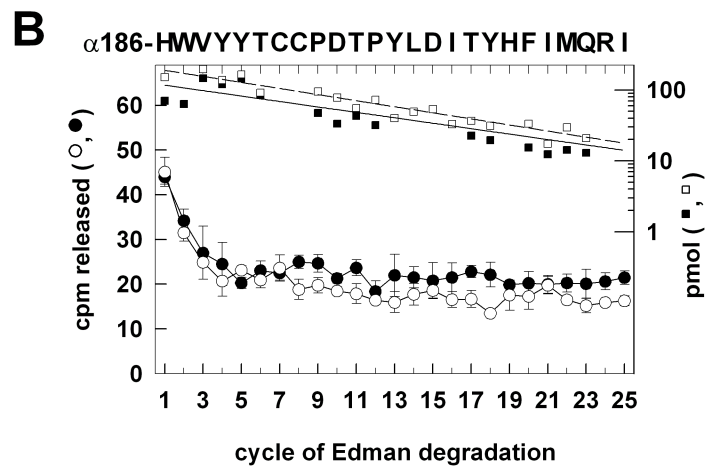
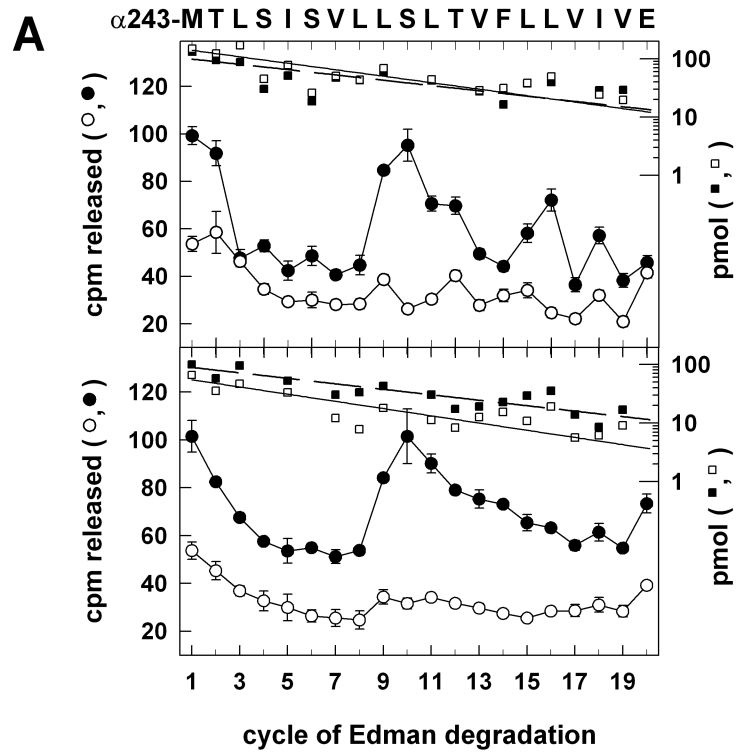
nAChR-rich membranes (800  $\mu$ g) were labeled with [<sup>3</sup>H]ethidium diazide in the presence of 10 mM oxidized glutathione and 2 mM carbamylcholine and the absence (lanes 1 & 2) or presence (lanes 3 & 4) of PCP and split for incubation with (lanes 2 & 4) or without (lanes 1 & 3) EndoglycosidaseH as described in methods. After incubation membranes were submitted to SDS-PAGE, and the  $\alpha$ -subunit was excised. The excised bands were transferred to the well of a 15% mapping gel and digested with V8 protease as described in methods. A, mapping gel stained with Coomassie Blue. B, fluorogram of mapping gel, exposed for 6 weeks. The mobility of the proteolytic fragments is indicated on the left. The incorporation in each polypeptide was additionally measured by scintillation counting of excised gel pieces. Incorporation in the presence of carbamylcholine (+/-) or the presence of carbamylcholine and PCP (+/+) in each  $\alpha$ -subunit fragment:  $\alpha$ V8-20: +/- : 2271 cpm, +/+ : 832 cpm;  $\alpha$ V8-18: +/-: 390 cpm, +/+ : 181 cpm;  $\alpha$ V8-10 (including  $\alpha$ V8-12): +/-: 346 cpm, +/+ : 251 cpm ( $\alpha$ V8-12: +/-: 262 cpm; +/+ : 185 cpm);  $\alpha$ V8-4: +/-: 43 cpm, +/+ : 26 cpm. +EndoH:  $\alpha$ V8-20: +/-: 1618 cpm, +/+ : 533 cpm;  $\alpha$ V8-18: +/-: 126 cpm, +/+ : 60 cpm;  $\alpha$ V8-10 (including  $\alpha$ V8-12): +/-: 38 cpm, +/+ : 45 cpm ( $\alpha$ V8-12: +/-: 282 cpm, +/+ : 210 cpm);  $\alpha$ V8-4: +/-: 27 cpm, +/+ : 23 cpm. Shown above is a schematic indicating the positions of the four fragments within the primary structure of the nAChR  $\alpha$  subunit.



**Figure 2-6. Reverse-phase HPLC purification of [<sup>3</sup>H]ethidium diazide labeled fragments from EndoLysC digest of  $\alpha$ V8-20.**

A. A map of the amino acid sequence of the nAChR  $\alpha$ -subunit contained within  $\alpha$ V8-20. Rectangles, M1, M2 and M3 hydrophobic segments. Arrows, location of two known sites of EndoLysC cleavage. The resulting cleavage products are indicated. Other potential cleavage sites indicated by K.

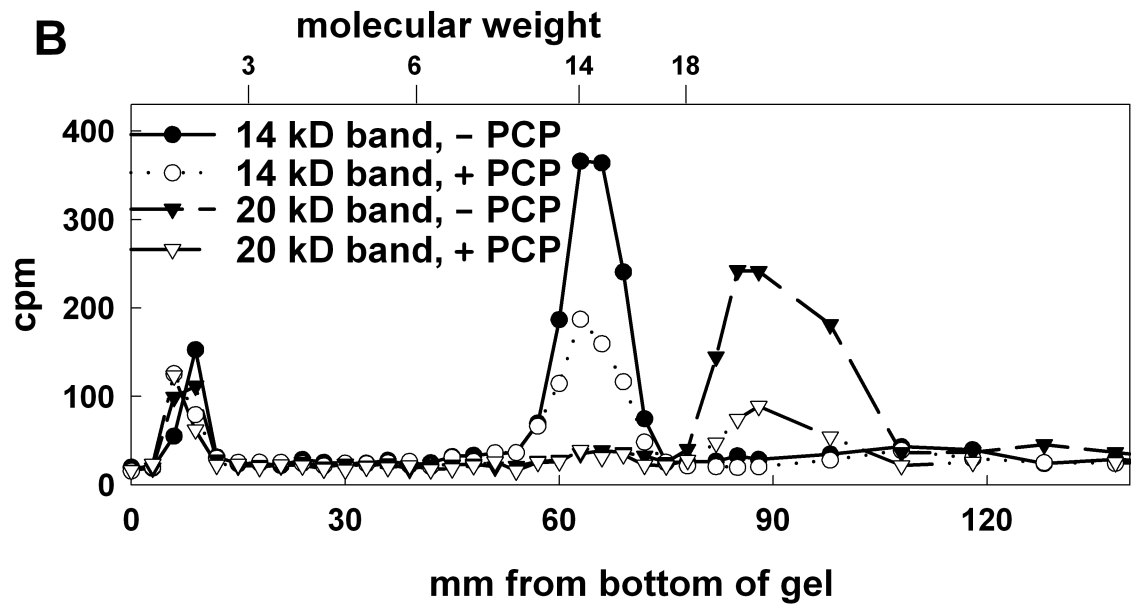
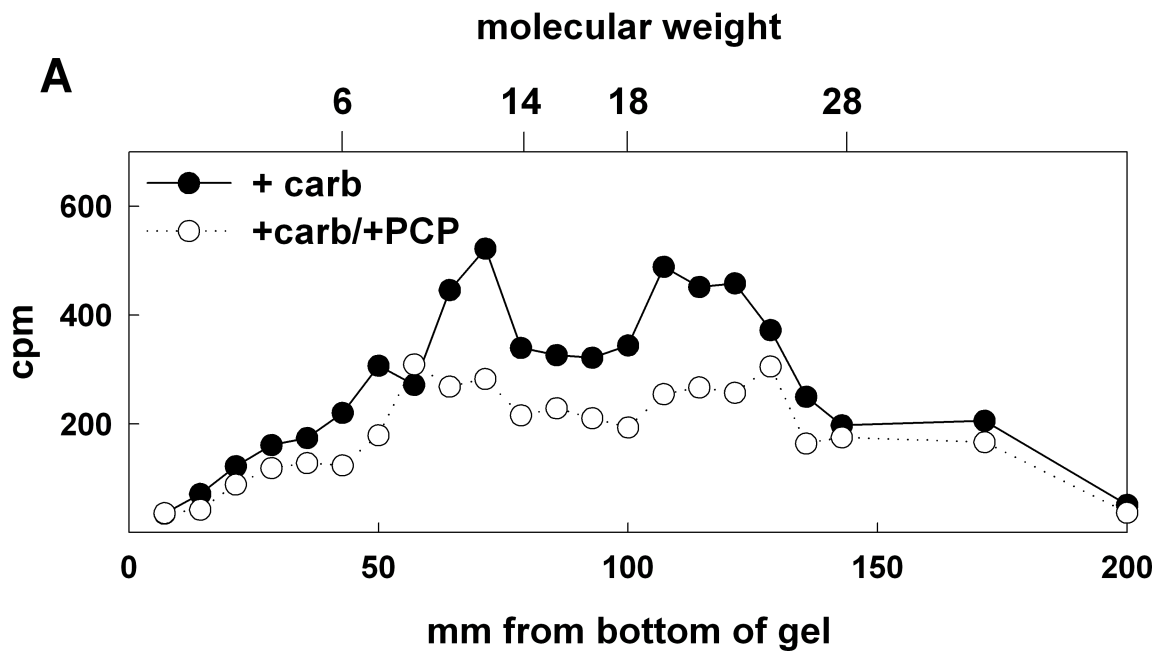
B. EndoLysC digested  $\alpha$ V8-20 isolated from nAChR-rich membranes photolabeled with [<sup>3</sup>H]ethidium diazide in the presence of carbamylcholine and the absence (●) or presence of PCP (○) was digested with EndoLysC. The digest was applied to a Brownlee Aquapore C4 column and fractionated by reverse-phase HPLC. Upper panel, <sup>3</sup>H elution profile calculated from a 10% aliquot of each fraction. Lower panel, fluorescence (·····) and absorbance profiles (—). Inset, <sup>3</sup>H elution profile when  $\alpha$ V8-20 (+/-) isolated by SDS-PAGE was purified by reverse-phase HPLC.



**Figure 2-7.  $^3\text{H}$  and mass release upon N-terminal sequence analysis of HPLC fractions of EndoLysC-digest of [ $^3\text{H}$ ]ethidium diazide labeled  $\alpha\text{V8-20}$  .**

A. Sequence analysis of fraction 34 from HPLC purification of Figure 2-6 (upper panel) and the same fraction from the purification of a second, independent labeling experiment. For each sample, 67% of each cycle of Edman degradation was analyzed for released  $^3\text{H}$  ( $\bullet, \circ$ ), and 33% for released PTH-amino acids ( $\blacksquare, \square$ ). For both labeling conditions, the only sequence detected began at  $\alpha\text{Met-243}$ , the N-terminus of  $\alpha\text{M2}$ . Labeling 1 (upper panel): +/- ( $\bullet, \blacksquare$ ):  $I_0=109$  pmol,  $R=90\%$ , 11600 cpm loaded, 2600 cpm remaining after 25 cycles. ++ ( $\circ, \square$ ):  $I_0=159$  pmol,  $R=88\%$ , 7900 cpm loaded, 1800 cpm remaining after 25 cycles. Labeling 2 (lower panel): +/- ( $\bullet, \blacksquare$ ):  $I_0=98$  pmol,  $R=90\%$ , 17000 cpm loaded, 5300 cpm remaining after 25 cycles. ++ ( $\circ, \square$ ):  $I_0=63$  pmol,  $R=87\%$ , 7000 cpm loaded, 2500 cpm remaining after 25 cycles. The sequence of the identified peptide is shown above.

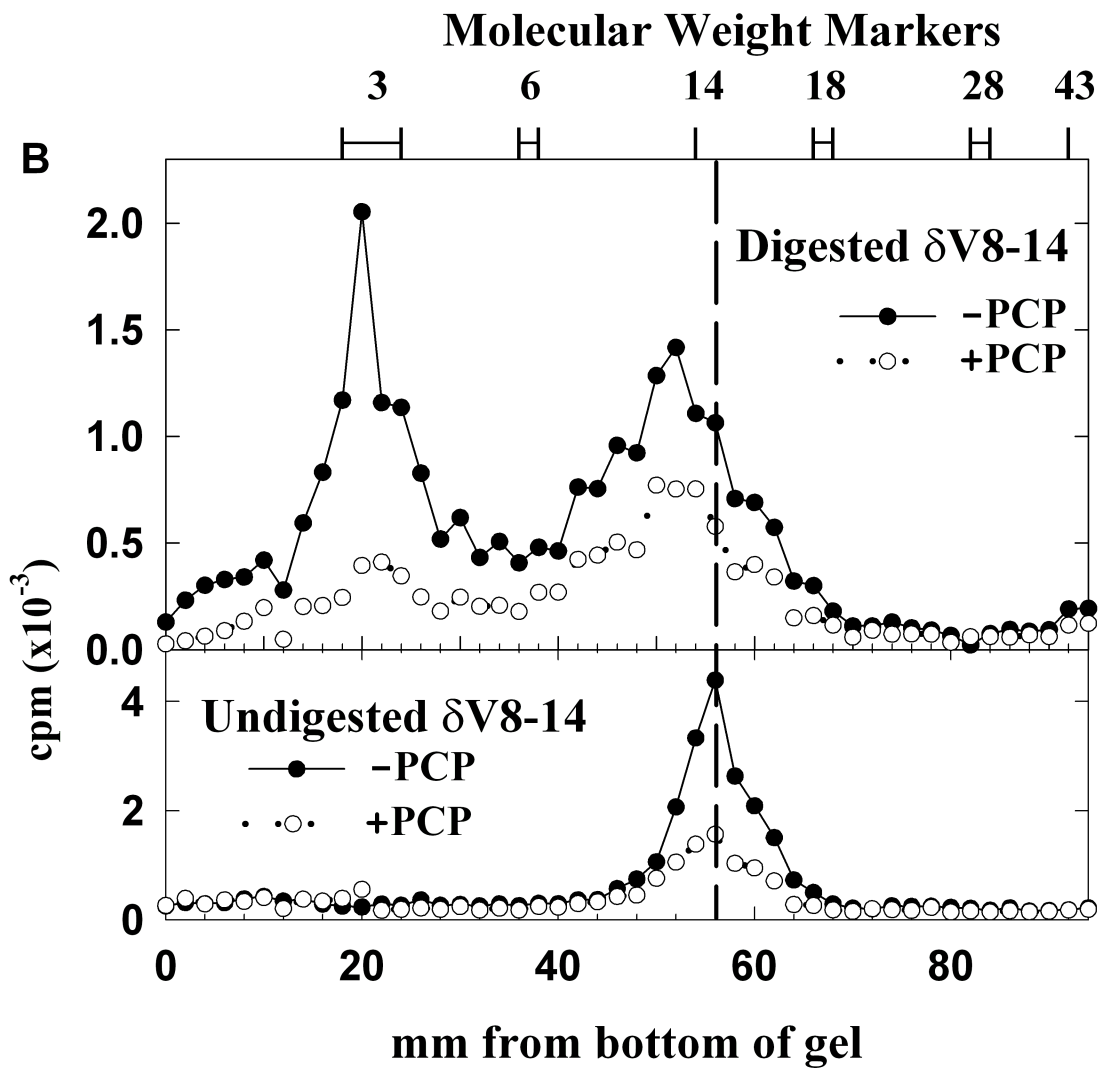
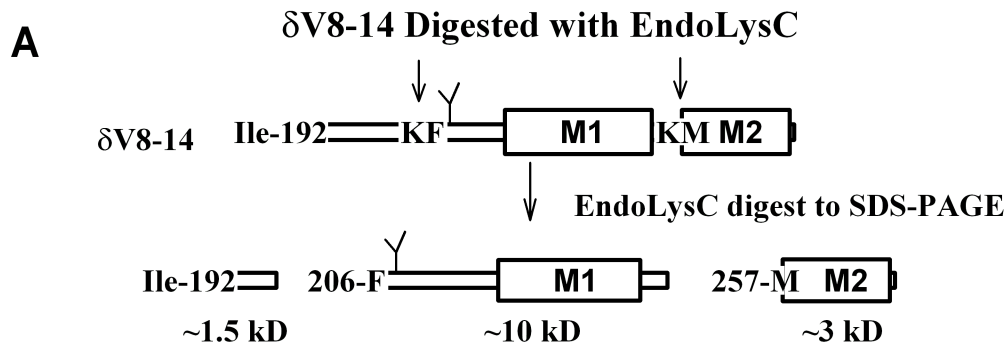
B. Sequence analysis of fraction 29 from HPLC purification of Figure 2-6. As above, for each sample, 67% of each cycle of Edman degradation was analyzed for released  $^3\text{H}$  ( $\bullet, \circ$ ), and 33% for released PTH-amino acids ( $\blacksquare, \square$ ). For both labeling conditions, the primary sequence detected began at  $\alpha\text{His-186}$  and a secondary sequence beginning at  $\alpha\text{Asp-180}$  (+/- ( $\bullet, \blacksquare$ ):  $\alpha\text{His-186}$   $I_0=128$  pmol,  $R=92\%$ ;  $\alpha\text{Asp-180}$   $I_0=18$  pmol,  $R=94\%$ , 5290 cpm loaded, 1250 cpm remaining after 25 cycles. ++ ( $\circ, \square$ ):  $\alpha\text{His-186}$   $I_0=208$  pmol,  $R=91\%$ ,  $\alpha\text{Asp-180}$   $I_0=39$  pmol,  $R=91\%$ , 3330 cpm loaded, 770 cpm remaining after 25 cycles). Level of released PTH-amino acids of the primary sequence is plotted ( $\blacksquare, \square$ ), and the sequence of the primary peptide is shown above.



**Figure 2-8. Proteolytic mapping of the sites of [<sup>3</sup>H]ethidium diazide incorporation in the nAChR  $\delta$ -subunit using V8 protease.**

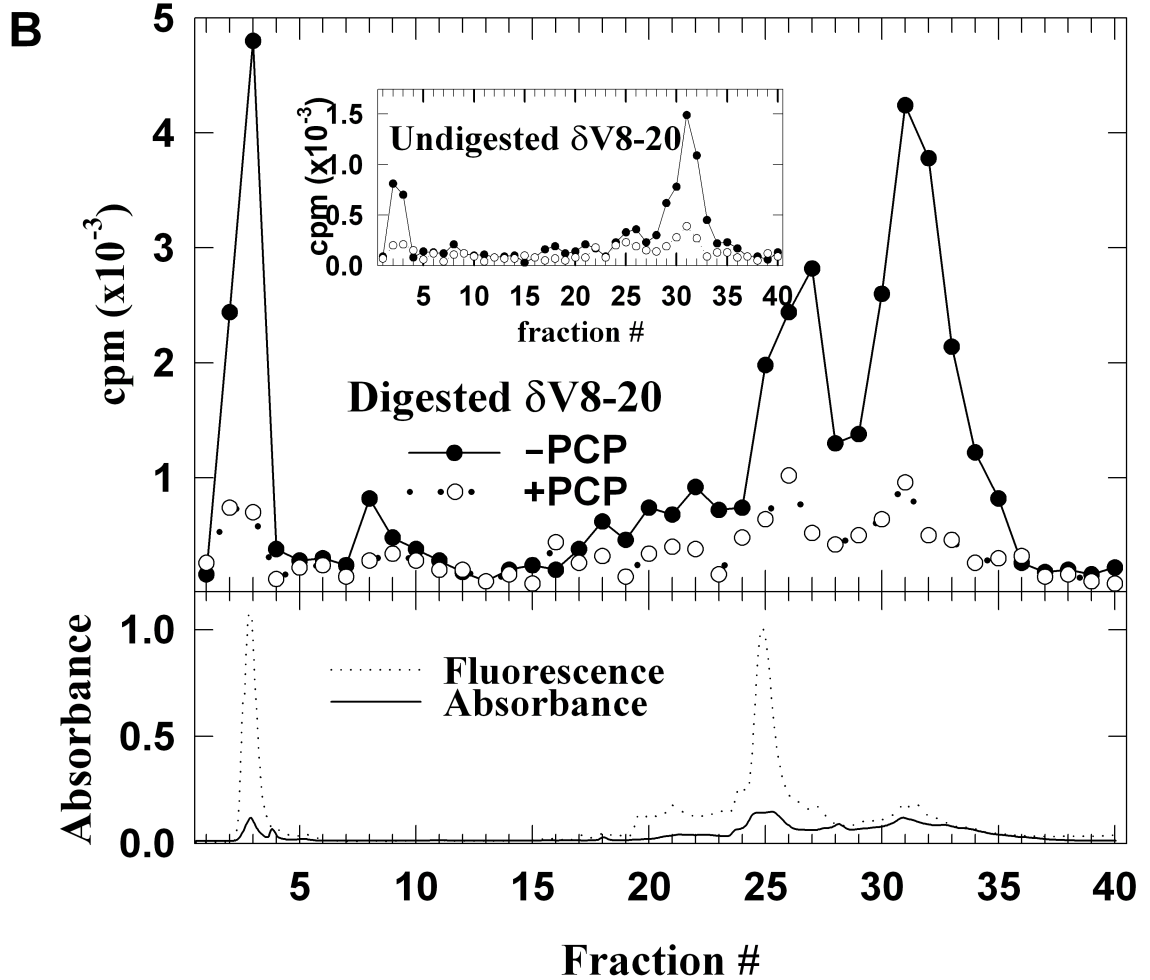
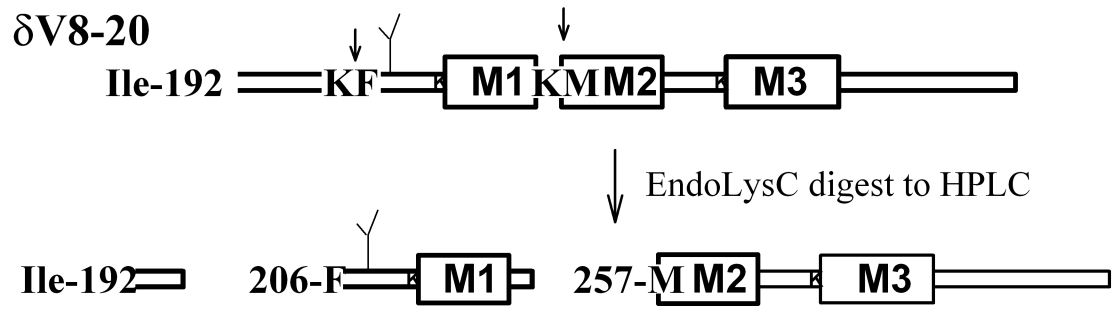
A. nAChR-rich membranes (400  $\mu$ g) were equilibrated with [<sup>3</sup>H]ethidium diazide in TPS in the presence of carbamylcholine and the absence (●) or presence of PCP (○). After photolysis in the presence of 10 mM GSSG, the samples were subjected to SDS-PAGE, and the  $\delta$ -subunit was excised after brief staining with Coomassie Blue. The excised bands were transferred to the wells of a 15% mapping gel and digested with V8 protease. The lanes were cut into 5 mm slices for the lower 100 mm and 20 mm slices for the upper portion of the gel. <sup>3</sup>H was quantified by scintillation counting. The mobility of molecular weight markers is indicated along the top axis.

B. Aliquots of ~14 kD ( $\delta$ V8-14, ●, ○) and ~20 kD ( $\delta$ V8-20, ▼, ▽) bands isolated from V8 mapping gel of nAChR  $\delta$ -subunit labeled in the absence (●, ▼) and presence (○, ▽) of PCP were diluted in sample buffer and submitted to SDS-PAGE using a 15% mapping gel without V8 protease. Gel was run at constant current overnight until dye front reached the bottom of the gel. Lanes were cut into 2 mm slices, and <sup>3</sup>H was quantified by scintillation counting. The mobility of molecular weight markers is indicated along the top axis.



**Figure 2-9. EndoLysC digest of  $\delta$ V8-14 fragment labeled with [ $^3$ H]ethidium diazide resolved by Tricine SDS-PAGE.**

- A. Map of  $\delta$ V8-14 sequence. Rectangles,  $\delta$ M1 and  $\delta$ M2 segments. Arrows, location of two potential sites of EndoLysC cleavage. The resulting cleavage products are indicated.
- B. Aliquots of  $\delta$ V8-14 labeled in the absence (●) and presence (○) of PCP were fractionated by Tricine SDS-PAGE. The lanes were cut into 2 mm slices, and  $^3$ H incorporation was quantified by scintillation counting. Upper panel, EndoLysC digest of  $\delta$ V8-14. Lower panel, undigested  $\delta$ V8-14. Mobility of molecular weight markers is indicated along top axis.

**A**

**Figure 2-10. Reverse-phase HPLC purification of [<sup>3</sup>H]ethidium diazide labeled fragments from EndoLysC digest of  $\delta$ V8-20.**

A. Sequence map of  $\delta$ V8-20. Rectangles,  $\delta$ M1,  $\delta$ M2 and  $\delta$ M3 segments. Arrows, location of two potential sites of EndoLysC cleavage. The resulting cleavage products are indicated.

B. The EndoLysC digests of  $\delta$ V8-20 labeled with [<sup>3</sup>H]ethidium diazide in the presence of carbamylcholine and the absence (●) and presence (○) of PCP were fractionated by reverse-phase HPLC. Upper panel, <sup>3</sup>H elution profiles calculated from 10% aliquot of fractions (Inset, <sup>3</sup>H elution profile of undigested  $\delta$ V8-20 labeled in the absence (●) and presence (○) of PCP). Lower panel, fluorescence (·····) and absorbance profiles (—).

δ257-MSTAI SVLLAQAVFLLLTSQRLPET  
δ206-FPNGTNYQDVTFYLI IRRKPLFYVI

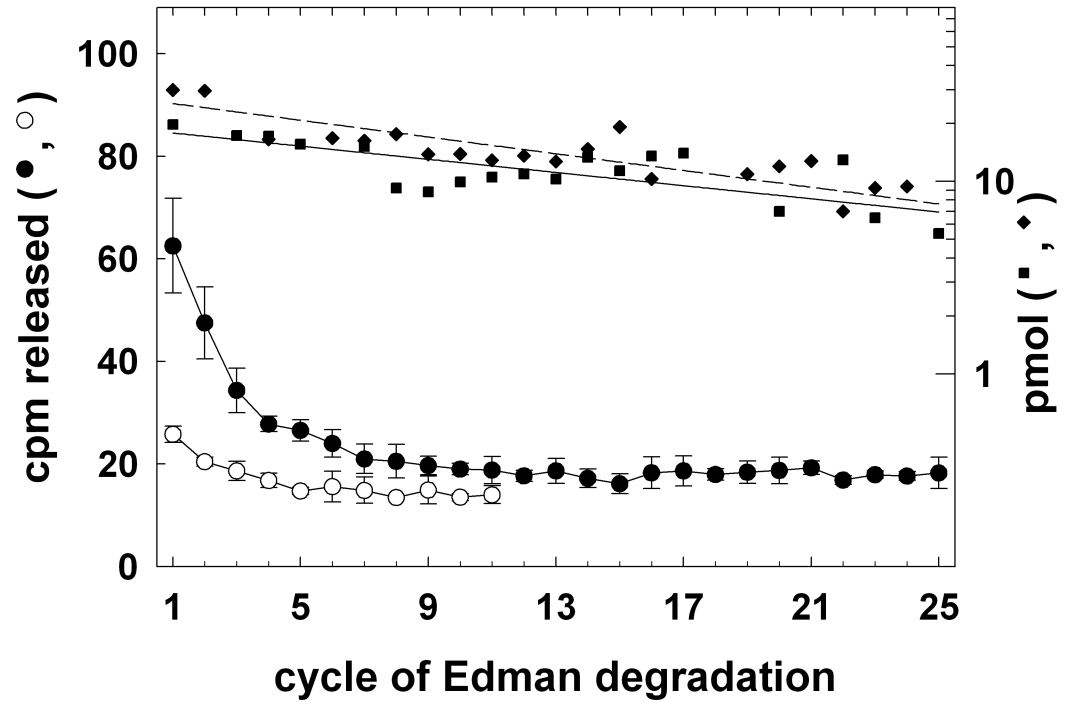


**Figure 2-11 Sequence Analysis of  $\delta$ V8-20 EndoLysC digest fragments.**

Sequence analysis of fraction 31 from HPLC purification of Figure 2-10. For each sample, 67% of each cycle of Edman degradation was analyzed for released  $^3\text{H}$  ( $\bullet$ ,  $\circ$ ), and 33% for released PTH-amino acids ( $\blacksquare$ ,  $\blacklozenge$ ). For both labeling conditions, two sequences were detected, one beginning at  $\delta$ Met-257, the N-terminus of the M2 segment, and one beginning at  $\delta$ Phe-206. +/- ( $\bullet$ ):  $\delta$ Met-257 ( $\blacksquare$ ):  $I_0=19$  pmol,  $R=96\%$ ;  $\delta$ Phe-206 ( $\blacklozenge$ ):  $I_0=27$  pmol,  $R=95\%$ , 3800 cpm loaded, 1100 cpm remaining after 25 cycles. +/- ( $\circ$ ):  $\delta$ Met-257:  $I_0=5$  pmol,  $R=99\%$ ;  $\delta$ Phe-206:  $I_0=12$  pmol,  $R=92\%$ , 860 cpm loaded, 170 cpm remaining after 11 cycles. The sequences of the identified peptides are shown above.

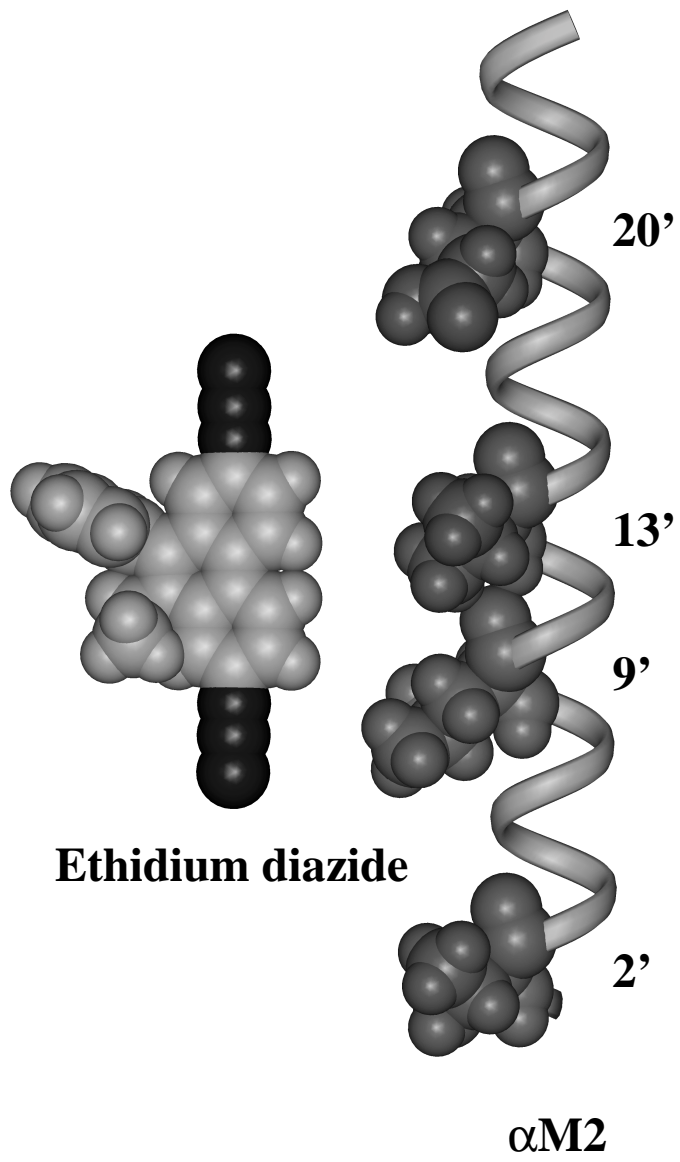


**Figure 2-12. Model of ethidium and  $\alpha$ M2 helix**

$\alpha$ -Helical model of the  $\alpha$ M2 segment and space filling model of ethidium were made using the molecular modeling software Insight (Biosym, Inc.). M2 residues 2' (threonine), 9' (leucine), and 20' (glutamate) are shown as space-filling models, and one amine group of ethidium is positioned in proximity to the  $\alpha$ M2 9' position, which was labeled with [ $^3$ H]ethidium diazide.

## Chapter 3 Identification of the Sites of Incorporation of [<sup>3</sup>H]3-Aziocanol in the nAChR

### ABSTRACT

A photoactivatable derivative of a long chain alcohol, [<sup>3</sup>H]3-aziocanol, has been used to localize the sites of interaction of alcohols with the *Torpedo* nicotinic acetylcholine receptor (nAChR). 3-Aziocanol inhibits the nAChR with an IC<sub>50</sub> ~33 μM. The sites of [<sup>3</sup>H]3-aziocanol incorporation in *Torpedo* nAChR-rich membranes were determined at 1 μM and 275 μM [<sup>3</sup>H]3-aziocanol. At both concentrations, [<sup>3</sup>H]3-aziocanol photoincorporated into all four nAChR subunits in the resting state. The incorporation of [<sup>3</sup>H]3-aziocanol into the α-subunit in the absence of agonist was mapped to two large proteolytic fragments, one, ~20 kD, containing the first three transmembrane segments and one, ~10 kD, containing the fourth transmembrane segment. In the presence of agonist, there was enhanced incorporation in the α-subunit that was mapped to the ~20 kD fragment of α, while the incorporation in the ~10 kD fragment was similar to that seen in the absence of other ligands. Further digestion of the 20 kD fragment showed a primary site of incorporation at αGlu-262, at the extracellular end of the αM2 segment, that was labeled preferentially in the desensitized state. In the absence of other drugs, [<sup>3</sup>H]3-aziocanol also photoincorporated into αTyr-190 and αTyr-198, residues within the binding site for agonists and competitive antagonists; this incorporation was blocked by the presence of carbamylcholine. No incorporation was attributable to the αM1 or αM3 segments. Digestion of the 10 kD fragment showed incorporation in the αM4 segment, at αHis-408 and αCys-412, residues known to be at the protein-lipid interface. These results indicate that the primary site of binding of 3-aziocanol is within the ion channel,

near the C-terminus of the  $\alpha$ M2 segment, with additional lower affinity interactions within the agonist binding site and at the protein-lipid interface.

## INTRODUCTION

In recent years, evidence for the direct interaction between general anesthetics and specific proteins has accumulated (Franks and Lieb, 1994). In particular, mutational analyses have identified amino acids in the inhibitory GABA<sub>A</sub> and glycine receptors as well as different positions within the nAChR which contribute to anesthetic action. Within the GABA<sub>A</sub> and glycine receptors, which, in general, are potentiated by general anesthetics, two residues, one in the M2 hydrophobic segment, the other in M3, are known to confer sensitivity to several classes of anesthetics, including long chain alcohols, volatile anesthetics (isoflurane and enflurane), and intravenous anesthetics (lorecleazole and etomidate) (Krasowski *et al.*, 1998; Mihic *et al.*, 1997; Wingrove *et al.*, 1994; McGurk *et al.*, 1998; Moody *et al.*, 1997; Belelli *et al.*, 1997; Ye *et al.*, 1998; Wick *et al.*, 1998). The position in M2, 15' based on numbering from the conserved positive charge at the N-terminus of M2 (lysine in nAChR, arginine in GABA<sub>A</sub> and glycine receptors), is located in the extracellular half of the M2 segment, on the face of the M2  $\alpha$ -helix opposite the lumen of the ion channel. The position in M3 is ~7 amino acids from the N-terminus of M3, but the orientation of this segment is not clearly established. However, the residue implicated in general anesthetic action on the GABA<sub>A</sub> and glycine receptors has been predicted to face the M2 helix, positioning it near the M2 15' residue (Wick *et al.*, 1998).

In contrast to the GABA<sub>A</sub> receptors, muscle and neuronal nAChR are inhibited by most general anesthetics. Single channel studies with long chain alcohols and other anesthetics, such as isoflurane, suggest that these anesthetics bind within the ion channel.

The open channel state in the presence of these drugs is characterized by flickering, similar to that seen with QX-222, an aromatic amine channel blocker (Dilger *et al.*, 1995). Site directed mutagenesis of the nAChR has shown that the nature of the residue at the M2 position 10', facing the lumen of the ion channel, can increase the potency of long chain alcohols and isoflurane as channel blockers (Forman *et al.*, 1995).

The residues implicated by the nAChR and GABA<sub>A</sub> receptor studies do not simply define a single, common binding site for long chain alcohols. Since alcohols potentiate most GABA<sub>A</sub> receptors but inhibit nAChRs, it is possible that long chain alcohols bind to different sites in the two receptors to exert their different actions. However, the sequence proximity of the positions in M2 that affect the binding of alcohols in the two receptors, only 5 amino acids apart, suggests that these positions both may affect a similar alcohol binding site, with one or both acting allosterically.

As an alternative to mutational analysis, the photoaffinity anesthetic 3-azioctanol was developed (Husain *et al.*, 1999) as a probe of the binding sites of long chain alcohols. This compound acts as an anesthetic in tadpoles, producing a loss of righting reflex with an EC<sub>50</sub> of ~160 μM, an EC<sub>50</sub> that is ~ 1/3 the potency of octanol. For the GABA<sub>A</sub> receptor, 3-azioctanol potentiates the response to submaximal concentrations of GABA, and inhibits agonist activation of muscle-type nAChR (IC<sub>50</sub> ~30 μM).

[<sup>3</sup>H]3-Azioctanol was used here as a photoaffinity probe to localize the sites of interaction of a long chain alcohol with *Torpedo* nAChR-rich membranes. Within the nAChR, incorporation was primarily within the α-subunit, with incorporation increased in the presence of agonist. The enhanced incorporation in the presence of agonist was within αGlu-262, at the C-terminus of αM2. In addition, [<sup>3</sup>H]3-azioctanol incorporated at lower efficiency into the αM4 segment, at equal levels in the presence and absence of

agonist, and in the absence of agonist, [<sup>3</sup>H]3-azioctanol also reacted with low efficiency with αTyr-190 and αTyr-198, residues implicated in the binding of agonist.

## **MATERIALS AND METHODS**

### **Materials**

nAChR-enriched membranes were isolated from *Torpedo californica* electric organ according to the method described by Sobel *et al.* (1977), modified as described by Pedersen *et al.* (1986). The final membrane suspensions were stored in 38% sucrose at -80 °C under argon. The membranes used here contained 0.5-2.0 nmol acetylcholine binding sites per milligram of protein. [<sup>3</sup>H]3-Azioctanol and nonradioactive 3-azioctanol were a kind gift from Dr. Keith Miller, synthesized as described in Husain *et al.* (1999). The specific activity of the [<sup>3</sup>H]3-azioctanol as prepared was ~11 Ci/mmol. This stock was stored at -20 °C in CH<sub>2</sub>Cl<sub>2</sub>, which was removed via evaporation immediately prior to the addition of membranes or isotopic dilution. For studies of incorporation at concentrations higher than 1 μM [<sup>3</sup>H]3-azioctanol, this stock was isotopically diluted with a stock of nonradioactive 3-azioctanol, 11 mM (concentration as reported in Husain, *et al.* (1999), based on the absorbance of 3-azioctanol at 350 nm) in *Torpedo* physiological saline (250 mM NaCl, 5 mM KCl, 3 mM CaCl<sub>2</sub>, 2 mM MgCl<sub>2</sub>, 5 mM sodium phosphate, pH 7.0; TPS), to a final specific activity of ~0.04 Ci/mmol. This dilution was prepared immediately before addition to membranes. *S. aureus* V8 protease was from ICN Biomedical Inc, EndoLysC from Boehringer Mannheim, phencyclidine (PCP) from Alltech Associates. Gallamine triethyl iodide was from Lederle, phenyltrimethylammonium (PTA) from Aldrich, and trifluoroacetic acid (TFA) was from Pierce. 1-Azidopyrene (1-AP) was purchased from Molecular Probes. 10% Genapol C-100 was from Calbiochem. Nicotine, d-tubocurarine (dTC), and carbamylcholine were

from Sigma. Pancuronium was from Organon;  $\alpha$ -bungarotoxin ( $\alpha$ BgTx) was purchased from Biotoxins, Inc.

### **Photoaffinity labeling of nAChR-enriched membranes with [<sup>3</sup>H]3-azioctanol**

For analytical labeling experiments, freshly thawed *Torpedo* membranes (100  $\mu$ g per condition) were diluted with TPS and pelleted (15000xg) for 30 minutes. The pellets were resuspended in TPS. Membrane aliquots were combined with [<sup>3</sup>H]3-azioctanol in the absence or presence of other ligands, as noted in the figure legends. The final membrane concentration was 2 mg/ml (~1  $\mu$ M nAChR). The final concentration of [<sup>3</sup>H]3-azioctanol was as noted in the figure legends. When one of the conditions contained  $\alpha$ BgTx, the samples were incubated for 2 hours in the dark at room temperature in glass vials; otherwise, the samples were irradiated within 3 minutes of the addition of drugs. The suspensions were irradiated at 365 nm (Spectroline lamp EN-16) for 10 minutes in a plastic 96-well plate on ice. The suspensions were diluted with sample loading buffer and directly submitted to SDS-PAGE.

For proteolytic mapping of [<sup>3</sup>H]3-azioctanol labeled  $\alpha$ -subunit with *S. aureus* V8 protease (Cleveland *et al.*, 1977; White and Cohen, 1992), labeling was carried out with 400  $\mu$ g (analytical mapping) or 10 mg (preparative) nAChR-rich *Torpedo* membranes. For analytical mapping, samples were photolyzed in a 24-well plate while for preparative mapping, the samples were photolyzed in glass screw-top vials with a stir bar. Following photolysis, the membrane suspensions were pelleted as described above. For analytical mapping, samples were resuspended in sample buffer and submitted to SDS-PAGE. For preparative mapping, samples were resuspended in TPS (2 mg/ml). The samples were labeled further with 1-azidopyrene (1-AP) (Blanton and Cohen, 1994) to ease identification and isolation of subunits and fragments from gels. 1-AP (62.5 mM in DMSO) was added to a final concentration of 500  $\mu$ M. After a 90 minute incubation, the

samples were photolyzed for 15 minutes on ice using a 365 nm lamp (Spectroline EN-16). Membranes were pelleted (15000xg) for 30 minutes, resuspended in sample buffer, and submitted to SDS-PAGE.

### **Gel Electrophoresis**

SDS-PAGE was performed as described by Laemmli (1970), modified as described by Pedersen *et al.* (1986). For analytical gels, the polypeptides were resolved on a 1 mm thick, 8% acrylamide gel and visualized by staining with Coomassie Blue (0.25% w/v in 45% methanol and 10% acetic acid). For autoradiography, the gels were impregnated with fluor (Amplify, Amersham), dried, and exposed at -80 °C to Kodak X-OMAT film for various times (6-8 weeks). Additionally, incorporation of  $^3\text{H}$  into individual polypeptides was quantified by scintillation counting of excised gel slices, as described in Middleton and Cohen (1991). For analytical V8 mapping gels, following electrophoresis, the gel was briefly stained with Coomassie Blue and destained to allow visualization of the subunits. The  $\alpha$ -subunits were then excised and placed directly into individual wells of a 1.5 mm mapping gel, composed of a 5 cm, 4.5% acrylamide stacking gel, and a 15 cm, 15% acrylamide separating gel. Into each well was added 1:1 gram subunit:gram *S. aureus* V8 protease in overlay buffer (5% sucrose, 125 mM Tris-HCl, 0.1% SDS, pH 6.8). The gel was run at 150V for two hours, and then the current was turned off for one hour. The gel was then run at constant current overnight until the dye front reached the end of the gel. The gel was stained, and the  $^3\text{H}$  was quantified by liquid scintillation. For preparative labelings, the polypeptides were resolved on a 1.5 mm, thick 8% acrylamide gel. The  $\alpha$ -subunit was identified in the 8% gels by 1-AP fluorescence, excised, and loaded directly onto the 1.5 mm mapping gels. The  $\alpha$ -subunit proteolytic fragments of ~20 kD ( $\alpha\text{V8-20}$ ) and ~10 kD ( $\alpha\text{V8-10}$ ) were identified by fluorescence and excised.

The region between  $\alpha$ V8-20 and  $\alpha$ V8-10 was excised to isolate  $\alpha$ V8-18. The excised proteolytic fragments were isolated by passive elution into 0.1 M  $\text{Na}_2\text{CO}_4$ , 0.1% SDS (Blanton and Cohen, 1994; Hager and Burgess, 1980). The eluate was filtered (Whatman No. 1) and concentrated using Millipore 5K concentrators. To remove excess SDS, acetone was added to the concentrate, and, following incubation at  $-20^\circ\text{C}$  overnight, the peptides were pelleted.

### **Proteolytic digestion:**

For EndoLysC digestion, acetone-precipitated peptides were resuspended in 15 mM Tris, pH 8.1, 0.1% SDS. EndoLysC (1.5 mU in resuspension buffer) was added to a final volume of 100  $\mu\text{l}$ . The digestion was allowed to proceed for 7-9 days before separation of fragments by HPLC. For *S. aureus* V8 protease digestion in solution, acetone precipitated peptides were resuspended in 15 mM Tris, pH 8.1, 0.1% SDS. V8 protease in resuspension buffer was added to a final concentration of 1:1 (w/w) and incubated at room temperature for 3-4 days before separation of fragments by HPLC. For trypsin digestion, acetone-precipitated peptides were resuspended in a small volume (40  $\mu\text{l}$ ) of 100 mM  $\text{NH}_4\text{CO}_3$ , 0.1% SDS, pH 7.8. Genapol C-100 and trypsin were added, with a final concentration of 0.02% SDS, 0.5% Genapol C-100, and 1:1 (w/w) trypsin. The digestion was allowed to proceed 3-4 days at room temperature prior to separation of the fragments by HPLC.

### **HPLC purification**

Proteolytic fragments from enzymatic digestion of [ $^3\text{H}$ ]3-azidoctanol labeled subunits were further purified by reverse-phase HPLC, as described by Blanton and Cohen (1992), using a Brownlee C4 Aquapore column (100 x 2.1 mm; 7  $\mu\text{m}$  particle size). Solvent A was

0.08% TFA in water, and solvent B was 0.05% TFA in 60% acetonitrile/40% 2-propanol. A nonlinear gradient (Waters Model 680 gradient controller, curve No. 7) from 25% to 100% solvent B in 80 minutes was used. The rate of flow was 0.2 ml/min, and 0.5 ml fractions were collected. The elution of peptides was monitored by absorbance at 215 nm, and the fluorescence from 1-AP was detected by fluorescence emission (357 nm excitation, 432 nm emission). Additionally, 25  $\mu$ L aliquots from the fractions were taken to determine the distribution of  $^3\text{H}$  by liquid scintillation counting.

$\alpha\text{V8-18}$  was purified by HPLC using solvents and gradients similar to those used by Cohen *et al.* (1991) to purify  $\alpha\text{V8-18}$  fragments, using a Brownlee C4 Aquapore column. Solvent A was 0.09% TFA in water, and solvent B was 0.1% TFA in acetonitrile. A linear gradient with several steps was used: 0 minutes, 10% solvent B; 10 minutes, 10% solvent B; 25 minutes, 25% solvent B; 45 minutes, 40% solvent B; 65 minutes 60% solvent B; 75 minutes, 100% solvent B. The rate of flow was 0.25 ml/min, and 0.5 ml fractions were collected. Measurements were determined as for the purification of the fragments of enzymatic digestion.

### **Sequence Analysis**

Automated amino terminal sequence analysis was performed on an Applied Biosystems Model 477A protein sequencer with an in-line 120A PTH analyzer. HPLC samples (450  $\mu$ l per fraction) were directly loaded onto chemically modified glass fiber disks (Beckman) in 20  $\mu$ l aliquots, allowing the solvent to evaporate at 40°C between loads. Sequencing was performed using gas-phase TFA to minimize possible hydrolysis. After conversion of the released amino acids to PTH amino acids, the suspension was divided into two parts. One portion, approximately one-third, went to the PTH analyzer while the remaining two-thirds was collected for scintillation counting. Yield of PTH amino acids was calculated from peak height compared with standards using the program Model 610A

Data Analysis Program Version 1.2.1. Initial yield and repetitive yield were calculated by a nonlinear least squares regression to the equation  $M=I_0 \cdot R^n$ , where M is the observed release,  $I_0$  is the initial yield, R is the repetitive yield, and n is the cycle number. PTH-derivatives known to have poor recovery (Ser, Arg, Cys, and His) were omitted from the fit.

Radioactivity incorporation in fragments and residues was quantified based on the results of sequence analysis. For the  $\alpha$ V8-20 and  $\alpha$ V8-10 fragments, approximately equal aliquots were subjected to either liquid scintillation counting or sequence analysis. These samples, since they contained SDS, were pre-treated on the sequencing filters for four minutes with gas-phase TFA, followed by a five minute wash with ethyl acetate. To estimate incorporation in large subunit fragments ( $\alpha$ V8-20 and  $\alpha$ V8-10) or in fragments isolated by HPLC, incorporation was calculated as the  $^3\text{H}$  loaded divided by three times the observed initial yield of the sequence (three times because only one-third of the PTH-amino acids were measured for mass calculations). Because even under favorable conditions less than 50% of the material loaded is sequenceable, this calculation is an overestimate. For incorporation at specific residues, the mass of that residue was calculated from the initial yield and repetitive yield. The increased  $^3\text{H}$  release in that cycle ( $\text{cpm}_n - \text{cpm}_{n-1}$ ) was divided by twice the mass of that cycle (twice since two-fold more PTH-amino acids were assayed for  $^3\text{H}$  than for mass). In this calculation, the radioactivity released and the mass levels reflect only the sequenced material.

## RESULTS

### **Photoincorporation of [ $^3\text{H}$ ]3-Aziotanol into nAChR-Rich Membranes.**

Initial experiments were designed to characterize the general pattern of photoincorporation of [ $^3\text{H}$ ]3-aziotanol and to test the sensitivity of photoincorporation to

various ligands. For these initial experiments, two concentrations of [<sup>3</sup>H]3-azioctanol were used, 1 μM (11 Ci/mmol) and 275 μM (0.04 Ci/mmol). The IC<sub>50</sub> of 3-azioctanol is ~30 μM. Therefore, 1 μM [<sup>3</sup>H]3-azioctanol was well below the concentration necessary for inhibition of 50% of the nAChR, while 275 μM [<sup>3</sup>H]3-azioctanol was a concentration sufficient to produce greater than 50% inhibition. Isotopic dilution of [<sup>3</sup>H]3-azioctanol resulted in the presence of similar levels of <sup>3</sup>H in the samples containing 1 μM and 275 μM [<sup>3</sup>H]3-azioctanol. Membranes (2 mg of protein/mL) were equilibrated with [<sup>3</sup>H]3-azioctanol in the presence and absence of 2 mM carbamylcholine. After irradiation for 10 minutes at 365 nm, the pattern of incorporation was assessed by SDS-PAGE followed by fluorography or scintillation counting of gel slices.

As seen in the fluorograph of the 8% polyacrylamide gel (Figure 3-1A), at both [<sup>3</sup>H]3-azioctanol concentrations, in the absence of carbamylcholine the principal polypeptide labeled was a 34 kD polypeptide, identified as a mitochondrial chloride channel (VDAC) (Blanton *et al.*, 1998a). Of the nAChR subunits, α was labeled most strongly. The labeled band at 43 kD contained rapsyn, a peripheral polypeptide associated with the cytoplasmic aspect of the nAChR (Carr *et al.*, 1987). Incorporation of [<sup>3</sup>H]3-azioctanol into the α-subunit was dependent on the conformational state of the nAChR, as the presence of agonist resulted in enhanced incorporation into the α-subunit, but not in non-nAChR polypeptides. Based on scintillation counting of excised gel slices, the increase in incorporation was, on average, ~5-fold at 1 μM [<sup>3</sup>H]3-azioctanol (Figure 3-1B), and ~3-fold at 275 μM. The presence of agonist also increased the incorporation in the β-subunit, though only by ~1.4-fold at 1 μM. The radioactivity incorporation at two non-receptor polypeptides, rapsyn (43K), and the α-subunit of Na<sup>+</sup>/K<sup>+</sup> ATPase (αNK), was not altered by the presence of carbamylcholine and appeared similar at 1 μM and 275 μM [<sup>3</sup>H]3-azioctanol. Since the [<sup>3</sup>H]3-azioctanol at 275 μM had an ~275-fold

lower specific activity, the observed similarity in the  $^3\text{H}$  incorporation in the  $\alpha$ -subunit at the two conditions indicated that the  $\alpha$ -subunit labeled in the presence of  $275\ \mu\text{M}$  [ $^3\text{H}$ ]3-azioctanol contained  $\sim 275$ -fold more moles of 3-azioctanol per mol subunit.

The dependence of the incorporation of [ $^3\text{H}$ ]3-azioctanol on the time of photolysis was measured over a range of time in the presence of carbamylcholine (Figure 3-2). For short photolyses, the incorporation increased approximately linearly, while at 20 minutes the incorporation in the  $\alpha$ -subunit in the presence of carbamylcholine appeared to saturate. The incorporation in the  $\alpha$ -subunit in the presence of carbamylcholine without irradiation was 4% the levels seen following 10 minutes irradiation. For the remainder of the experiments, the photolysis was carried out for 10 minutes.

The concentration dependence for the enhancement of [ $^3\text{H}$ ]3-azioctanol photolabeling by carbamylcholine (Figure 3-3) as well as the effects of other cholinergic agonists and competitive antagonists (Figure 3-4) was determined by quantification of  $^3\text{H}$  incorporation in gel slices. The data for the concentration dependence of carbamylcholine was well fit by a single binding site, with a  $K=4\ \mu\text{M}$ . While this value for the concentration of carbamylcholine producing 50% enhancement was higher than the directly measured  $K_{\text{eq}}$  of  $0.1\ \mu\text{M}$  (Boyd and Cohen, 1980b), this was not unexpected, since the photolabeling experiment was carried out at a concentration of ACh sites of  $2.2\ \mu\text{M}$ . At concentrations sufficient to fully occupy the ACh site, the agonists phenyltrimethylammonium (PTA) and nicotine increased [ $^3\text{H}$ ]3-azioctanol photoincorporation in the  $\alpha$ -subunit to the same extent as carbamylcholine (Figure 3-4). The presence of the competitive antagonists dTC and gallamine, known to partially desensitize the receptor (Pedersen and Papineni, 1995; Medynski, 1983), resulted in incorporation in  $\alpha$ -subunit  $\sim 60\%$  of that seen in the presence of carbamylcholine, while for pancuronium, a competitive antagonist which is not known to desensitize the receptor,

[<sup>3</sup>H]3-azidoctanol incorporation in the  $\alpha$ -subunit was similar to that seen in the absence of carbamylcholine. No effect of these cholinergic drugs was seen on the incorporation of [<sup>3</sup>H]3-azidoctanol into non-nAChR polypeptides including rapsyn (43 kD), calectrin (37 kD), or the Na<sup>+</sup>/K<sup>+</sup> ATPase  $\alpha$ -subunit (not shown).

The effects of several noncompetitive antagonists on the incorporation of [<sup>3</sup>H]3-azidoctanol at 1  $\mu$ M were also tested (Figure 3-5A,B). For membranes equilibrated with carbamylcholine, the <sup>3</sup>H incorporation in  $\alpha$  was insensitive to the presence of 1 mM octanol. At 100  $\mu$ M, meproadifen, an aromatic amine noncompetitive antagonist, reduced the incorporation by ~50%. Two other aromatic amine noncompetitive antagonists, phencyclidine (PCP) and QX-222, failed to inhibit the incorporation of [<sup>3</sup>H]3-azidoctanol in the  $\alpha$ -subunit (Figure 3-5B). The presence of noncompetitive antagonists did not affect the incorporation in the other nAChR subunits (not shown) nor the incorporation in non-nAChR polypeptides, including rapsyn (43 kD), VDAC (34 kD), and calectrin (37 kD) (not shown).

The effects of meproadifen were also studied in the presence of 275  $\mu$ M [<sup>3</sup>H]3-azidoctanol (Figure 3-5C). At that concentration the presence of carbamylcholine resulted in a ~3-fold increase in the incorporation of [<sup>3</sup>H]3-azidoctanol in the  $\alpha$ -subunit over that seen in the absence of carbamylcholine. In the presence of carbamylcholine, meproadifen reduced the incorporation by ~50%. In the absence of carbamylcholine, meproadifen actually enhanced the [<sup>3</sup>H]3-azidoctanol incorporation. In the presence of  $\alpha$ BgTx, meproadifen did not alter the [<sup>3</sup>H]3-azidoctanol incorporation in the  $\alpha$ -subunit. The incorporation in rapsyn (43 kD) was not affected by the presence of these cholinergic drugs.

The incorporation of [<sup>3</sup>H]3-azidoctanol in nAChR  $\alpha$ -subunit was measured over a range of [<sup>3</sup>H]3-azidoctanol concentrations, using a constant specific activity of [<sup>3</sup>H]3-

azioctanol (Figure 3-6). The incorporation in the Na<sup>+</sup>/K<sup>+</sup> ATPase  $\alpha$ -subunit (open symbols) increased linearly across the range of concentrations tested and was not affected by the presence of cholinergic drugs. For membranes equilibrated with carbamylcholine, the incorporation in the  $\alpha$ -subunit increased nearly linearly up to ~ 1 mM and then appeared to saturate. At all concentrations, the incorporation in the presence of  $\alpha$ BgTx was less than that seen in the absence of added drugs, though at ~2 mM the incorporation in the presence of  $\alpha$ BgTx was similar to that seen in the presence of carbamylcholine. In the absence of drug, the incorporation appeared to increase nearly linearly up to 1 mM, and then the incorporation increased sharply, surpassing the incorporation in the presence of carbamylcholine at 2 mM. However, the higher incorporation in the absence of carbamylcholine showed high variability. The total <sup>3</sup>H incorporation at ~ 2 mM [<sup>3</sup>H]3-azioctanol was ~0.25 mol [<sup>3</sup>H]3-azioctanol/mol  $\alpha$ , based on the reported counting efficiency (25%) of the toluene-based gel cocktail used (Middleton and Cohen, 1991).

### **Mapping of [<sup>3</sup>H]3-azioctanol photoincorporation into $\alpha$ -subunit proteolytic fragments**

The distribution of [<sup>3</sup>H]3-azioctanol incorporation within the  $\alpha$ -subunit was examined by digestion of the labeled subunit with *S. aureus* V8 protease under conditions which are known to generate four large, non-overlapping fragments resolvable by SDS-PAGE (Figure 3-7A). The largest fragment, a 20 kD peptide ( $\alpha$ V8-20<sup>1</sup>), begins at  $\alpha$ Ser-

---

<sup>1</sup> Staining of the mapping gel with Coomassie Blue revealed the four expected proteolytic fragments in all conditions. Additionally, a band was present at ~22 kD in the conditioned labeled with 275  $\mu$ M [<sup>3</sup>H]3-azioctanol in the presence of carbamylcholine (not shown). This band was excised from this condition, and this region was also excised in the other conditions. This band was assumed to be  $\alpha$ V8-20 that was highly labeled with [<sup>3</sup>H]3-azioctanol, resulting in reduced mobility. Therefore, the <sup>3</sup>H present in this region was attributed to labeling in  $\alpha$ V8-20 and was added to that of the  $\alpha$ V8-20 band.

173 and contains the first three membrane spanning regions,  $\alpha$ M1,  $\alpha$ M2, and  $\alpha$ M3 (Pedersen *et al.*, 1986). The 10 kD peptide ( $\alpha$ V8-10) contains the fourth membrane spanning region,  $\alpha$ M4, and begins at  $\alpha$ Asn-339. The 18 kD ( $\alpha$ V8-18) and 4 kD ( $\alpha$ V8-4) peptides begin at  $\alpha$ Val-46 and  $\alpha$ Ser-1, respectively. Membranes labeled with [ $^3$ H]3-azidoctanol were subjected to SDS-PAGE, and the  $\alpha$ -subunit was excised. This gel piece was loaded onto a mapping gel along with V8 protease. The  $\alpha$ -subunit was cleaved in the gel with the protease, and the fragments were separated on the gel. Again, like the studies of the incorporation in the intact subunits, the incorporation was measured at both 1  $\mu$ M and 275  $\mu$ M [ $^3$ H]3-azidoctanol. Similar levels of  $^3$ H were used at the two concentrations, with a specific activity of 11 Ci/mmol at 1  $\mu$ M and 0.04 Ci/mmol at 275  $\mu$ M, resulting in a  $\sim$ 275-fold reduction in specific activity in the samples labeled in the presence of 275  $\mu$ M [ $^3$ H]3-azidoctanol compared to those labeled in the 1  $\mu$ M condition. Based on liquid scintillation counting of these  $\alpha$ -subunit proteolytic fragments, the main sites of photoincorporation in the absence of agonist were within the  $\alpha$ V8-20 and  $\alpha$ V8-10 fragments (Figure 3-7B). The  $^3$ H incorporation in each fragment was similar at both concentrations of [ $^3$ H]3-azidoctanol. In the absence of agonist, the incorporation in  $\alpha$ V8-10 was  $\sim$ 60% that of  $\alpha$ V8-20. The addition of agonist increased the labeling of the  $\alpha$ V8-20 fragment, nine-fold at 1  $\mu$ M and five-fold at 275  $\mu$ M, while the  $^3$ H incorporated in  $\alpha$ V8-10 was unchanged by the presence of carbamylcholine. In the presence of carbamylcholine, the incorporation in  $\alpha$ V8-20 accounted for  $\sim$ 90% of the incorporation at both [ $^3$ H]3-azidoctanol concentrations, while  $\alpha$ V8-10 contained  $\sim$ 6% of the total [ $^3$ H]3-azidoctanol incorporation within the  $\alpha$ -subunit fragments. The similar levels of  $^3$ H incorporation in the fragments between the two concentrations, with [ $^3$ H]3-azidoctanol at an  $\sim$ 275-fold lower specific activity at 275  $\mu$ M, indicated that  $\sim$ 275-fold more molecules

of 3-azidoctanol were incorporated at 275  $\mu\text{M}$  [ $^3\text{H}$ ]3-azidoctanol. In all conditions, the incorporation in  $\alpha\text{V8-18}$  and  $\alpha\text{V8-4}$  was unchanged and lower than the incorporation in  $\alpha\text{V8-10}$ .

The carbamylcholine-dependent labeling of nAChR with [ $^3\text{H}$ ]3-azidoctanol was in the  $\alpha\text{V8-20}$  fragment containing  $\alpha\text{M1}$ ,  $\alpha\text{M2}$ , and  $\alpha\text{M3}$ . To further localize the site of labeling, 10 mg of membranes were labeled with 1  $\mu\text{M}$  or 275  $\mu\text{M}$  [ $^3\text{H}$ ]3-azidoctanol in the presence or absence of carbamylcholine, meproadifen, or  $\alpha\text{BgTx}$ . Additionally, these membranes were labeled with 1-azidopyrene, a fluorescent compound that photoincorporates in transmembrane segments, to aid in the localization of transmembrane segments. Following the digestion of  $\alpha$ -subunit with V8 protease, the  $\alpha\text{V8-20}$ ,  $\alpha\text{V8-18}$ , and  $\alpha\text{V8-10}$  fragments were excised and eluted. To quantify the  $^3\text{H}$  incorporation, the eluted  $\alpha\text{V8-20}$  and  $\alpha\text{V8-10}$  fragments were subjected to sequence analysis. Based on sequence analysis of the fragments, at 1  $\mu\text{M}$  [ $^3\text{H}$ ]3-azidoctanol, in the absence of carbamylcholine  $\sim 0.008$  moles of [ $^3\text{H}$ ]3-azidoctanol incorporated into a mole of  $\alpha\text{V8-20}$ , and  $\sim 0.004$  moles into  $\alpha\text{V8-10}$ . In the presence of carbamylcholine, 0.06 moles incorporated into  $\alpha\text{V8-20}$  and 0.004 moles into  $\alpha\text{V8-10}$ . At 275  $\mu\text{M}$  [ $^3\text{H}$ ]3-azidoctanol, the incorporation increased, with  $\sim 0.55$  moles incorporated per mole of  $\alpha\text{V8-20}$  and 0.24 moles per mole  $\alpha\text{V8-10}$  in the absence of carbamylcholine. In the presence of carbamylcholine at 275  $\mu\text{M}$  [ $^3\text{H}$ ]3-azidoctanol,  $\sim 1.3$  moles [ $^3\text{H}$ ]3-azidoctanol incorporated into  $\alpha\text{V8-20}$  and  $\sim 0.40$  moles into  $\alpha\text{V8-10}$ .

## Localization of the sites of incorporation of [<sup>3</sup>H]3-azioctanol in αV8-20 segment

### M2

To determine if there was incorporation in the αM2 segment, the eluted αV8-20 fragment, labeled with [<sup>3</sup>H]3-azioctanol, was digested with EndoLysC. Digestion with EndoLysC is known to create a ~10 kD fragment starting at αMet-243, the N-terminus of the αM2 segment, that can be purified by reverse-phase HPLC (Pedersen *et al.*, 1992), previous chapter). When the EndoLysC-digested αV8-20 which had been labeled with 275 μM [<sup>3</sup>H]3-azioctanol in the presence of carbamylcholine was fractionated by reverse-phase HPLC, ~80% of the <sup>3</sup>H eluted in a peak centered at fraction 33 (~88% organic) (Figure 3-8A). For the samples labeled in the presence of αBgTx or the absence of other drugs, the <sup>3</sup>H in fraction 33 was only ~20% that seen for the sample labeled in the presence of carbamylcholine.

For each labeling condition, fraction 33, which contained the peak of <sup>3</sup>H from the sample labeled in the presence of carbamylcholine, was subjected to Edman degradation (Figure 3-8B) which showed that the only sequence present was that beginning at αMet-243 (-carb: I<sub>0</sub>=23 pmol; +carb: I<sub>0</sub>=30 pmol). No other sequences were present at more than 10% the mass of the peptide beginning at αMet-243. For the sample labeled in the presence of carbamylcholine, there was a peak of <sup>3</sup>H release in cycle 20, corresponding to incorporation at αGlu-262, and that release was reduced by ~60% in the sample labeled in the absence of carbamylcholine or in the presence of αBgTx (not shown). Based upon the <sup>3</sup>H release in cycle 20, in the presence of carbamylcholine, there were ~0.33 mol [<sup>3</sup>H]3-azioctanol incorporated per mol αGlu-262. In the absence of other drugs or the presence of αBgTx, there were ~0.14 mol [<sup>3</sup>H]3-azioctanol incorporated per mol αGlu-262.

The HPLC profile of the EndoLysC-digest of  $\alpha$ V8-20 labeled in the presence of 1  $\mu$ M [ $^3$ H]3-azioctanol was similar to that at 275  $\mu$ M (not shown). For the sample labeled in the presence of carbamylcholine, ~70% of the  $^3$ H eluted as a single peak at ~90% organic. As with fraction 33 from the sample labeled in the presence of 275  $\mu$ M [ $^3$ H]3-azioctanol, sequence analysis of the fraction containing the peak of  $^3$ H from the samples labeled with 1  $\mu$ M [ $^3$ H]3-azioctanol revealed the presence of a single sequence beginning at  $\alpha$ Met-243 with release of  $^3$ H in cycle 20 (not shown). In the presence of carbamylcholine, the release in cycle 20 was equivalent to 0.06 mol per mol  $\alpha$ Glu-262, and that labeling was reduced by ~75% for the sample labeled in the presence of meproadiifen and carbamylcholine (0.014 mol [ $^3$ H]3-azioctanol per mol  $\alpha$ Glu-262). In the absence of carbamylcholine, the incorporation of [ $^3$ H]3-azioctanol at  $\alpha$ Glu-262 (0.0012 mol [ $^3$ H]3-azioctanol incorporated per mol  $\alpha$ Glu-262) was ~2% that seen in the presence of carbamylcholine.

#### Agonist site

For the  $\alpha$ V8-20 labeled with either 1  $\mu$ M or 275  $\mu$ M [ $^3$ H]3-azioctanol in the absence of carbamylcholine, the HPLC chromatogram of the EndoLysC digest of  $\alpha$ V8-20 (Figure 3-8A) contained a peak of  $^3$ H at fraction 29 (69% organic) in addition to the peak at fraction 33. When the material in fraction 29 was sequenced, the primary sequence began at  $\alpha$ His-186 (-carb:  $I_0=35$  pmol; + $\alpha$ BgTx:  $I_0=55$  pmol; +carb:  $I_0=36$  pmol) (Figure 3-8C). This fragment contains residues contributing to the ACh site ( $\alpha$ 190-200) as well as the  $\alpha$ M1 segment, since there is no lysine between  $\alpha$ His-186 and  $\alpha$ Lys-242, prior to  $\alpha$ M2. At 275  $\mu$ M [ $^3$ H]3-azioctanol,  $^3$ H release was evident in cycles 5 and 13 for the fragment labeled in the absence of carbamylcholine but not for the samples labeled in the presence of carbamylcholine or  $\alpha$ BgTx. Release of  $^3$ H in these cycles correspond to

$\alpha$ Tyr-190 and  $\alpha$ Tyr-198, residues known to contribute to the agonist binding site (Chiara and Cohen, 1997; Middleton and Cohen, 1991; Dennis *et al.*, 1988; Sine *et al.*, 1994; Tomaselli *et al.*, 1991). The amount of incorporation in these residues was ~10% that in  $\alpha$ Glu-262 in the absence of carbamylcholine, with [ $^3$ H]3-azioctanol only incorporating at ~0.013 mol per mol  $\alpha$ Tyr-190 and ~0.017 mol per mol  $\alpha$ Tyr-198. A similar pattern of release, though with lower levels of  $^3$ H incorporation, was seen in the sample labeled with 1  $\mu$ M [ $^3$ H]3-azioctanol in the absence of carbamylcholine (see Table 3-1 in Discussion). In the presence of carbamylcholine, while there was no release in cycle 5 or 13, there was release evident in cycle 3, which, if originating from the fragment beginning at  $\alpha$ His-186, indicated ~0.003 mol incorporated per mol  $\alpha$ Val-189.

### M1 and M3

As seen in Figure 3-8, EndoLysC digestion of  $\alpha$ V8-20 generated two fragments, one beginning at  $\alpha$ Met-243 and one beginning at  $\alpha$ His-186, which were separated by HPLC (Figure 3-8A) and sequenced (Figure 3-8B). The fragment beginning at  $\alpha$ His-186, which eluted in fraction 29, contained residues contributing to the agonist site as well as the  $\alpha$ M1 segment. Based on the radioactivity in the fragment and the mass levels sequenced, this fragment from the sample labeled at 275  $\mu$ M [ $^3$ H]3-azioctanol in the presence of carbamylcholine contained ~0.05 mol incorporated per mol fragment, ~4% that in the major radiolabeled fragment, recovered in fraction 33, that contained the  $\alpha$ M2 and  $\alpha$ M3 segments. Therefore, if there is any incorporation within the  $\alpha$ M1 segment, it was less than 4% of the level of the incorporation in the  $\alpha$ M2 segment.

Solution digestion of  $\alpha$ V8-20 with V8 protease generates a ~9 kD fragment beginning at  $\alpha$ Leu-263, the N-terminus of the  $\alpha$ M2-M3 linker and containing the  $\alpha$ M3 segment (Blanton and Cohen, 1994). To determine if [ $^3$ H]3-azioctanol incorporated into

the  $\alpha$ M3 segment,  $\alpha$ V8-20 labeled with 275  $\mu$ M [ $^3$ H]3-azidoctanol was digested with V8 protease, and the fragments were separated by HPLC (Figure 3-9). V8 protease cleaves at the C-terminal side of glutamates, and in order to generate the fragment beginning at  $\alpha$ Leu-263, cleavage must occur at  $\alpha$ Glu-262, which is labeled by [ $^3$ H]3-azidoctanol. Therefore, it was expected that only fragments not labeled at  $\alpha$ Glu-262 would be digested to generate the fragment beginning at  $\alpha$ Leu-263. In the sample labeled in the presence of carbamylcholine, ~85% of the  $^3$ H eluted at fraction 33 (Figure 3-9, inset). This fraction, based on sequence analysis, contained a fragment beginning at the N-terminus of  $\alpha$ V8-20, and, based on the high levels of  $^3$ H in the fraction, this fragment should have contained the  $\alpha$ M2 segment. The fragment beginning at  $\alpha$ Leu-263 was expected to elute at ~55% organic (Blanton and Cohen, 1994). A small peak of  $^3$ H was present in fraction 23 (~50% organic), and one half of this fraction from each condition was subjected to Edman degradation (not shown). Two sequences were present, one the fragment beginning at  $\alpha$ Leu-263 (-carb:  $I_0=4.8$  pmol; + $\alpha$ BgTx:  $I_0=3.4$  pmol; +carb:  $I_0=1.5$  pmol) as well as a fragment beginning at  $\alpha$ Thr-52 (-carb:  $I_0=72$  pmol; + $\alpha$ BgTx:  $I_0=24$  pmol; +carb:  $I_0=37$  pmol), an N-terminus of the  $\alpha$ V8-18 fragment, arising from contamination of the  $\alpha$ V8-20 sample with  $\alpha$ V8-18. Based upon the mass levels present, if the  $^3$ H in this fraction were attributable only to the sequence beginning at  $\alpha$ Leu-263, then, in the presence of carbamylcholine, 0.08 mol [ $^3$ H]3-azidoctanol incorporated per mol fragment, ~6% of the incorporation in the fragment beginning at  $\alpha$ Met-243. Therefore, the  $\alpha$ M3 segment was labeled at less than 6% the levels of incorporation in the  $\alpha$ M2 segment.

### **Incorporation of [ $^3$ H]3-azidoctanol into $\alpha$ V8-18**

To characterize the levels of incorporation in the  $\alpha$ V8-18 fragment compared to the incorporation in  $\alpha$ V8-20,  $\alpha$ V8-18 was purified by reverse-phase HPLC (Figure

3-10A). A peak of  $^3\text{H}$  eluted at fraction 23, as well as in two hydrophobic peaks. The hydrophobic peaks corresponded to contamination by  $\alpha\text{V8-20}$ . Sequence analysis of fraction 23 showed two sequences present at similar levels, one beginning at  $\alpha\text{Val-46}$  (–carb:  $I_0=41$  pmol; + $\alpha\text{BgTx}$ :  $I_0=19$  pmol; +carb:  $I_0=32$  pmol) and the other beginning at  $\alpha\text{Thr-52}$  (–carb:  $I_0=38$  pmol; + $\alpha\text{BgTx}$ :  $I_0=24$  pmol; +carb:  $I_0=31$  pmol) (Figure 3-10B). These two peptides are the known N-termini of  $\alpha\text{V8-18}$ . Radioactivity release was evident in the 6th cycle. Since these two sequences were present at similar levels, however, it was unclear to which sequence the release was attributable. Similar levels of release were seen in the presence or absence of carbamylcholine or  $\alpha\text{BgTx}$ . The residue, either  $\alpha\text{Glu-51}$  or  $\alpha\text{Arg-57}$ , was labeled by  $\sim 0.003$  mol [ $^3\text{H}$ ]3-azioctanol per mol residue.

Additional incorporation is also present within  $\alpha\text{V8-18}$ , though at an undetermined site(s). EndoLysC digestion of  $\alpha\text{V8-18}$  followed by HPLC separation showed a peak of  $^3\text{H}$  that contained a single sequence, that beginning at Lys-77 (–carb  $I_0=22$  pmol, + $\alpha\text{BgTx}$   $I_0=15$  pmol, +carb  $I_0=13$  pmol) (not shown). The fragment showed  $\sim 10\%$  incorporation in each of the three conditions. Based on the radioactivity released in the cycle containing  $\alpha\text{Tyr-93}$ , a residue contributing to the agonist binding site, this position is labeled by less than  $0.00003$  mol [ $^3\text{H}$ ]3-azioctanol per mol residue (not shown).

### **Localization of the sites of incorporation of [ $^3\text{H}$ ]3-azioctanol in $\alpha\text{V8-10}$**

At  $275$   $\mu\text{M}$  [ $^3\text{H}$ ]3-azioctanol, the  $\alpha\text{V8-10}$  fragment labeled in the presence or absence of other cholinergic drugs showed similar levels of  $^3\text{H}$  incorporation. Additionally, the levels of incorporation in  $\alpha\text{V8-10}$  labeled with  $1$   $\mu\text{M}$  [ $^3\text{H}$ ]3-azioctanol were similar in the presence and absence of other drugs. HPLC purification of  $\alpha\text{V8-10}$

labeled with 275  $\mu\text{M}$  [ $^3\text{H}$ ]3-azidoctanol revealed that ~60% of the incorporated  $^3\text{H}$  eluted in the flow-through (Figure 3-11A, inset), while only ~20% eluted in a broad peak between fractions 32-35, where intact  $\alpha\text{V8-10}$  was known to elute (Blanton and Cohen, 1992). Sequence analysis confirmed the presence of  $\alpha\text{V8-10}$  in these fractions. The presence of  $^3\text{H}$  in the flow-through indicated that most of the [ $^3\text{H}$ ]3-azidoctanol incorporated into  $\alpha\text{V8-10}$  was not stably incorporated under the conditions of HPLC.

To localize the  $^3\text{H}$  incorporation within  $\alpha\text{V8-10}$  that is stably incorporated, [ $^3\text{H}$ ]3-azidoctanol labeled  $\alpha\text{V8-10}$  that had been eluted from gel was digested with trypsin, under conditions known to cleave the fragment at  $\alpha\text{Arg-400}$  (Blanton and Cohen, 1992). HPLC purification of the digest showed the major peak of  $^3\text{H}$  in the flow-through, as well as a peak of  $^3\text{H}$  at fractions 30-33 (Figure 3-11A). Based upon the  $^3\text{H}$  elution profile seen when intact  $\alpha\text{V8-10}$  was purified by HPLC, the  $^3\text{H}$  in the flow-through, ~60% of the eluted  $^3\text{H}$ , was assumed to result from [ $^3\text{H}$ ]3-azidoctanol incorporation which was unstable to HPLC conditions. The  $^3\text{H}$  present between fractions 30-33 accounted for ~15% of the total eluted  $^3\text{H}$ . Sequence analysis of the pooled fractions 30-33 showed the presence of a primary sequence beginning at  $\alpha\text{Tyr-401}$  (-carb:  $I_0=502$  pmol; + $\alpha\text{BgTx}$ :  $I_0=457$  pmol; +carb:  $I_0=423$  pmol), near the beginning of  $\alpha\text{M4}$ , along with a secondary sequence beginning at  $\alpha\text{Ser-388}$  (-carb:  $I_0=68$  pmol; + $\alpha\text{BgTx}$ :  $I_0=70$  pmol; +carb:  $I_0=72$  pmol) (Figure 3-11B). In all conditions tested,  $^3\text{H}$  release was observed in cycles 8 and 12, indicating incorporation in  $\alpha\text{His-408}$  and  $\alpha\text{Cys-412}$ . Additional low level release was seen reproducibly in cycle 3, corresponding to  $\alpha\text{Ala-403}$ . [ $^3\text{H}$ ]3-Azidoctanol incorporated into  $\alpha\text{His-408}$  and  $\alpha\text{Cys-412}$  at ~0.0025 mol per mol residue at 275  $\mu\text{M}$ , at ~1% that level at 1  $\mu\text{M}$ . However, at both concentrations most of the  $^3\text{H}$  eluted with the flow-through of the HPLC, and this  $^3\text{H}$  could have been incorporated into these residues but labile under HPLC conditions. Alternatively, there could have been another residue or

residues in  $\alpha$ V8-10 that were labeled more prominently, but the incorporation at this site(s) was highly labile under the conditions of HPLC.

## DISCUSSION

[<sup>3</sup>H]3-Aziotanol photoincorporates with high efficiency into the  $\alpha$ -subunit of the nAChR, with the primary site of incorporation being  $\alpha$ Glu-262, within the ion channel at the extracellular end of  $\alpha$ M2. Additional incorporation was present in the  $\alpha$ M4 segment, at  $\alpha$ His-408 and  $\alpha$ Cys-412, and in the agonist binding site, at  $\alpha$ Tyr-190 and  $\alpha$ Tyr-198, as well as minor incorporation elsewhere. While the incorporation in  $\alpha$ M4 was independent of the presence of other drugs, the incorporation at  $\alpha$ Glu-262 increased for nAChR in the desensitized state, while incorporation at  $\alpha$ Tyr-190/ $\alpha$ Tyr-198 was seen only in the absence of carbamylcholine or  $\alpha$ BgTx.

When labeling was analyzed at the level of the subunit, the most prominent pharmacology of labeling was the dependence of the  $\alpha$ -subunit incorporation on the presence of carbamylcholine. This increased incorporation was due to the desensitization of the nAChR since other agonists also increased the incorporation, while the incorporation was lowest in the presence of pancuronium or  $\alpha$ BgTx. The competitive antagonists dTC and gallamine caused only a partial increase in the incorporation in the  $\alpha$ -subunit. Sequence analysis showed that the increased photoincorporation in the presence of carbamylcholine was due to increased incorporation at  $\alpha$ Glu-262, at the C-terminus of  $\alpha$ M2. The incorporation of 1  $\mu$ M [<sup>3</sup>H]3-aziotanol at  $\alpha$ Glu-262 in the absence of carbamylcholine or  $\alpha$ BgTx was ~2% the incorporation in the presence of carbamylcholine, likely due to the fact that even in the absence of agonist ~10% of the nAChR are in the desensitized state in isolated *Torpedo* membranes (Boyd, 1994).

While the primary pharmacology observed at the level of the intact subunit was the increased incorporation in the presence of carbamylcholine, attributable to increased incorporation at  $\alpha$ Glu-262, analysis of subunit fragments revealed that there was also photolabeling of  $\alpha$ Tyr-190 and  $\alpha$ Tyr-198 inhibitable by the presence of carbamylcholine or  $\alpha$ BgTx. These residues have both been labeled previously by competitive antagonists, such as [ $^3$ H]d-tubocurare (Chiara and Cohen, 1997) and DDF (Dennis *et al.*, 1988), and agonists, such as [ $^3$ H]nicotine (Middleton and Cohen, 1991). The efficiency of incorporation in these residues, 0.012% of Tyr-190 labeled at 1  $\mu$ M and 1.3% labeled at 275  $\mu$ M [ $^3$ H]3-azioctanol, was lower than the incorporation in  $\alpha$ Glu-262 even in the absence of carbamylcholine, 0.12% at 1  $\mu$ M and 14% at 275  $\mu$ M [ $^3$ H]3-azioctanol. The inhibition of this incorporation by the presence of carbamylcholine or  $\alpha$ BgTx established that the occupancy of the agonist binding site prevented the accessibility of [ $^3$ H]3-azioctanol to these side chains.

In the presence of carbamylcholine, the aromatic amine noncompetitive antagonist meproadifen partially inhibited the incorporation in the  $\alpha$ -subunit, although two other aromatic amine noncompetitive antagonists, PCP and QX-222, did not. The presence of meproadifen resulted in an ~60% inhibition in the incorporation at the subunit level, as well as an ~70% inhibition at  $\alpha$ Glu-262. This residue was also labeled by [ $^3$ H]meproadifen mustard (Pedersen and Cohen, 1990). While charged noncompetitive antagonists fully inhibit the incorporation of [ $^3$ H]meproadifen mustard, indicating that these drugs bind in a mutually exclusive manner, it is not known whether a charged and an uncharged noncompetitive antagonist can bind the channel simultaneously. Therefore, further studies of the binding of these noncompetitive antagonists are necessary before the partial inhibition of the incorporation can be clearly understood.

Although the photoincorporation of most drugs studied which photoincorporate into residues in M2 in the ion channel domain, including [<sup>3</sup>H]chlorpromazine, [<sup>3</sup>H]triphethylphosphonium, [<sup>125</sup>I]TID, and [<sup>3</sup>H]tetracaine, are inhibited by the presence of high concentrations of the nonradioactive analog, the presence of 1 mM octanol did not inhibit the incorporation of 1 μM [<sup>3</sup>H]3-azioctanol in the α-subunit in the presence of carbamylcholine. However, if octanol behaves similarly to 3-azioctanol, this result is not unexpected. As shown in Figure 3-6, the incorporation of [<sup>3</sup>H]3-azioctanol in the α-subunit in the presence of carbamylcholine increased approximately linearly up to ~1.5 mM [<sup>3</sup>H]3-azioctanol. This linearity indicates a lack of saturation of [<sup>3</sup>H]3-azioctanol incorporation in the entire subunit (although the incorporation at certain sites may have been saturated). Therefore, if the concentration of [<sup>3</sup>H]3-azioctanol were held constant while the concentration of non-radioactive 3-azioctanol was increased, then the incorporation of [<sup>3</sup>H]3-azioctanol would appear constant in this range (for example, see Figure 3-1). While 1 mM octanol would be expected to inhibit the incorporation at sites that were fully bound below 1 mM octanol, it would not inhibit the incorporation at the several sites that were not fully bound at 1 mM octanol.

The IC<sub>50</sub> of 3-azioctanol is ~30 μM (Husain, *et al*, 1999). The incorporation of [<sup>3</sup>H]3-azioctanol in α-subunit in the presence of carbamylcholine, however, was half-maximum at ~1 mM, well above the concentration at which the binding at the inhibitory site should have been fully occupied. As was demonstrated, multiple sites of labeling contributed to the total incorporation in the α-subunit at 1 μM [<sup>3</sup>H]3-azioctanol. A comparison of the incorporation of [<sup>3</sup>H]3-azioctanol at 1 μM and 275 μM (Table 3-1) showed that the only site of incorporation which did not increase approximately linearly with concentration was αGlu-262 which was labeled at ~6% at 1 μM and ~33% at 275 μM, an increase of only ~6-fold. The other sites, those in αM4 and the agonist site,

which were labeled similarly in the absence and presence of carbamylcholine, showed an ~100-fold increase between 1  $\mu\text{M}$  and 275  $\mu\text{M}$ , indicating a lack of saturation at these sites at these concentrations. More detailed studies are required to determine the concentration of [ $^3\text{H}$ ]3-azioctanol necessary to produce half-maximum incorporation in  $\alpha\text{Glu-262}$  as well as the maximum labeling at this residue.

Between 1  $\mu\text{M}$  and 275  $\mu\text{M}$  [ $^3\text{H}$ ]3-azioctanol there was a linear increase in the level of incorporation at  $\alpha\text{Tyr-190}/\alpha\text{Tyr-198}$  in the agonist site. Although no studies have been carried out with [ $^3\text{H}$ ]3-azioctanol, octanol at concentrations up to 4 mM did not inhibit [ $^3\text{H}$ ]ACh binding, while butanol, which could be studied at high concentrations, inhibited the binding with a  $K_I$  of ~80 mM (Firestone *et al.*, 1994). Since [ $^3\text{H}$ ]3-azioctanol labeled the agonist site, but only in the absence of carbamylcholine or  $\alpha\text{BgTx}$ , it is possible that the inhibition of agonist binding by alcohols is due to direct, low affinity competition of the alcohol with the agonist for the agonist binding site. Further studies are required to determine whether the labeling at the agonist site saturates at higher concentrations of [ $^3\text{H}$ ]3-azioctanol or increases linearly over the range of accessible concentrations.

Although the non-M2 sites did not show saturating incorporation between 1 and 275  $\mu\text{M}$  [ $^3\text{H}$ ]3-azioctanol, it is possible that the levels of incorporation in a given residue were underestimated. While the incorporation in  $\alpha\text{V8-20}$  and  $\alpha\text{V8-18}$  appeared stable under the HPLC conditions used, ~60% of the  $^3\text{H}$  in the  $\alpha\text{V8-10}$  fragment was eluted in the flow-through of the HPLC. Therefore, at all concentrations the incorporation at  $\alpha\text{His-408}$  or  $\alpha\text{Cys-412}$ , or possibly another site, was most likely underestimated, due to instability of the photoadduct.

The high efficiency of the incorporation of [ $^3\text{H}$ ]3-azioctanol into  $\alpha\text{Glu-262}$  could be due to preferential reactivity of [ $^3\text{H}$ ]3-azioctanol with glutamates. However, while the

only other reported amino acid labeled by an aliphatic diazirine was a glutamate of a hexosaminidase (Liessem *et al.*, 1995), in our study [<sup>3</sup>H]3-azioctanol photoincorporated into a variety of side chains, including histidine, cysteine, alanine, valine, and tyrosine. Acidic side chains at some binding sites showed no [<sup>3</sup>H]3-azioctanol incorporation. For example, in  $\alpha$ M4 there was reactivity with alanine, histidine, and cysteine, but no reaction with  $\alpha$ Asp-407 at the N-terminus of  $\alpha$ M4. Therefore, the high reactivity with  $\alpha$ Glu-262 is most likely due primarily to a higher affinity of [<sup>3</sup>H]3-azioctanol for that region of the ion channel.

The preferential labeling of the M2 segment of the  $\alpha$ -subunit by [<sup>3</sup>H]3-azioctanol contrasts with the labeling seen in the desensitized state for other NCAs (including chlorpromazine, triphenylphosphonium, and 3-trifluoromethyl-3-phenyl diazirine (Karlin and Akabas, 1995)) which labeled amino acids in the M2 segment of each subunit in the desensitized state. Meproadifen mustard also reacted selectively with  $\alpha$ Glu-262, however. Although the observed preference may be partially attributable to higher reactivity of the reactive intermediate with glutamates, in the  $\beta$ -subunit the equivalent residue is an aspartate, which should not react very differently from a glutamate. This position in  $\beta$ , however, when mutated to a cysteine, is not modified by water-soluble modification reagents, while a cysteine at  $\alpha$ 262 is (Akabas *et al.*, 1994; Zhang and Karlin, 1998). Therefore, the three-dimensional structure of the nAChR  $\beta$ -subunit, and perhaps the  $\gamma$ - and  $\delta$ -subunits, is not similar to that of  $\alpha$  in this region of the ion channel domain, and the preferential incorporation into the  $\alpha$ -subunit may reflect a unique conformation of the  $\alpha$  subunit in this region.

Previous studies aimed at elucidating the site of long chain alcohol binding on the nAChR have implicated residues at the 10' position (Forman, 1997; Forman *et al.*, 1995), while studies with the GABA<sub>A</sub> receptor have indicated the contribution of a residue in

M2 at the 15' position, which faces away from the channel lumen on a turn of the helix between the 13' and 17' residues (Wick *et al.*, 1998). Modeling the M2 segment as an  $\alpha$ -helix with the azi group of 3-azioctanol near  $\alpha$ Glu-262 (Figure 3-12) shows that the carbon chain of 3-azioctanol only reaches to the 13' residues, and is incapable of reaching to this level on the opposite face of the helix. The photolabeling and electrophysiology results, then, are in apparent disagreement. However, the electrophysiology studies measure octanol inhibition of the open state of the receptor, while the photoaffinity labeling studies are done with a desensitized receptor. It is possible that octanol binds differently in the two states, perhaps closer to the 10' position in the open state, and closer to  $\alpha$ Glu-262 in the desensitized state. Alternatively, the mutations studied may have changed the nature of the region near  $\alpha$ Glu-262.

The studies presented here provide strong evidence that, in the desensitized state of the nAChR, [<sup>3</sup>H]3-azioctanol binds within the ion channel domain near  $\alpha$ Glu-262. Further studies, such as photoincorporation of [<sup>3</sup>H]3-azioctanol in the open channel or the effects of site directed mutagenesis of the N-terminal end of the M2 segment on the inhibition of the nAChR by octanol, will be necessary to further refine the site of action of long chain alcohols on the nAChR.

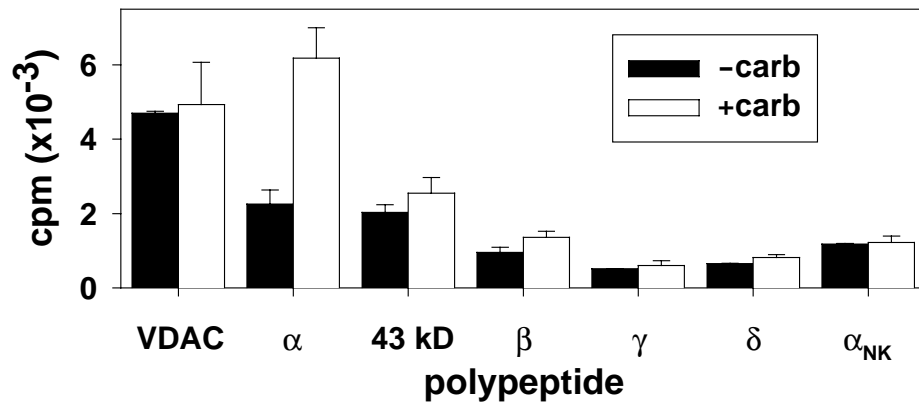
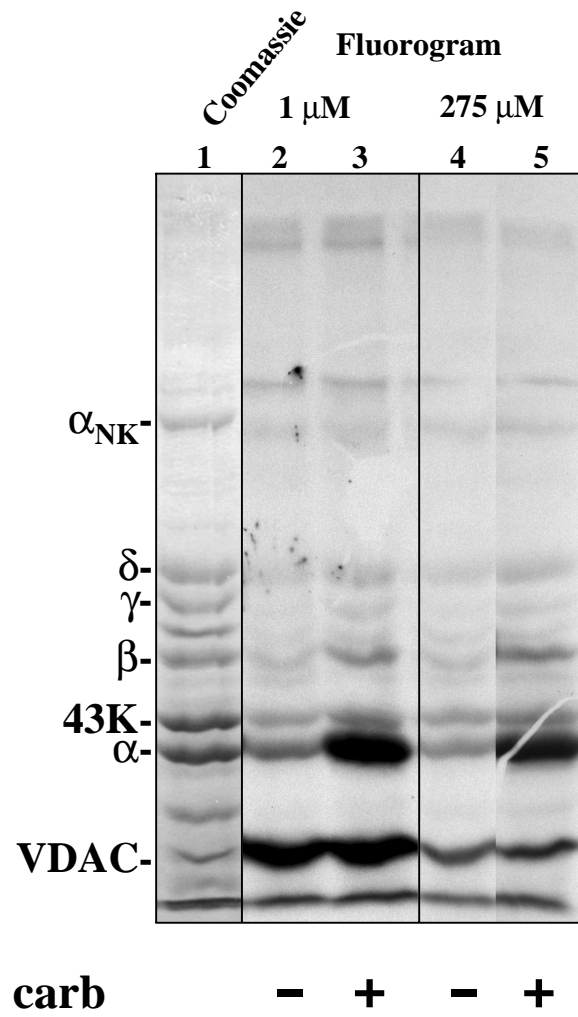


**Figure 3-1. Photoincorporation of [<sup>3</sup>H]3-azioctanol into integral and peripheral membrane proteins of nAChR-rich membranes in the presence or absence of carbamylcholine.**

A, nAChR-rich membranes (100 μg at 2 mg/ml) were equilibrated with 1 μM (11 Ci/mmol) (lanes 2 and 3) and 275 μM (0.04 Ci/mmol) (lanes 4 and 5) [<sup>3</sup>H]3-azioctanol in TPS, in the absence (lanes 2 and 4) or presence (lanes 3 and 5) of 2 mM carbamylcholine and irradiated at 365 nM for 10 minutes. After photolysis, samples were subjected to SDS-PAGE, visualized by Coomassie Blue (lane 1), processed for fluorography, and exposed to film for 6 weeks (A, lanes 2-5). Indicated on the left in A are the mobilities of nAChR subunits, rapsyn (43K), the α-subunit of the Na<sup>+</sup>/K<sup>+</sup> ATPase (αNK), and the mitochondrial chloride channel (VDAC).

B, The <sup>3</sup>H incorporated in the absence or presence of carbamylcholine at 1 μM [<sup>3</sup>H]3-azioctanol was quantified by scintillation counting as described in Methods. Values shown are the averages of duplicate samples with standard deviations.

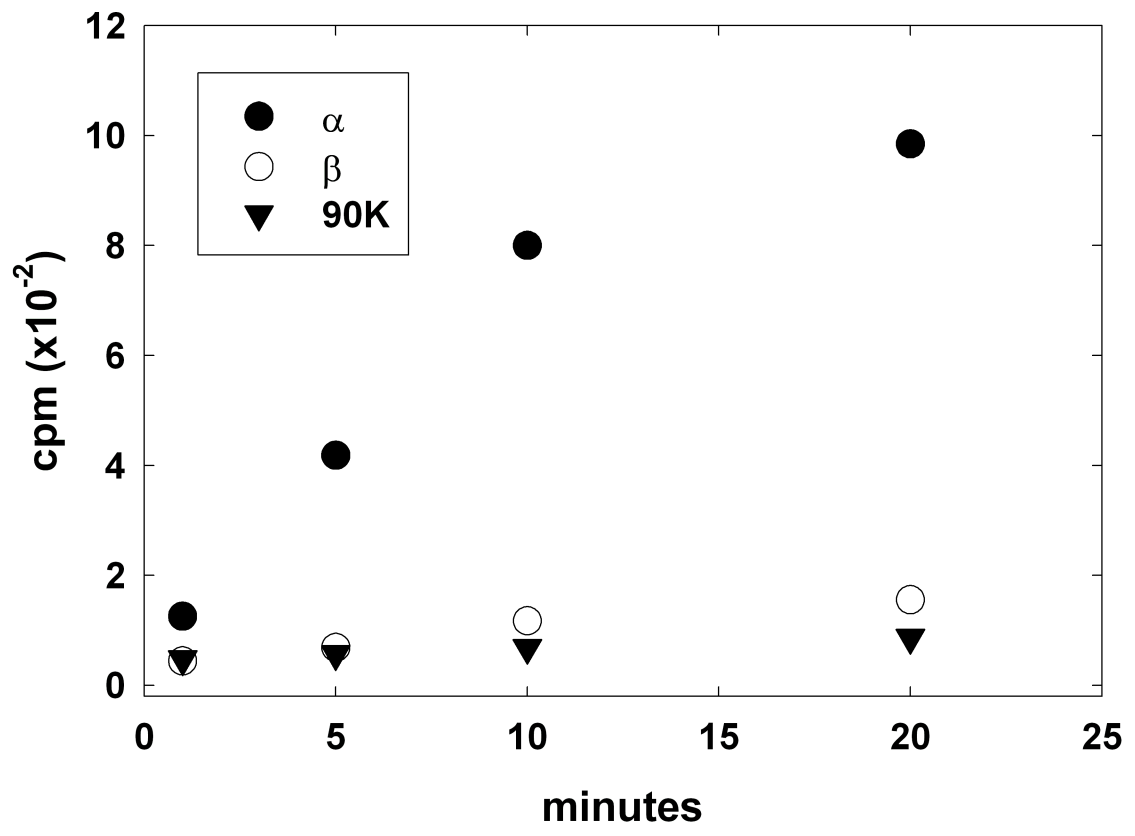


**Figure 3-2 Time course of incorporation of [<sup>3</sup>H]3-azidoethanol into integral membrane proteins of nAChR-rich membranes in the presence of carbamylcholine.**

nAChR-rich membranes (100 μg at 2 mg/ml) were equilibrated with 1 μM [<sup>3</sup>H]3-azidoethanol in TPS in the presence of 2 mM carbamylcholine and irradiated at 365 nm for the times indicated. After photolysis, samples were subjected to SDS-PAGE, visualized by Coomassie Blue, and the polypeptides were excised. <sup>3</sup>H in nAChR α (●) or β (○) subunits as well as the α-subunit of Na<sup>+</sup>/K<sup>+</sup> ATPase (▼) was quantified by scintillation counting.

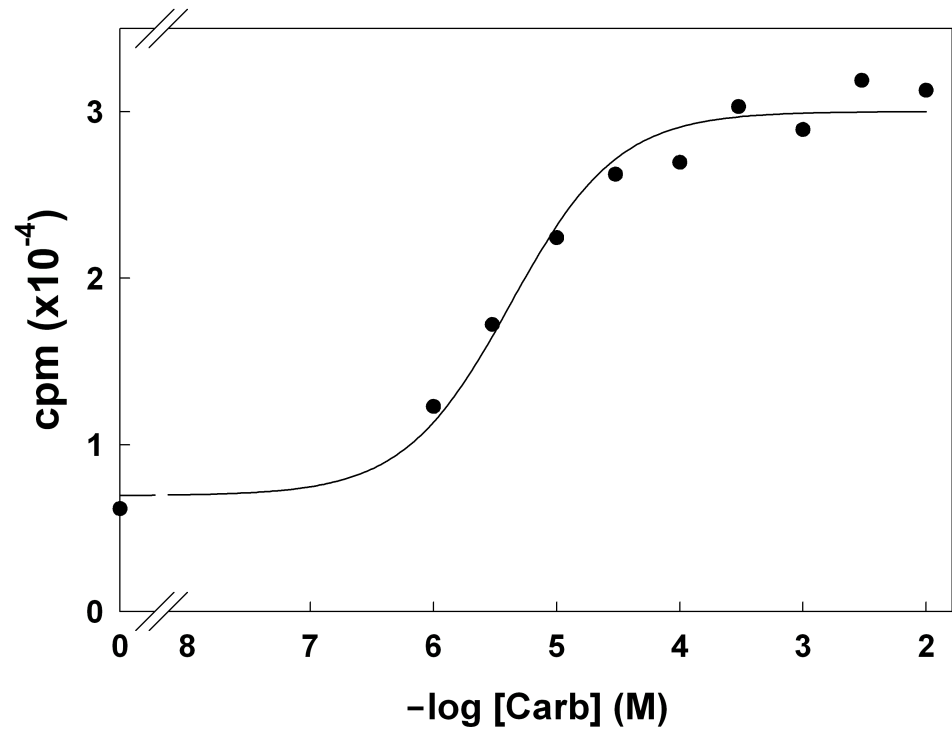


**Figure 3-3. Dependence of [<sup>3</sup>H]3-azidoctanol incorporation into  $\alpha$ -subunit on the concentration of carbamylcholine.**

nAChR-rich membranes (100  $\mu$ g at 2 mg/ml) were equilibrated with 1  $\mu$ M [<sup>3</sup>H]3-azidoctanol in TPS in the presence of varying concentrations of carbamylcholine and irradiated at 365 nm for 10 minutes. Samples were subjected to SDS-PAGE and visualized by Coomassie Blue. Bands corresponding to nAChR  $\alpha$ -subunit were excised and <sup>3</sup>H incorporation was quantified by scintillation counting. The data were fit to a

single site model  $B = \frac{B_A}{1 + \frac{K}{L}} + B_0$  where B was the observed <sup>3</sup>H incorporation at each

concentration, L was the concentration of carbamylcholine, B<sub>A</sub> and B<sub>0</sub> were the agonist dependent and independent incorporation, respectively, and K was the apparent dissociation constant for carbamylcholine. K, B<sub>A</sub>, and B<sub>0</sub> were varied. Based on the data, B<sub>A</sub>=23100 $\pm$ 1400 cpm; B<sub>0</sub>=6900 $\pm$ 1300 cpm; K=4.2 $\pm$ 1.0  $\mu$ M

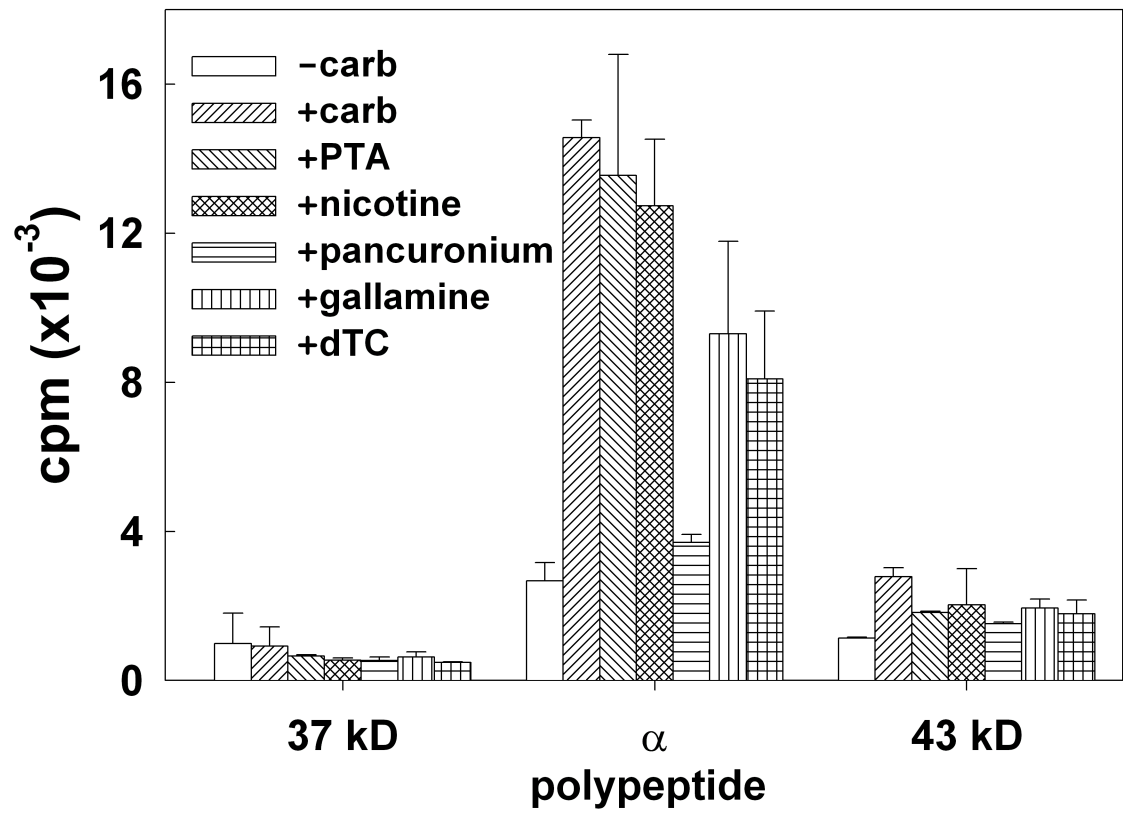


**Figure 3-4. Photoincorporation of [<sup>3</sup>H]3-azidoctanol into nAChR-rich membranes in the presence of various cholinergic agonists and competitive antagonists.**

nAChR-rich membranes (100 µg at 2 mg/ml) were equilibrated with 1 µM [<sup>3</sup>H]3-azidoctanol in TPS in the absence of other drugs, or in the presence of 2 mM carbamylcholine (carb), 200 µM PTA, 100 µM nicotine, 100 µM pancuronium, 1 mM gallamine, or 30 µM d-tubocurarine (dTC) and irradiated for 10 minutes at 365 nm. After photolysis, samples were subjected to SDS-PAGE and visualized by Coomassie Blue. Bands corresponding to α-subunit, as well as the 37 kD (calectrin) and 43 kD (rapsyn) bands were excised. <sup>3</sup>H incorporation was quantified by scintillation counting.

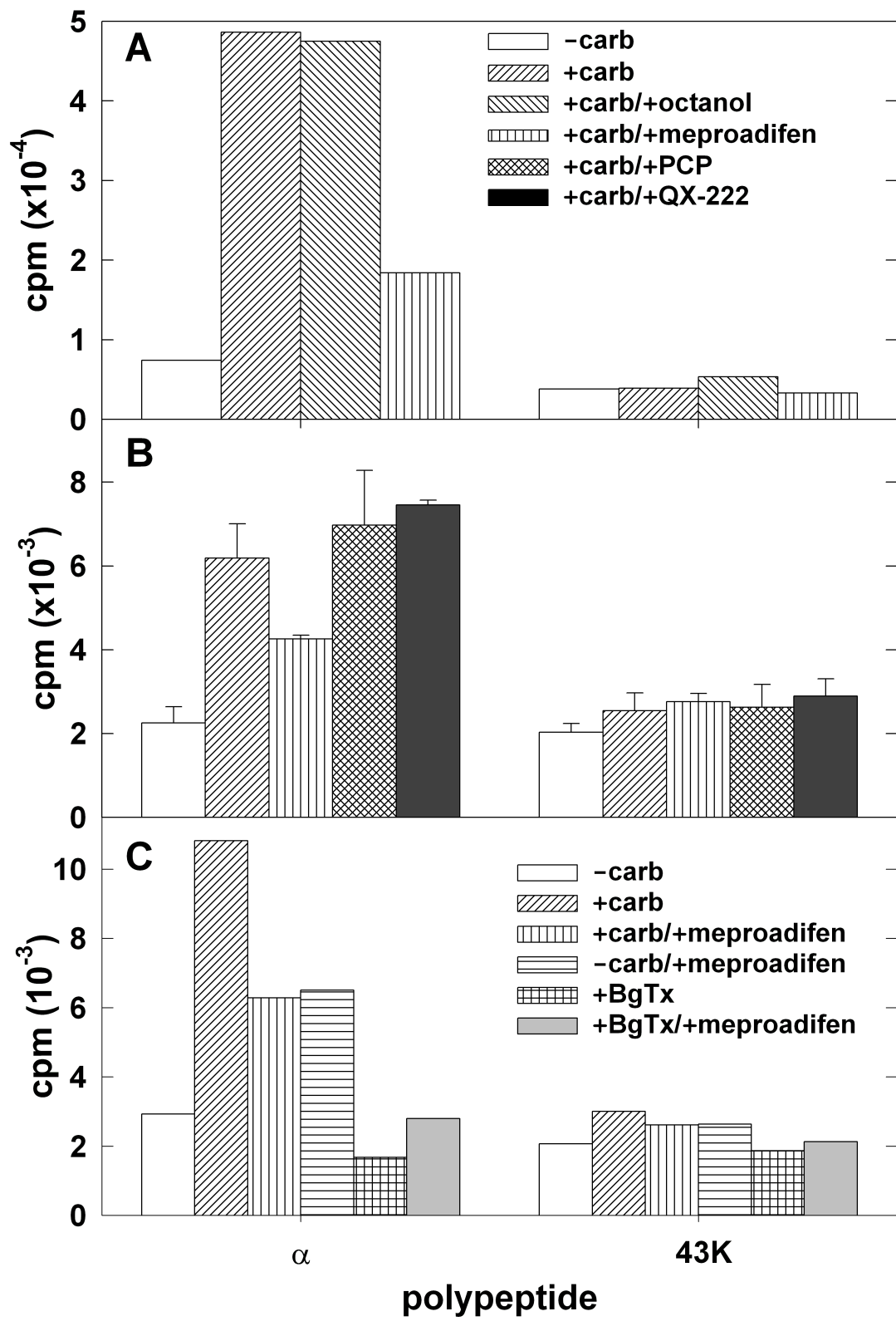


**Figure 3-5. Photoincorporation of [<sup>3</sup>H]3-azioctanol into nAChR-rich membranes in the presence and absence of various cholinergic drugs.**

nAChR-rich membranes (100 µg at 2 mg/ml) were labeled with 1 µM (11 Ci/mmol; A and B) or 275 µM (0.04 Ci/mmol; C) [<sup>3</sup>H]3-azioctanol. At 1 µM [<sup>3</sup>H]3-azioctanol, membranes were labeled in the absence of other drugs, in the presence of 2 mM carbamylcholine with no other drug, or with 1 mM octanol, 100 µM meproadifen, 100 µM PCP, or 1 mM QX-222. Data from two experiments are shown. Averages and errors in panel B were from duplicate samples within the experiment. At 275 µM [<sup>3</sup>H]3-azioctanol, membranes were labeled in the absence or the presence of 2 mM carbamylcholine or 10 µM αBgtx, in the absence or presence of 100 µM meproadifen. Following irradiation at 365 nm for 10 minutes, samples were subjected to SDS-PAGE and visualized by Coomassie Blue. Bands corresponding to nAChR α-subunit and the 43 kD (rapsyn) polypeptide were excised. <sup>3</sup>H was quantified by scintillation counting.

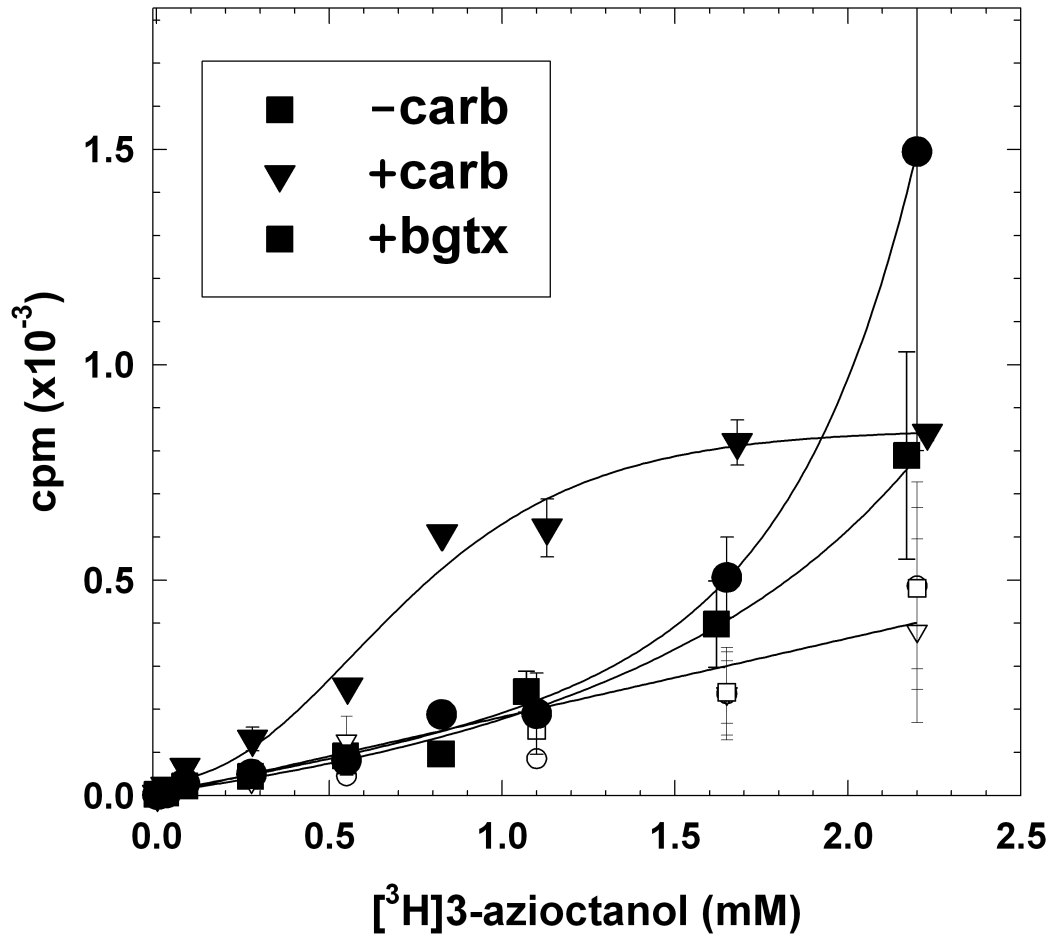


**Figure 3-6. Effect of [<sup>3</sup>H]3-azidoctanol concentration on the incorporation into  $\alpha$ -subunit.**

nAChR-rich membranes (100  $\mu$ g at 2 mg/ml) were equilibrated with varying concentrations of [<sup>3</sup>H]3-azidoctanol (~0.04 Ci/mmol), in the absence of other drugs ( $\bullet$ ,  $\circ$ ), in the presence of 2 mM carbamylcholine ( $\blacktriangledown$ ,  $\triangledown$ ), or in the presence of 10  $\mu$ M  $\alpha$ BgTx ( $\blacksquare$ ,  $\square$ ). After irradiation at 365 nm for 10 minutes, samples were subjected to SDS-PAGE and visualized by Coomassie Blue. Bands corresponding to nAChR  $\alpha$ -subunit (solid symbols), as well as the 90 kD band, containing the  $\alpha$ -subunit of Na<sup>+</sup>/K<sup>+</sup> ATPase (open symbols), were excised, and <sup>3</sup>H incorporation was quantified by scintillation counting. Error bars are from the average of 4 separate experiments normalized to a common specific activity by assuming common level of incorporation in  $\alpha$ -subunit in the presence of carbamylcholine at 2.2 mM [<sup>3</sup>H]3-azidoctanol.

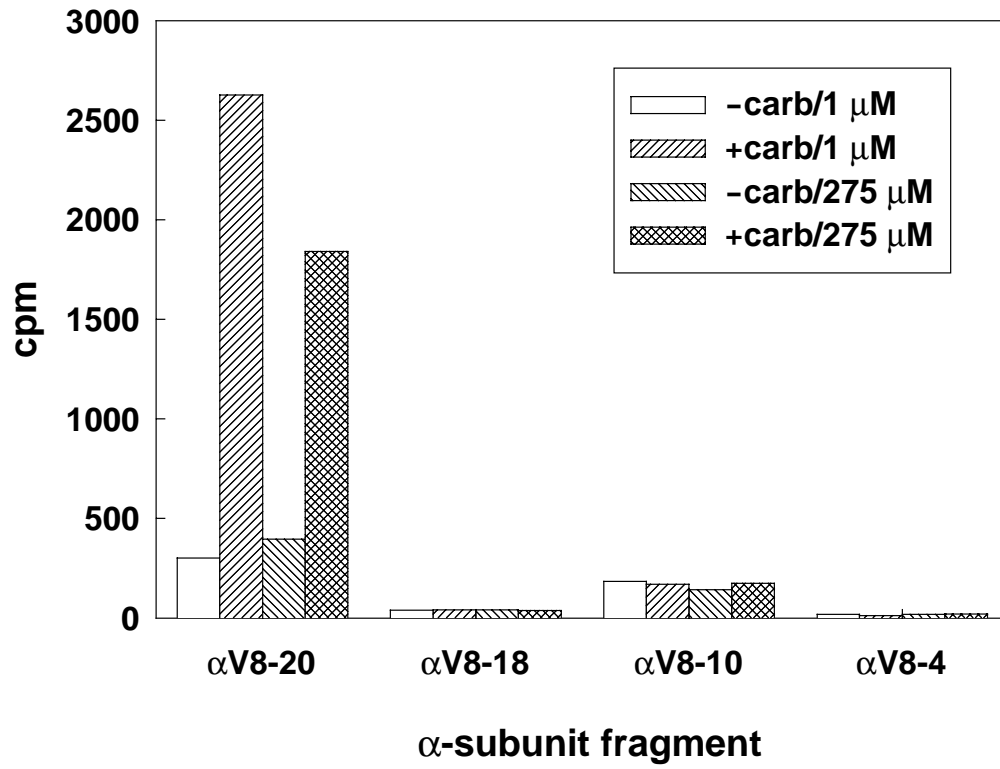
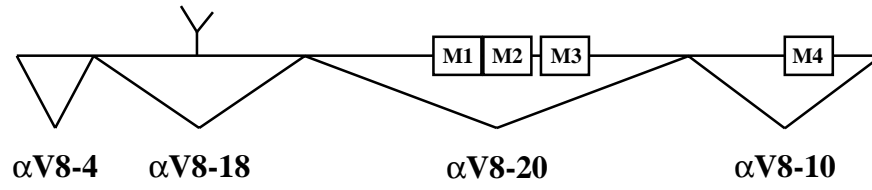


**Figure 3-7. Proteolytic mapping of sites of [<sup>3</sup>H]3-azioctanol incorporation into the nAChR  $\alpha$ -subunit using *S. aureus* V8 protease.**

nAChR-rich membranes (400  $\mu$ g at 2 mg/ml) were labeled with 1  $\mu$ M (11 Ci/mmol) or 275  $\mu$ M (0.04 Ci/mmol) [<sup>3</sup>H]3-azioctanol in the absence or presence of 2 mM carbamylcholine. After photolysis at 365 nm for 10 minutes, membranes were pelleted, resuspended in sample buffer, and submitted to SDS-PAGE. Following electrophoresis, the  $\alpha$ -subunit was excised and transferred to the well of a 15% mapping gel for digestion with V8 protease. Bands were visualized with Coomassie blue, and <sup>3</sup>H incorporation was quantified by scintillation counting. <sup>3</sup>H present in proteolytic fragments of nAChR  $\alpha$ -subunit labeled in the absence or presence of 2 mM carbamylcholine at 1  $\mu$ M and 275  $\mu$ M [<sup>3</sup>H]3-azioctanol is shown. A schematic of digestion of  $\alpha$ -subunit with V8 protease is shown above.

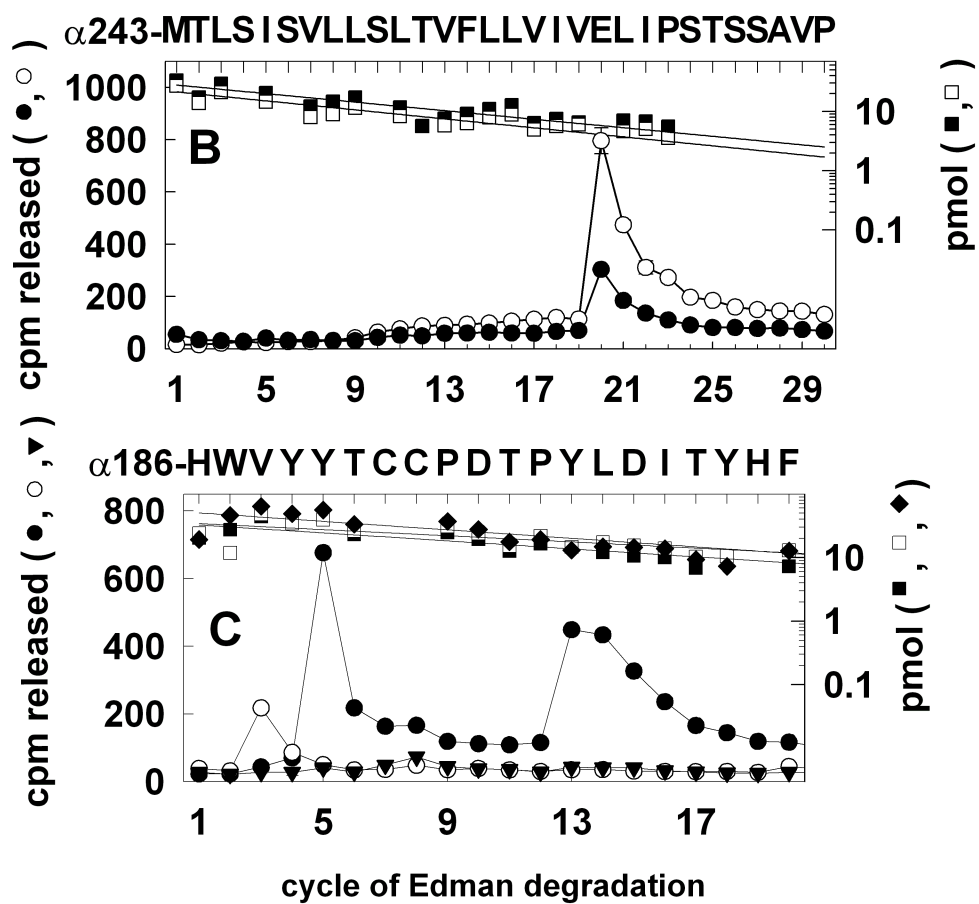
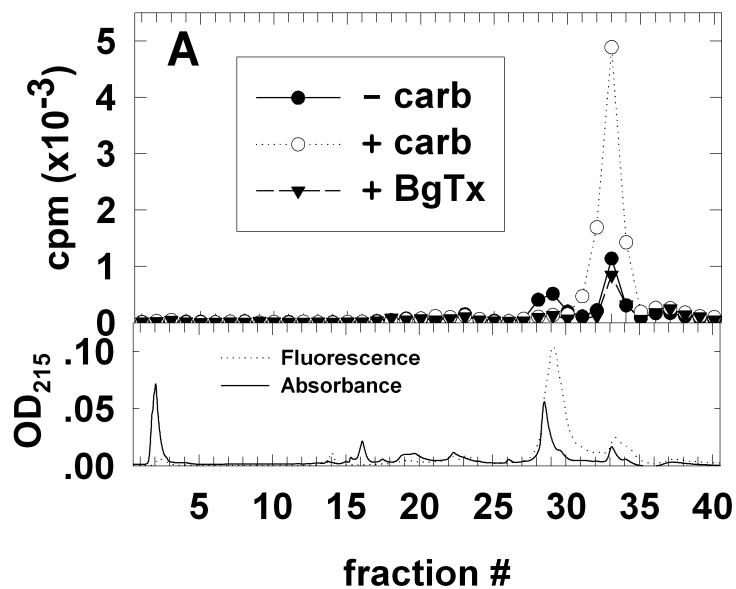


**Figure 3-8. Reverse phase HPLC purification of [<sup>3</sup>H]3-azioctanol labeled fragments from an EndoLysC digest of  $\alpha$ V8-20 and sequence analysis of HPLC fractions**

A.  $\alpha$ V8-20 isolated from nAChRs photolabeled with 275  $\mu$ M [<sup>3</sup>H]3-azioctanol in the absence (●) or presence of 10  $\mu$ M  $\alpha$ BgTx (▼) or 2 mM carbamylcholine (○) was digested with EndoLysC. The digest was applied to a Brownlee Aquapore C4 column and fractionated by reverse-phase HPLC. Upper panel, <sup>3</sup>H elution profiles (5% of each fraction counted). Lower panel, fluorescence (·····) and absorbance profiles (—).

B, C. <sup>3</sup>H (●, ○, ▼) and mass released (■, □, ◆) on N-terminal sequencing of material in HPLC fraction 33 (B) and 29 (C). B, Fraction 33 from the sample labeled in the absence (●, ■) and presence of carbamylcholine (○, □) showed a single sequence, beginning at  $\alpha$ Met-243, the N-terminus of the  $\alpha$ M2 segment (–carb:  $I_0=23$  pmol, R=92%, 9800 cpm loaded, 3900 cpm remaining after 30 cycles; +carb:  $I_0=30$  pmol, R=92%, 26000 cpm loaded, 3900 cpm remaining after 30 cycles). C, Fraction 29 from the sample labeled in the absence (●, ■) or presence of  $\alpha$ BgTx (▼, ◆) or carbamylcholine (○, □) showed a primary sequence beginning at  $\alpha$ His-186 and a secondary sequence beginning at  $\alpha$ Asp-180 (–carb:  $\alpha$ His-186  $I_0=35$  pmol, R=93%,  $\alpha$ Asp-180  $I_0=4.6$  pmol, R=86%, 16700 cpm loaded, 3400 cpm remaining after 25 cycles; + $\alpha$ BgTx:  $\alpha$ His-186  $I_0=55$  pmol, R=93%,  $\alpha$ Asp-180  $I_0=2.4$  pmol, R=95%, 4100 cpm loaded, 1000 cpm remaining after 25 cycles; +carb:  $\alpha$ His-186  $I_0=36$  pmol, R=95%,  $\alpha$ Asp-180  $I_0=7.8$  pmol, R=82%, 4800 cpm loaded, 1200 cpm remaining after 25 cycles). Primary sequence for each fraction is shown on top axes.

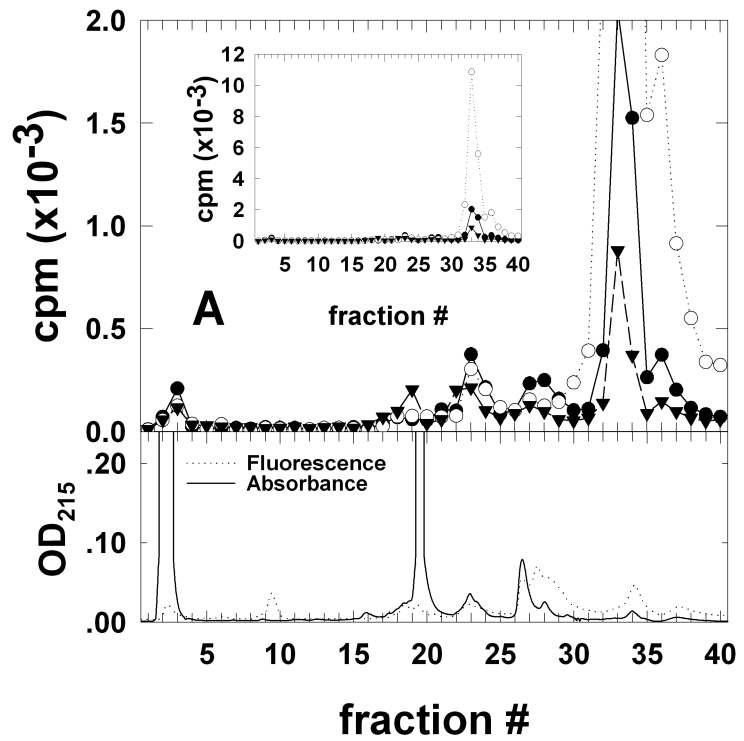


**Figure 3-9. Reverse phase HPLC purification of [<sup>3</sup>H]3-azioctanol labeled fragments from *S. aureus* V8 protease digest of  $\alpha$ V8-20.**

$\alpha$ V8-20 isolated from nAChRs labeled with 275  $\mu$ M [<sup>3</sup>H]3-azioctanol in the absence (●) or presence of 10  $\mu$ M  $\alpha$ BgTx (▼) or 2 mM carbamylcholine (○) was digested with V8 protease in solution. The digest was applied to a Brownlee Aquapore C4 column and fractionated by reverse-phase HPLC. Upper panel, <sup>3</sup>H release profiles (5% of each fraction). Inset, replot of <sup>3</sup>H to include peak of <sup>3</sup>H in fraction 33. Lower panel, fluorescence (·····) and absorbance profiles (—).

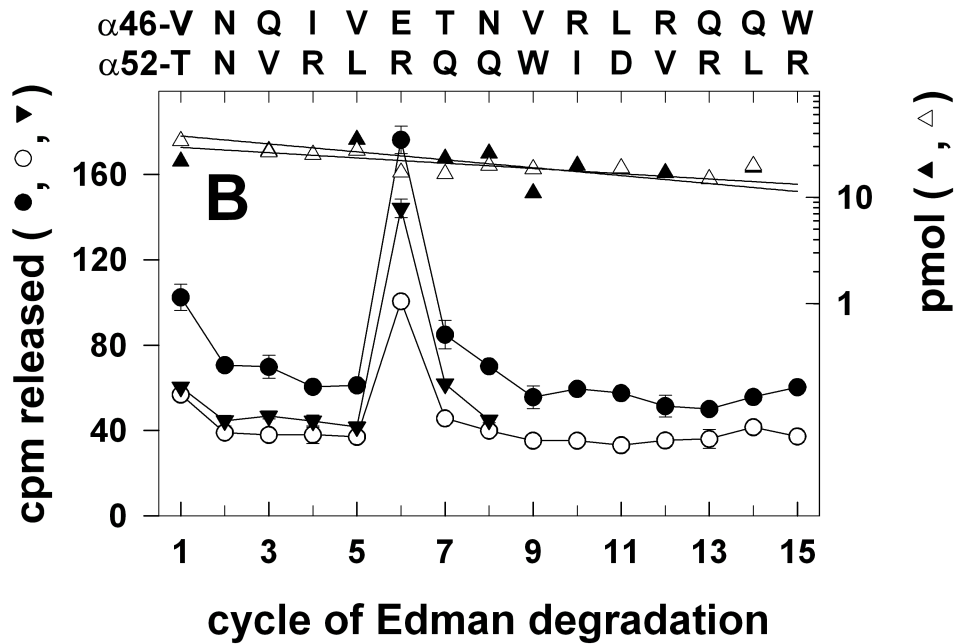
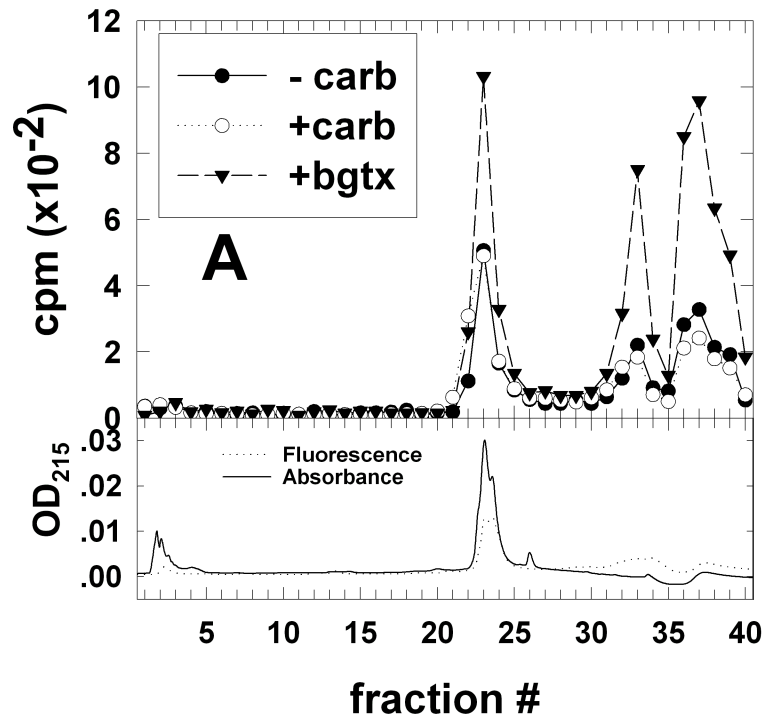


**Figure 3-10. Reverse phase HPLC purification of [<sup>3</sup>H]3-azidoctanol labeled  $\alpha$ V8-18 and sequence analysis of HPLC fraction.**

A.  $\alpha$ V8-18 isolated from nAChR labeled with 275  $\mu$ M [<sup>3</sup>H]3-azidoctanol in the absence (●) or presence of 10  $\mu$ M  $\alpha$ BgTx (▼) or 2 mM carbamylcholine (○) was applied to a Brownlee Aquapore C4 column and purified by reverse-phase HPLC. Upper panel, <sup>3</sup>H elution profiles (5% of each fraction). Lower panel, fluorescence (·····) and absorbance profiles (—).

B. <sup>3</sup>H (●, ○, ▼) and mass released (▲, △) on N-terminal sequencing of material from HPLC fraction 23. The sample labeled in the absence (●, ▲, △) or presence of  $\alpha$ BgTx (▼) or carbamylcholine (○) showed two sequences, one beginning at  $\alpha$ Val-46 and one beginning at  $\alpha$ Thr-52 (–carb:  $\alpha$ Val-46 (△)  $I_0=41$  pmol, R=92%,  $\alpha$ Thr-52 (▲)  $I_0=38$  pmol, R=94%, 10120 cpm loaded, 2400 cpm remaining after 15 cycles; + $\alpha$ BgTx:  $\alpha$ Val-46  $I_0=19$  pmol, R=91%,  $\alpha$ Thr-52  $I_0=24$  pmol, R=91%, 10320 cpm loaded, 2000 cpm remaining after 8 cycles; +carb:  $\alpha$ Val-46  $I_0=32$  pmol, R=92%,  $\alpha$ Thr-52  $I_0=31$  pmol, R=94%, 9800 cpm loaded, 1800 cpm remaining after 15 cycles). The two sequences that were present are shown along top axis.

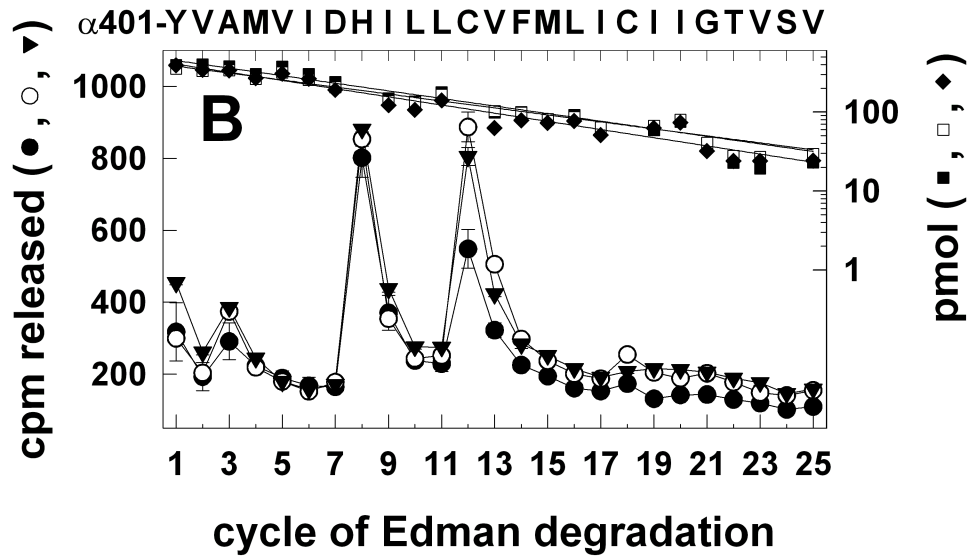
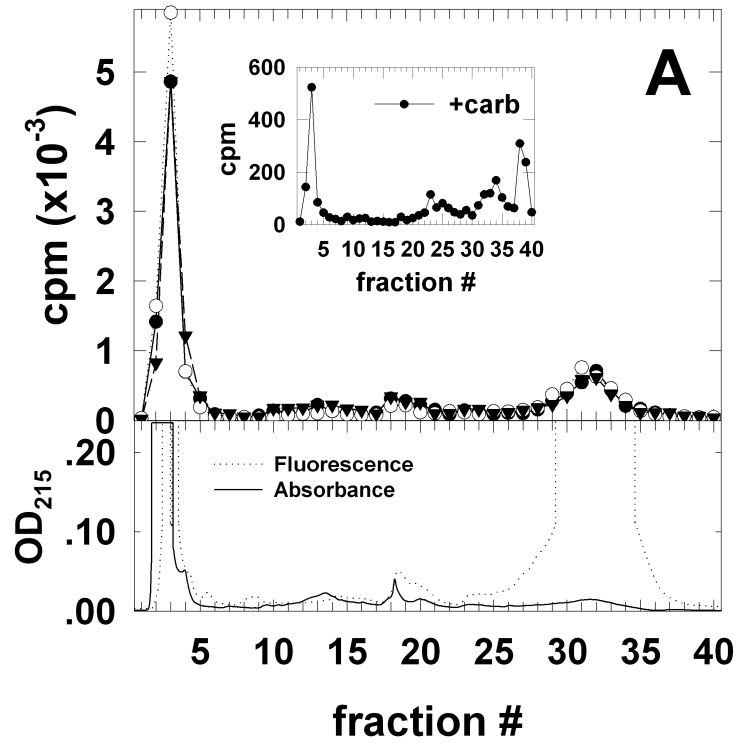


**Figure 3-11. Reverse phase HPLC purification of [<sup>3</sup>H]3-azioctanol labeled fragments from trypsin digestion of αV8-10 and sequence analysis of HPLC fractions.**

A. αV8-10 labeled with 275 μM [<sup>3</sup>H]3-azioctanol in the absence (●) or presence of 10 μM αBgTx (▼) or 2 mM carbamylcholine (○) was digested with trypsin and applied to a Brownlee Aquapore C4 column for fractionation by reverse-phase HPLC. Upper panel, <sup>3</sup>H elution profiles from the digest of αV8-10 labeled under the given conditions. Lower panel, fluorescence (·····) and absorbance profiles (—). Inset, <sup>3</sup>H elution profile of undigested αV8-10 labeled with 1 μM [<sup>3</sup>H]3-azioctanol in the presence of 2 mM carbamylcholine purified by reverse-phase HPLC.

B. <sup>3</sup>H (●, ○, ▼) and mass released (■, □, ◆) on N-terminal sequencing of material from HPLC fractions 31-34. The sample labeled in the absence (●, ■) or presence of αBgTx (▼, ◆) or carbamylcholine (○, □) showed a primary sequence beginning at αTyr-401 and a secondary sequence beginning at αSer-388 (–carb: αTyr-401 I<sub>0</sub>=502 pmol, R=90%, αSer-388 I<sub>0</sub>=68 pmol, R=87%, 52400 cpm loaded, 12700 cpm remaining after 25 cycles; +αBgTx: αTyr-401=I<sub>0</sub> 457 pmol, R=89%, αSer-388 I<sub>0</sub>=70 pmol, R=87%, 48500 cpm loaded, 16700 cpm remaining after 25 cycles; +carb: αTyr-401 I<sub>0</sub>=423 pmol, R=90%, αSer-388 I<sub>0</sub>=72 pmol, R=88%, 57800 cpm loaded, 19400 cpm remaining after 25 cycles). The primary sequence is shown along top axis.

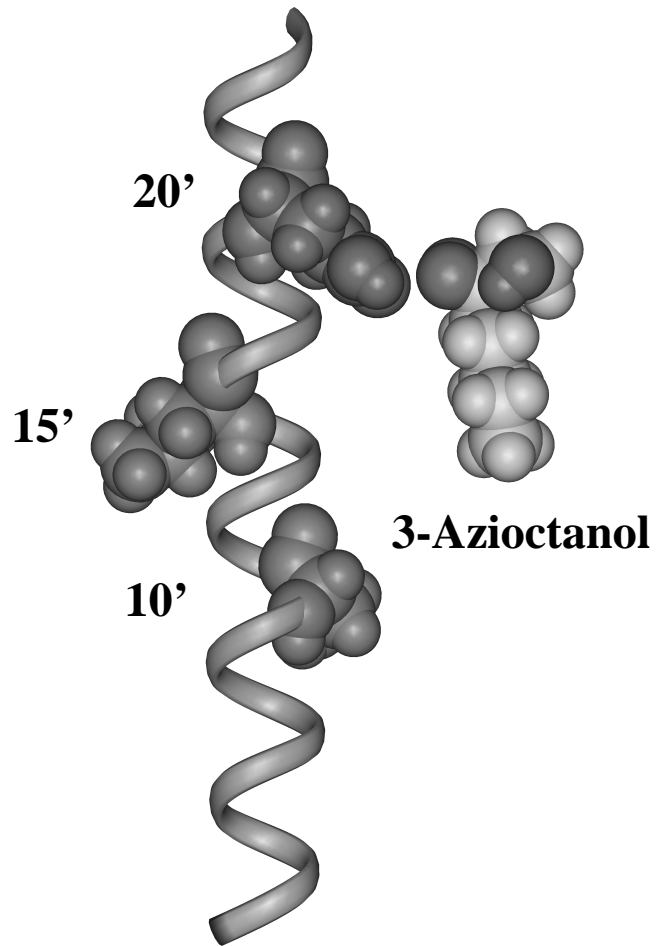


**Figure 3-12. Model of 3-azioctanol and  $\alpha$ M2 helix**

$\alpha$ -Helical model of the  $\alpha$ M2 segment and space filling model of octanol were made using the molecular modeling software Insight (Biosym, Inc.). M2 residues 10', 15', and 20' are shown as space-filling models. The diazirine of 3-azioctanol (dark) is positioned near  $\alpha$ Glu-262, the residue labeled by [ $^3$ H]3-azioctanol. The hydroxyl group is also shown darker than the other atoms.

<b><math>\alpha</math>V8-20</b>									
conc.	$\alpha$ V8-20		$\alpha$ M243- $\alpha$ K340		$\alpha$ Glu-262		$\alpha$ H186- $\alpha$ K242	$\alpha$ Tyr-190	
	-carb	+carb	-carb	+carb	-carb	+carb	-carb	-carb	
275 $\mu$ M	0.55	1.3	0.6 $\pm$ 0.1	1.4 $\pm$ 0.1	0.14 $\pm$ 0.04	0.33 $\pm$ 0.10	0.18	0.013	
1 $\mu$ M	0.008	0.06	0.012 $\pm$ 0.009	0.27 $\pm$ 0.19	0.0012 $\pm$ 0	0.06 $\pm$ 0.04	0.0017	0.00012	

<b><math>\alpha</math>V8-10</b>									
	$\alpha$ V8-10		$\alpha$ Y401- $\alpha$ G437		$\alpha$ His-408		$\alpha$ Cys-412		
	-carb	+carb	-carb	+carb	-carb	+carb	-carb	+carb	
275 $\mu$ M	0.24	0.40	0.05	0.06	0.003	0.003	0.002	0.005	
1 $\mu$ M	0.0038	0.0035	0.00093	0.00098	0.00003	0.00003	0.00004	0.00004	

<b><math>\alpha</math>V8-18</b>						
	$\alpha$ V8-18		$\alpha$ Glu-51/ $\alpha$ Arg-57		$\alpha$ K77- $\alpha$ K?	
	-carb	+carb	-carb	+carb	-carb	+carb
275 $\mu$ M	0.06	0.07	0.003	0.002	0.10	0.15

**Table 3-1. Incorporation of [<sup>3</sup>H]3-azioctanol into fragments and residues of  $\alpha$ -subunit.**

The ratio of moles [<sup>3</sup>H]3-azioctanol incorporated per mole of the fragments or residues labeled were calculated from the <sup>3</sup>H incorporation and the known specific activity of [<sup>3</sup>H]3-azioctanol. The <sup>3</sup>H incorporation in each fragment and residue was calculated as described in the methods. For the incorporation into fragments, the mass levels were based on the observed mass sequenced and the total radioactivity loaded. For the incorporation into specific residues, the mass was based on the initial and repetitive yields and the radioactivity was based on the observed release. Averages shown are from duplicate preparative labeling experiments.

## Chapter 4 Identification of the Sites of Incorporation of [<sup>3</sup>H]Progesterin Aryl Azide in the nAChR

### ABSTRACT

Progesterone at micromolar concentrations is a noncompetitive antagonist of the *Torpedo* nicotinic acetylcholine receptor (nAChR). To localize the sites of interaction of progesterone with the nAChR, we have used a photoactivatable derivative of progesterone, [<sup>3</sup>H]progesterin aryl azide. At 0.4 μM, [<sup>3</sup>H]progesterin aryl azide photoincorporated into all four subunits of the nAChR. The incorporation was not affected by the presence of other cholinergic drugs. Within the α subunit, ~75% of the incorporation was mapped to a 10 kD fragment containing the fourth transmembrane segment (αM4), known to contribute to the protein-lipid interface. Approximately 10% of the [<sup>3</sup>H]progesterin aryl azide incorporation in the α subunit was in a 20 kD fragment containing the first three transmembrane segments (αM1, αM2, and αM3). Efforts to further localize the incorporation provided evidence that [<sup>3</sup>H]progesterin aryl azide incorporated into the αM4 segment as well as the M4 segments of the other subunits. However, the yields of these segments recovered for sequence analysis, along with the instability of the adducts formed with the β, γ, and δ subunits to purification conditions, precluded the identification of labeled amino acids.

### INTRODUCTION

The anesthetic properties of steroids were first reported by Seyle (1941). Since then, some steroids, such as alphaxalone-alphadalone, have been used clinically for inducing and maintaining anesthesia. The action of ligand-gated ion channels is altered by steroids, consistent with the effects of several other general anesthetics. However, while several recent studies have begun to identify specific residues in the GABA<sub>A</sub>,

glycine, and nACh receptors which affect the potency of other general anesthetics (Wick *et al.*, 1998; Forman, 1997), the site of action of steroids on these receptors is unclear. Although the potentiation of the GABA<sub>A</sub> receptor by steroids is not due to non-specific effects on lipid order (Paul and Purdy, 1992), the site of action is distinct from the binding sites of GABA and competitive antagonists, barbiturates, or benzodiazepines. Additionally, mutations within the second (M2) and third (M3) segments that have been shown to affect the potency of several general anesthetics, such as the long chain alcohols, do not affect the potency of steroid anesthetics (Belelli *et al.*, 1997; McGurk *et al.*, 1998). Recent work by Rick *et al.* (1998) using chimeric GABA<sub>A</sub> receptors has indicated that N-terminal region of the GABA<sub>A</sub> receptor, prior to the M2 segment, confers sensitivity to steroids.

Unlike the GABA<sub>A</sub> receptor, steroids act as noncompetitive antagonists (NCAs) on the nAChR. Their method of action on the nAChR, however, appears different than that of other NCAs such as the aromatic amines. When progesterone is applied before agonist, and then washed off, the current is still inhibited (Valera *et al.*, 1992). Hydrocortisone and 11-deoxycortisone cause a decrease in burst duration, indicating that the channel may be able to adopt a closed conformation while still being bound by the steroid (Bouzat and Barrantes, 1993). Additionally, the application of hydrocortisone with QX-222 alters the single channel properties from those seen with QX-222 alone, suggesting that the two drugs bind different sites (Bouzat and Barrantes, 1996). These results suggest that steroids are not traditional channel-blockers, if they even bind in the channel at all.

The high lipophilicity of steroids suggests a possible interaction at the protein-lipid interface. However, electrophysiological experiments with the nAChR have provided evidence that the steroids do not act via the protein-lipid interface. Binding to a

site accessible only from the extracellular side is supported by a decrease in inhibition when hydrocortisone and 11-deoxycortisone are applied intracellularly (Bouzat and Barrantes, 1993). Experiments with a modified progesterone coupled to bovine serum albumin show that even a strongly hydrophilic steroid could still inhibit current, suggesting that the steroid does not need to enter the lipid bilayer to exert its effects (Valera *et al.*, 1992; Ke and Lukas, 1999).

Photoaffinity labeling studies with the steroid noncompetitive antagonist of the nAChR, [<sup>3</sup>H]promegestone, however, showed incorporation only into the fourth transmembrane segment (M4), in amino acids known to contribute to the protein-lipid interface (Blanton *et al.*, 1999). There was no detectable incorporation of [<sup>3</sup>H]promegestone into any residues in the M2 segment, which lines the lumen of the channel and has been photoaffinity labeled by several other noncompetitive antagonists. This lack of incorporation, however, may be attributable either to a lack of binding within the channel or the absence of side chains within the lumen of the channel into which the promegestone reactive group can incorporate.

As an alternative to promegestone, Kym *et al.* (1995) synthesized [<sup>3</sup>H]progesterin aryl azide (Figure 4-1) as a photoaffinity probe of the progesterone receptor. With the progesterone receptor, [<sup>3</sup>H]progesterin aryl azide showed photoattachment efficiency of ~60%, while promegestone only showed an efficiency of ~5%. These two steroids utilize different photoreactive groups, one an enone and the other an aryl azide. Additionally, these reactive groups are at opposite ends of the steroid, ring A as opposed to ring D, perhaps allowing reaction with different regions of the receptor.

Here we present studies examining the photolabeling of nAChR-rich membranes by the photoaffinity steroid [<sup>3</sup>H]progesterin aryl azide. This compound incorporated into each nAChR subunit. Within the  $\alpha$  subunit, the primary site of labeling was contained

within a ~10 kD fragment which included the M4 segment. However, the low levels of incorporation as well as low mass levels were compounded by the instability of the adducts to HPLC and sequencing conditions, so no information could be obtained regarding the specific side chains labeled.

## **MATERIALS AND METHODS**

### **Materials**

nAChR-enriched membranes were isolated from *Torpedo californica* electric organ according to the method described by Sobel *et al.* (1977), modified as described by Pedersen *et al.* (1986). The final membrane suspensions were stored in 38% sucrose at -80 °C under argon. The membranes used here contained 0.5-1.0 nmol acetylcholine binding sites per milligram of protein. [<sup>3</sup>H]Progesterin aryl azide (16 $\alpha$ ,17 $\alpha$ -[(*S*)-1'-(4-azidophenyl)(ethylenedioxy)]pregn-4-ene-3,20-dione) was a kind gift from Dr. John Katzenellenbogen, synthesized according to the methods described in Kym *et al.* (1995), with a specific activity of 16 Ci/mmol. *S. aureus* V8 protease was from ICN Biomedical Inc, EndoLysC from Boeringher Mannheim, trifluoroacetic acid (TFA) from Pierce. 1-Azidopyrene (1-AP) was purchased from Molecular Probes. 10% Genapol C-100 was from Calbiochem. Tetracaine, progesterone, oxidized glutathione, Tricine, trypsin, and carbamylcholine were from Sigma. EndoglycosidaseH was from Genzyme.

### **Photoaffinity labeling of nAChR-enriched membranes with [<sup>3</sup>H]progesterin aryl azide**

For analytical labeling experiments, freshly thawed *Torpedo* membranes (100  $\mu$ g per condition) were diluted with TPS and pelleted (15000xg) for 30 minutes. The pellets were resuspended in *Torpedo* physiological saline (250 mM NaCl, 5 mM KCl, 3 mM CaCl<sub>2</sub>, 2 mM MgCl<sub>2</sub>, 5 mM sodium phosphate, pH 7.0; TPS), and [<sup>3</sup>H]progesterin aryl

azide was added. The membranes were split into aliquots, and additional ligands were added to the final concentrations indicated in the figure legends. The final concentration of membranes was approximately 2 mg/ml (~1  $\mu$ M nAChR), and the [ $^3$ H]progesterin aryl azide was present at 0.4  $\mu$ M. The presence of 0.1 mM oxidized glutathione (GSSG) as a scavenger during photolysis reduced the incorporation into both nAChR and non-nAChR polypeptides by ~40%, and no further reduction was seen at GSSG concentrations up to 1 mM GSSG. Therefore, after a 1 hour incubation at room temperature, oxidized glutathione (GSSG) was routinely added to a final concentration of 1 mM. Since [ $^3$ H]progesterin aryl azide was reported to absorb strongly at 246 nm (Kym *et al.*, 1993), the suspensions were irradiated at 254 nm (Spectroline EF-16) for 2 minutes in a plastic 96-well plate on ice. Five minute photolysis did not increase the incorporation appreciably. The suspensions were diluted with sample loading buffer and directly submitted to SDS-PAGE.

For proteolytic mapping of [ $^3$ H]progesterin aryl azide labeled  $\alpha$  subunit with *S. aureus* V8 protease (Cleveland *et al.*, 1977; White and Cohen, 1992), labeling was carried out with 400  $\mu$ g (analytical mapping) or 10 mg (preparative) nAChR-rich *Torpedo* membranes. For analytical mapping, samples were photolyzed in a 24-well plate, while for preparative mapping, the samples were photolyzed in glass dishes (5.5 cm diameter). Following photolysis, the membrane suspensions were pelleted. For analytical mapping, samples were resuspended in 40  $\mu$ l 50 mM sodium phosphate, pH 7, 1% SDS, and 40  $\mu$ l of 50 mM sodium phosphate, pH 6, with or without 5 mU endoglycosidase H was added to each. After an overnight incubation, samples were diluted with sample buffer and submitted to SDS-PAGE. For preparative mapping, samples were resuspended in TPS (2 mg/ml) and then labeled further with 1-azidopyrene (1-AP) (Blanton and Cohen, 1994) to ease identification and isolation of subunits and fragments from gels. 1-AP (62.5 mM in

DMSO) was added to a final concentration of 500  $\mu$ M. After a 90 minute incubation, the samples were photolyzed for 15 minutes on ice using a 365 nm lamp (Spectroline EN-16). Membranes were pelleted (15000xg) for 30 minutes, resuspended in sample buffer, and submitted to SDS-PAGE.

### **Gel Electrophoresis**

Gel electrophoresis was carried out as described in Chapter 3.

### **Proteolytic digestion**

For EndoLysC digestion, acetone precipitated peptides were resuspended in 15 mM Tris, pH 8.1, 0.1% SDS. EndoLysC (1.5 mU in resuspension buffer) was added to a final volume of 100  $\mu$ l. The digestion was allowed to proceed for 7-9 days before separation of fragments by Tricine SDS-PAGE (Schagger and von Jagow, 1987). For trypsin digestion, acetone precipitated peptides were resuspended in a small volume (40  $\mu$ l) of 100 mM  $\text{NH}_4\text{CO}_3$ , 0.1% SDS, pH 7.8. Genapol C-100 and trypsin were added, with a final concentration of 0.02% SDS, 0.5% Genapol C-100, and 1:1 (w/w) trypsin. The digestion was allowed to proceed 3-4 days at room temperature prior to separation of the fragments by Tricine SDS-PAGE. Following Tricine SDS-PAGE, bands were excised based on fluorescence and molecular weight, and fragments were isolated as above. Pellets were resuspended in either 40  $\mu$ l (for sequencing directly) or 200  $\mu$ l (for HPLC purification) 15 mM Tris pH 8.1, 0.1% SDS.

### **HPLC purification**

Proteolytic fragments from enzymatic digestion of [ $^3\text{H}$ ]progesterone aryl azide labeled subunits were further purified by reverse-phase HPLC, as described by Blanton and Cohen (1992), using a Brownlee C4 Aquapore column (100 x 2.1 mm; 7  $\mu$ m particle size). Solvent A was 0.08% TFA in water, and solvent B was 0.05% TFA in 60%

acetonitrile/40% 2-propanol. A nonlinear gradient (Waters Model 680 gradient controller, curve No. 7) from 25% to 100% solvent B in 80 minutes was used. The rate of flow was 0.2 ml/min, and 0.5 ml fractions were collected. The elution of peptides was monitored by absorbance at 215 nm, and the fluorescence from 1-AP was detected by fluorescence emission (357 nm excitation, 432 nm emission). Additionally, 50  $\mu$ L aliquots from the fractions were taken to determine the distribution of  $^3\text{H}$  by liquid scintillation counting.

### **Sequence Analysis**

Automated amino terminal sequence analysis was performed on an Applied Biosystems Model 477A protein sequencer with an in-line 120A PTH analyzer. When multiple HPLC fractions were combined, solvent was removed by vacuum centrifugation, and samples were resuspended in 40  $\mu$ l 15 mM Tris pH 8.1, 0.1% SDS. The SDS present in the storage buffer was removed using a pre-wash step. The pre-wash step consisted of a four minute treatment with gas-phase TFA followed by a five minute wash with ethyl acetate (this pre-wash step was not used for samples labeled with [ $^3\text{H}$ ]ethidium diazide (Chapter 2) or [ $^3\text{H}$ ]3-azioctanol (Chapter 3)). When single HPLC samples (450  $\mu$ l per fraction) were sequenced, they were directly loaded onto chemically modified glass fiber disks (Beckman) in 20  $\mu$ l aliquots, allowing the solvent to evaporate at 40°C between loads. Sequencing was performed using gas-phase TFA to minimize possible hydrolysis. After conversion of the released amino acids to PTH amino acids, the suspension was divided into two parts. One portion, approximately one-third, went to the PTH analyzer while the remaining two-thirds was collected for scintillation counting. Yield of PTH amino acids was calculated from peak height compared with standards using the program Model 610A Data Analysis Program Version 1.2.1. Initial yield and repetitive yield were calculated by a nonlinear least squares regression to the equation  $M=I_0 * R^n$ , where M is

the observed release,  $I_0$  is the initial yield,  $R$  is the repetitive yield, and  $n$  is the cycle number. Derivatives known to have poor recovery (Ser, Arg, Cys, and His) were omitted from the fit.

## RESULTS

### Photoincorporation of [ $^3\text{H}$ ]progesterin aryl azide into nAChR-rich membranes

Initial experiments were designed to characterize the general pattern of [ $^3\text{H}$ ]progesterin aryl azide photoincorporation as well as to test the sensitivity of the incorporation to various drugs. Membranes (2 mg of protein/mL) were equilibrated with 0.4  $\mu\text{M}$  [ $^3\text{H}$ ]progesterin aryl azide in the presence and absence of several drugs. After irradiation for 2 minutes at 254 nm, the pattern of incorporation was assessed by SDS-PAGE followed by fluorography. As is evident in the fluorograph of the 8% polyacrylamide gel (Figure 4-2), [ $^3\text{H}$ ]progesterin aryl azide photoincorporated into all four subunits of the nAChR as well as into the  $\alpha$ -subunit of  $\text{Na}^+/\text{K}^+$  ATPase. Incorporation was greatest in the  $\alpha$  and  $\gamma$  subunits and was present to a lesser extent in  $\beta$  and  $\delta$ . The presence of carbamylcholine had no effect on the incorporation. Additionally, the presence or absence of 10  $\mu\text{M}$  or 100  $\mu\text{M}$  progesterone was without effect. Proadifen, an aromatic amine nAChR NCA, at 100  $\mu\text{M}$  also showed no inhibition of [ $^3\text{H}$ ]progesterin aryl azide incorporation. 100  $\mu\text{M}$  Tetracaine appeared to have reduced the incorporation in all polypeptide bands, though that effect is most likely due to the UV absorbance of tetracaine itself. Based upon scintillation counting of excised gel bands,  $\sim 30$  cpm/pmol was incorporated in the  $\alpha$  subunit. This incorporation, with  $\sim 0.3\%$  of the  $\alpha$ -subunits labeled, is similar to the levels of labeling by promegestone ( $\sim 0.1\%$  of  $\alpha$ -subunits labeled) at similar concentrations (Blanton, 1999).

## **Mapping the [<sup>3</sup>H]progesterone aryl azide incorporation in nAChR $\alpha$ subunit with V8 protease**

The distribution of [<sup>3</sup>H]3-azidoethanol incorporation within the  $\alpha$ -subunit was examined by digestion of the labeled subunit with *S. aureus* V8 protease. V8 protease cleavage in the gel generates 4 large fragments,  $\alpha$ V8-20,  $\alpha$ V8-18,  $\alpha$ V8-10, and  $\alpha$ V8-4, named according to their apparent molecular weights (Pedersen *et al.*, 1986).  $\alpha$ V8-20 (Ser-173–Glu-338) contains the  $\alpha$ M1,  $\alpha$ M2 and  $\alpha$ M3 transmembrane segments, as well as a portion of the N-terminal extracellular segment. The  $\alpha$ M4 transmembrane segment is within  $\alpha$ V8-10 (Asn-339–Gly-437).  $\alpha$ V8-18 (Val-46–Glu-172) contains a glycosylation sensitive to EndoglycosidaseH, and when membranes are treated with EndoglycosidaseH, the deglycosylated fragment now runs at ~12 kD ( $\alpha$ V8-12). When the incorporation of [<sup>3</sup>H]progesterone aryl azide was mapped using *S. aureus* V8 protease, incorporation was primarily within the  $\alpha$ V8-10 fragment, as seen in the fluorogram (Figure 4-3). Based upon liquid scintillation counting of excised gel bands, in the absence of other drugs, ~75% of the incorporated <sup>3</sup>H was in  $\alpha$ V8-10, ~10% in  $\alpha$ V8-20, and ~6% in  $\alpha$ V8-18.

## **Localization of [<sup>3</sup>H]progesterone aryl azide incorporation within $\alpha$ V8-10**

To further characterize the incorporation of [<sup>3</sup>H]progesterone aryl azide in the  $\alpha$ V8-10 fragment, 10 mg of nAChR membranes were labeled with [<sup>3</sup>H]progesterone aryl azide in the presence of 1 mM GSSG. These membranes were also labeled with 1-azidopyrene (1-AP) (Blanton and Cohen, 1992) for ease of identifying subunits and fragments following SDS-PAGE, as described in Methods. Following separation of subunits by SDS-PAGE, the  $\alpha$ -subunit was transferred to the well of a mapping gel for digestion with V8 protease. Proteolytic fragments were identified after electrophoresis by illumination

at 365 nm to detect 1-AP incorporation.  $\alpha$ V8-10 was identified by fluorescence and mobility, excised, eluted, and concentrated.

$\alpha$ V8-10 labeled with [ $^3$ H]progesterone aryl azide was digested with trypsin, and the fragments were separated by HPLC (Figure 4-4A). A peak of  $^3$ H eluted between fractions 34-37 (~84% organic), with little  $^3$ H in the flow through, indicating that [ $^3$ H]progesterone aryl azide incorporation in  $\alpha$ M4 is stable to HPLC conditions. A tryptic fragment of  $\alpha$ V8-10 beginning at  $\alpha$ Tyr-401 which was labeled with [ $^3$ H]promegestone was reported to have eluted at ~82% organic (Blanton *et al.*, 1999). Fractions 34-36 were pooled, dried, resuspended in 40  $\mu$ l buffer, and subjected to sequence analysis. Since SDS was present in the resuspension buffer, the filter was pre-treated with TFA and washed with ethyl acetate to remove SDS. The ethyl acetate wash was assayed for  $^3$ H, and contained ~20% of the  $^3$ H originally present in the 3 HPLC fractions. Sequence analysis of these fractions (Figure 4-4B) following pooling, drying, and resuspension showed the presence of three sequences, beginning at  $\alpha$ Tyr-401 ( $I_0$ =27 pmol), at the N-terminus of  $\alpha$ M4;  $\alpha$ Ser-388 ( $I_0$ =25 pmol), which also contained the  $\alpha$ M4 segment; and  $\alpha$ Met-243 ( $I_0$ =10 pmol), which is the N-terminus of  $\alpha$ M2. The presence of the sequence beginning at  $\alpha$ Met-243 was due to accidental contamination of the  $\alpha$ V8-10 sample with  $\alpha$ V8-20. While low levels of release appeared consistent through triplicate counting of cycles 17 and 23, ~10 cpm above background, no release was evident when similar fractions from a separate labeling experiment were sequenced. This second experiment contained only two sequences, one beginning at  $\alpha$ Tyr-401 (15 pmol) and one beginning at  $\alpha$ Ser-388 (20 pmol). However, the sequence which showed low levels of  $^3$ H in cycle 17 and 23 of release had ~2-fold more mass of  $\alpha$ Tyr-401, and additionally there was more  $^3$ H within the fractions pooled (~6000 cpm vs. ~3500 cpm).

### Localization of [<sup>3</sup>H]progesterin aryl azide incorporation in the nAChR $\beta$ subunit

A ~5 kD proteolytic fragment of  $\beta$  which contains the  $\beta$ M4 segment can be generated by a trypsin digestion of the  $\beta$ -subunit (Blanton *et al.*, 1998a).  $\beta$ -subunit labeled with [<sup>3</sup>H]progesterin aryl azide was therefore digested with trypsin, and the fragments were separated by Tricine SDS-PAGE. After elution, the fragments were either sequenced directly, as was done with those from the first labeling experiment, or further separated by HPLC before sequence analysis, in the second labeling. When samples were sequenced directly following gel elution, the band spanning ~5-7 kD contained four fragments containing  $\beta$ M4 (total  $I_0$ =167 pmol) as well as a sequence beginning at  $\beta$ Ser-126 ( $I_0$ =44 pmol). No <sup>3</sup>H release above background was seen, though only 2000 cpm was loaded on the filter. Since these samples contained SDS, pretreatment of the sequencing filter with TFA was necessary prior to sequencing. During this treatment, ~15% of the loaded <sup>3</sup>H was removed.

As an alternative approach, from a separate labeling experiment, the tryptic digest of  $\beta$ -subunit was fractionated by Tricine SDS-PAGE, and then the eluted fragments were further purified by HPLC. Upon HPLC purification of the band containing fragments of ~4-8 kD (band 2), ~50% of the <sup>3</sup>H eluted in the flow-through (Figure 4-5), indicating instability of incorporation to the conditions of HPLC. Hydrophobic fractions which contained <sup>3</sup>H were loaded directly onto sequencing filters, avoiding the pre-wash step, and subjected to Edman degradation. The results are summarized in Table 4-1. Sequence analysis of fraction 31 (~78% organic), containing ~540 cpm, revealed the presence of two fragments, one beginning at  $\beta$ Lys-216 (15 pmol), the N-terminus of the  $\beta$ M1 segment, and one beginning at  $\beta$ Asp-427 (7 pmol), the N-terminus of the  $\beta$ M4 segment. No <sup>3</sup>H release above background was evident in 20 cycles, with the <sup>3</sup>H in the first cycle ~20 cpm (not shown). Sequence analysis of fraction 34 (~93% organic), containing ~560

cpm, revealed the presence of a fragment beginning at  $\beta$ Met-249 (18 pmol), the N-terminus of the  $\beta$ M2 segment. When Band 1 was purified by HPLC, ~30% of the  $^3\text{H}$  was present in the flow-through. Fractions 22, 25, 26, and 28 were sequenced (summarized in Table 4-1) and showed sequences attributable to both the nAChR  $\beta$  subunit and several contaminating fragments (from nAChR  $\delta$ -subunit as well as the  $\beta$ -subunit of  $\text{Na}^+/\text{K}^+$  ATPase).

### **Localization of [ $^3\text{H}$ ]progesterin aryl azide incorporation in the nAChR $\gamma$ -subunit**

A ~5 kD peptide containing  $\gamma$ M4 can be generated by digestion of the  $\gamma$ -subunit with trypsin (Blanton *et al.*, 1999).  $\gamma$ -subunit labeled with [ $^3\text{H}$ ]progesterin aryl azide was therefore digested with trypsin, and the fragments were separated by Tricine SDS-PAGE. Two bands containing  $^3\text{H}$  were excised from the Tricine gel based upon molecular weight. Upon HPLC purification of the band containing fragments of ~3-6 kD (band 2), ~50% of the  $^3\text{H}$  eluted in the flow-through (Figure 4-6A), indicating instability of incorporation to the conditions of HPLC. Hydrophobic fractions which contained  $^3\text{H}$  were loaded directly onto sequencing filters, avoiding the pre-wash step, and subjected to Edman degradation. The results are summarized in Table 4-1. Sequence analysis of fraction 31 (~78% organic), containing ~610 cpm, revealed the presence of two fragments, one beginning at  $\gamma$ Val-466 (7 pmol), the N-terminus of the  $\gamma$ M4 segment, and one beginning at  $\gamma$ Lys-218 (2 pmol), the N-terminus of the  $\gamma$ M1 segment. No  $^3\text{H}$  release above background was evident in 20 cycles. When Band 1, which contained fragments ~1-3 kD, was purified by HPLC, ~50% of the  $^3\text{H}$  eluted in the flow-through (Figure 4-6B). Fractions 25 and 26 were sequenced (summarized in Table 4-1), and contamination by  $\delta$ -subunit was evident. Again, no  $^3\text{H}$  release above background was evident from either of these sequences.

### **Localization of [<sup>3</sup>H]progesterin aryl azide incorporation in the nAChR $\delta$ -subunit**

EndoLysC digest of  $\delta$ -subunit generates a fragment beginning at  $\delta$ Met-257, the N-terminus of  $\delta$ M2, which runs on a Tricine gel between 6 and 10 kD (Gallagher and Cohen, 1999).  $\delta$ -subunit labeled with [<sup>3</sup>H]progesterin aryl azide was therefore digested with EndoLysC, and the fragments were separated by Tricine SDS-PAGE. A band containing fragments of ~3-10 kD was excised, and the eluted fragments were further purified by reverse-phase HPLC (Figure 4-7). Approximately ~20% of the <sup>3</sup>H eluted in the flow-through. Hydrophobic fractions which contained <sup>3</sup>H were loaded directly onto sequencing filters, avoiding the pre-wash step, and subjected to Edman degradation. The results are summarized in Table 4-1. Sequence analysis of fraction 31 (~80% organic), containing ~470 cpm, showed the presence of only one sequence, that beginning at  $\delta$ Met-257 (17 pmol), the N-terminus of  $\delta$ M2. Fraction 28 (~66% organic), containing ~410 cpm, contained two sequences, one beginning at  $\delta$ Ser-421 (15 pmol) and one beginning at  $\delta$ Asn-437 (11 pmol), both of which contain the  $\delta$ M4 segment. Sequence analysis of fraction 26, containing ~600 cpm, showed the presence of two sequences, one beginning at  $\delta$ Phe-206 (88 pmol) and one beginning at  $\delta$ Asn-200 (102 pmol), both of which should contain the  $\delta$ M1 segment. The separation of these fragments showed the high resolution of the reverse-phase HPLC conditions for these hydrophobic fragments. These fractions were only sequenced for 6 cycles, since no release was expected from such low levels of loaded <sup>3</sup>H, and ~20 cpm was present in the first cycle of each.

### **DISCUSSION**

[<sup>3</sup>H]Progesterin aryl azide photoincorporated into all four subunits of the nAChR. Within the  $\alpha$  subunit, ~75% of the incorporation was within a fragment containing  $\alpha$ M4. Incorporation in the other subunits was not clearly mapped, although there was evidence

for incorporation in the M4 segments, as well as possible incorporation in other transmembrane segments.

The incorporation of [<sup>3</sup>H]progesterin aryl azide at the subunit level was not altered by any of the cholinergic drugs tested. Inhibition at a specific site, however, could have been masked by nonspecific incorporation elsewhere. For example, if the site were in the  $\alpha$ V8-20 fragment, which contained only ~10% of the incorporation, a decrease in incorporation would have been undetectable in the intact subunit. An apparent decrease in the incorporation in  $\alpha$ V8-20 was observed in the presence of carbamylcholine, with an increase in the incorporation in  $\alpha$ V8-18, ~2-fold, though this study was performed only once (Figure 4-3). Further information on the sites of incorporation in these fragments is lacking.

The incorporation in  $\alpha$ V8-10 was within the  $\alpha$ M4 segment. This incorporation was stable to the conditions of HPLC, and, after trypsin digestion of  $\alpha$ V8-10, radioactivity was revealed to be within a hydrophobic fragment beginning at the N-terminus of  $\alpha$ M4. In one experiment sequence analysis of this fragment resulted in very low levels of release in cycles 17 and 23, approximately 10 cpm, although this release was not seen in a second experiment which, unfortunately, contained lower levels of mass and radioactivity. Unlike [<sup>3</sup>H]progesterin aryl azide, the sequence analysis of this same fragment labeled with [<sup>3</sup>H]promegestone showed ~300 cpm release in cycle 13,  $\alpha$ Cys-412 (Blanton, 1999). However, 129 pmol of the sequence beginning at  $\alpha$ Tyr-401 was present, and 44000 cpm was loaded. Here, 6000 cpm were present in the HPLC fractions which were pooled, and two sequences containing  $\alpha$ M4 were present, one beginning at  $\alpha$ Tyr-401 (27 pmol) and one beginning at Ser-388 (25 pmol). Therefore, under the conditions seen here, the release from the sequence beginning at  $\alpha$ Tyr-401 labeled by [<sup>3</sup>H]promegestone would have only showed ~25 cpm of release. This level of release

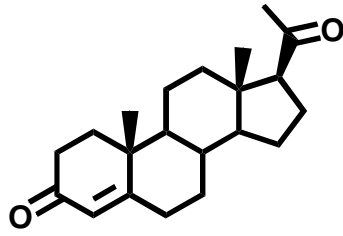
would have been detectable had [ $^3\text{H}$ ]progesterin aryl azide photoincorporated into  $\alpha\text{Cys-412}$ . Additionally, the release from the fragment labeled by [ $^3\text{H}$ ]progesterin aryl azide was in cycles 17 and 23, which, due to loss in the repetitive yield, would have even lower levels of release if labeled at similar levels as  $\alpha\text{Cys-412}$  was by [ $^3\text{H}$ ]promegestone. Although ~20% of the radioactivity loaded on the sequencer filter was released during prewash, perhaps due to loss from a single site, the lack of release in cycle 13, and the presence in cycles 17 and 23, may indicate that the steroids bind in a single orientation and that the photoreactive group on ring A may be able to access  $\alpha\text{Cys-412}$  while the photoreactive group on ring D only accesses residues closer to the center of the lipid bilayer.

Within the other subunits, incorporation within the M4 segments is also likely. Sequence analysis of HPLC fractions showed the presence of fragments containing the M4 segments within fractions containing  $^3\text{H}$ . However, in the case of  $\beta$  and  $\gamma\text{M4}$  segments, other fragments were also present, and no release of  $^3\text{H}$  was seen. Additionally, unlike the incorporation of [ $^3\text{H}$ ]progesterin aryl azide in  $\alpha\text{M4}$ , the incorporation in the  $\beta$ -,  $\gamma$ - and  $\delta$ -subunits was unstable to the conditions of HPLC. Aryl azides are known to rearrange to ketenimine azepines, and photoadducts formed with this group are expected to be labile under acidic conditions, like those used for HPLC. Additional evidence of instability to acid came from the loss of  $^3\text{H}$  during the pre-wash of the sequencing filter.

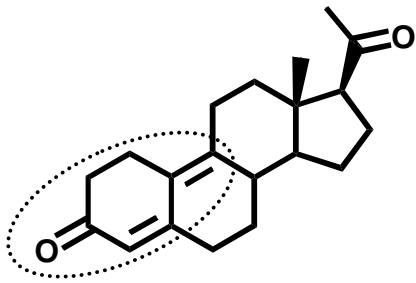
In addition to incorporation in the M4 segments, it is likely that there was incorporation within other transmembrane segments of  $\beta$  and  $\delta$ . In HPLC fraction 26 from band 1 of  $\beta$ , the only nAChR sequence present was  $\delta\text{M2}$ . The size of this fragment, ~2-4 kD, indicated that this fragment contained the  $\delta\text{M2}$  segment without the  $\delta\text{M3}$  segment. Additionally, a fragment containing the  $\delta\text{M2}$  and  $\delta\text{M3}$  segments was the only

sequence present in fraction 31 from the HPLC purification of band 2 of  $\delta$ . Similarly, fraction 34 from the HPLC of  $\beta$  band 2 showed only the sequence beginning at  $\beta$ Met-249, the N-terminus of  $\beta$ M2, and this fragment should contain both the  $\beta$ M2 and  $\beta$ M3 segments, based on the molecular weight. If the  $^3\text{H}$  in these HPLC fractions were attributable to these fragments containing the M1 and M2 sequences, then they should contain similar levels of incorporation to the  $\beta$  and  $\delta$ M4 segments.

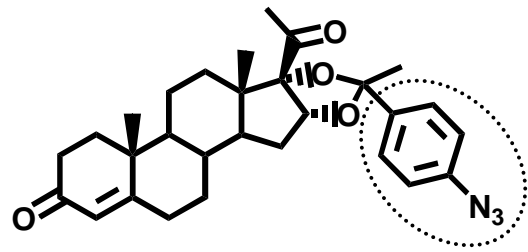
The loss of  $^3\text{H}$  during HPLC and pre-wash treatment and the low mass levels precluded the identification of residues into which [ $^3\text{H}$ ]progesterin aryl azide might have photoincorporated. In order to identify particular amino acids labeled by [ $^3\text{H}$ ]progesterin aryl azide, further studies would require labeling at higher concentrations of [ $^3\text{H}$ ]progesterin aryl azide, and identification would depend upon efficient isolation of labeled fragments. Alternatively, studies with another steroid containing a photoactivatable group which photoincorporates into the nAChR with higher efficiency and forms bonds upon photoincorporation which are more stable to the conditions of HPLC and sequencing, such as a diazirine or benzophenone, could help define the site of action of neurosteroids on the nAChR.



**Progesterone**



**Promegestone**



**Progestin Aryl Azide**

**Figure 4-1. Structure of progesterone and photoaffinity derivatives**

Structures of progesterone, promegestone, and progestin aryl azide are shown. Dotted ovals show location of photoreactive group.



**Figure 4-2. Photoincorporation of [<sup>3</sup>H]progesterin aryl azide into integral and peripheral membrane proteins of nAChR-rich membranes in the presence or absence of various cholinergic drugs.**

nAChR-rich membranes (100 µg) were equilibrated with [<sup>3</sup>H]progesterin aryl azide in TPS (2 mg/ml) in the presence of 1 mM oxidized glutathione in the absence (lanes 1-4) or presence (5-8) of carbamylcholine, and in the presence of 10 µM (lanes 2 and 6) or 100 µM (lanes 3 and 7) progesterone, 100 µM tetracaine (lane 4), or 100 µM proadifen (lane 8). After photolysis at 254 nm for 2 minutes, the samples were subjected to SDS-PAGE, visualized by Coomassie Blue (Panel A), processed for fluorography, and exposed to film for 3 weeks (Panel B). Indicated on the left are the mobilities of the nAChR subunits, calectrin (37K), and the α-subunit of the Na<sup>+</sup>/K<sup>+</sup> ATPase (αNK). Based on scintillation counting of parallel lanes, the radioactivity incorporated in the absence of carbamylcholine was: α: 3544; β: 2385; γ: 1423; δ: 1149; 43K: 2385; αNK: 2688.

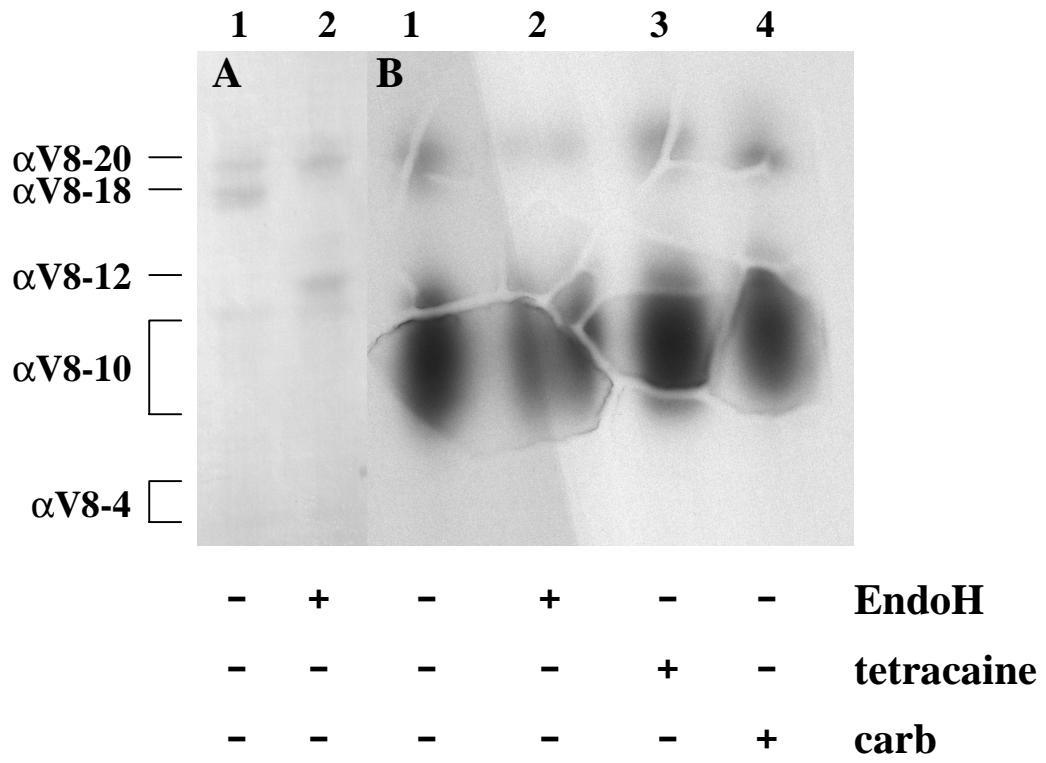


**Figure 4-3. Proteolytic mapping of sites of [<sup>3</sup>H]progesterin aryl azide incorporation into the nAChR  $\alpha$ -subunit using *S. aureus* V8 protease.**

nAChR-rich membranes (400  $\mu$ g) were labeled with [<sup>3</sup>H]progesterin aryl azide in the presence of 1 mM oxidized glutathione and in the absence of other cholinergic drugs (lanes 1 and 2) or in the presence of 100  $\mu$ M tetracaine (lane 3) or 2 mM carbamylcholine (lane 4). One sample labeled in the absence of other drugs was treated with EndoglycosidaseH (lane 2) as described in methods, while the other samples incubated in buffer without EndoglycosidaseH overnight. After incubation, membranes were submitted to SDS-PAGE, and the  $\alpha$ -subunit was excised. The excised bands were transferred to the well of a 15% mapping gel and digested with V8 protease as described in methods. A, mapping gel stained with Coomassie Blue. B, fluorogram of mapping gel, exposed for 4 weeks. The mobility of the proteolytic fragments is indicated on the left. Shown above is a schematic indicating the positions of the four fragments within the primary structure of the nAChR  $\alpha$  subunit. Based on scintillation counting of parallel lanes, the cpm incorporated in the absence of carbamylcholine was:  $\alpha$ V8-20: 911;  $\alpha$ V8-18: 498;  $\alpha$ V8-10: 6749.

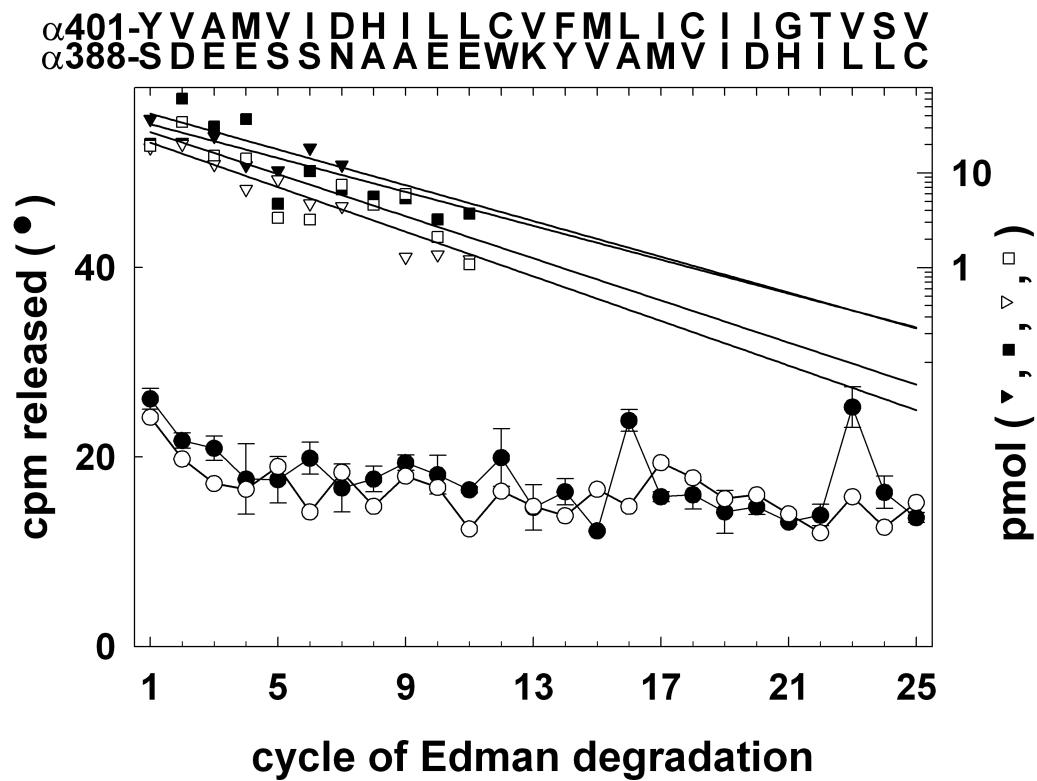
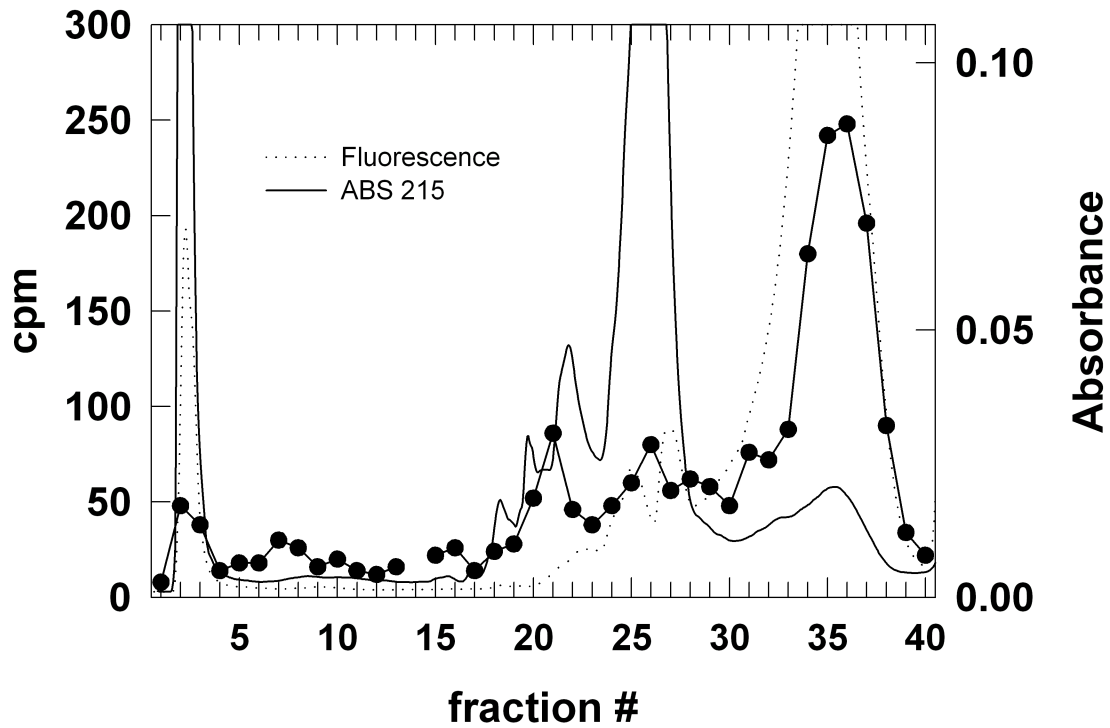


**Figure 4-4. Reverse phase HPLC purification of [<sup>3</sup>H]progesterin aryl azide labeled fragments from trypsin digest of  $\alpha$ V8-10**

A,  $\alpha$ V8-10 isolated from nAChR photolabeled with [<sup>3</sup>H]progesterin aryl azide was digested with trypsin. The digest was applied to a Brownlee Aquapore C4 column and fractionated by reverse-phase HPLC. <sup>3</sup>H elution profiles (●) are from scintillation counting of 10% of each fraction. Fluorescence (·····) and absorbance profiles (—) were measured as described in methods.

B, <sup>3</sup>H (●,○) and mass released (■, ▼, □, ▽) on N-terminal sequencing of material in HPLC fractions 34-36 from two separate preparative labeling experiments. In one experiment (●), two sequences containing  $\alpha$ M4 were present, one beginning at  $\alpha$ Tyr-401 (■, I<sub>0</sub>=27 pmol, R=83%), and one beginning at  $\alpha$ Ser-388 (▼, I<sub>0</sub>=25 pmol, R=83%), as well as a sequence beginning at  $\alpha$ Met-243 (I<sub>0</sub>=10 pmol, R=86%), containing the  $\alpha$ M2 and  $\alpha$ M3 segments. Total <sup>3</sup>H in the HPLC fractions was 6000 cpm, with 1300 cpm released during pre-wash, and 1300 cpm remaining on the filter. In the other experiment (○), only the sequences containing  $\alpha$ M4 were present ( $\alpha$ Tyr-401 (□): I<sub>0</sub>=15 pmol, R=80%;  $\alpha$ Ser-388 (▽): I<sub>0</sub>=20 pmol, R=82%). Total <sup>3</sup>H in the HPLC fractions was 3500 cpm, with 1100 cpm released during pre-wash, and 310 cpm remaining on the filter.

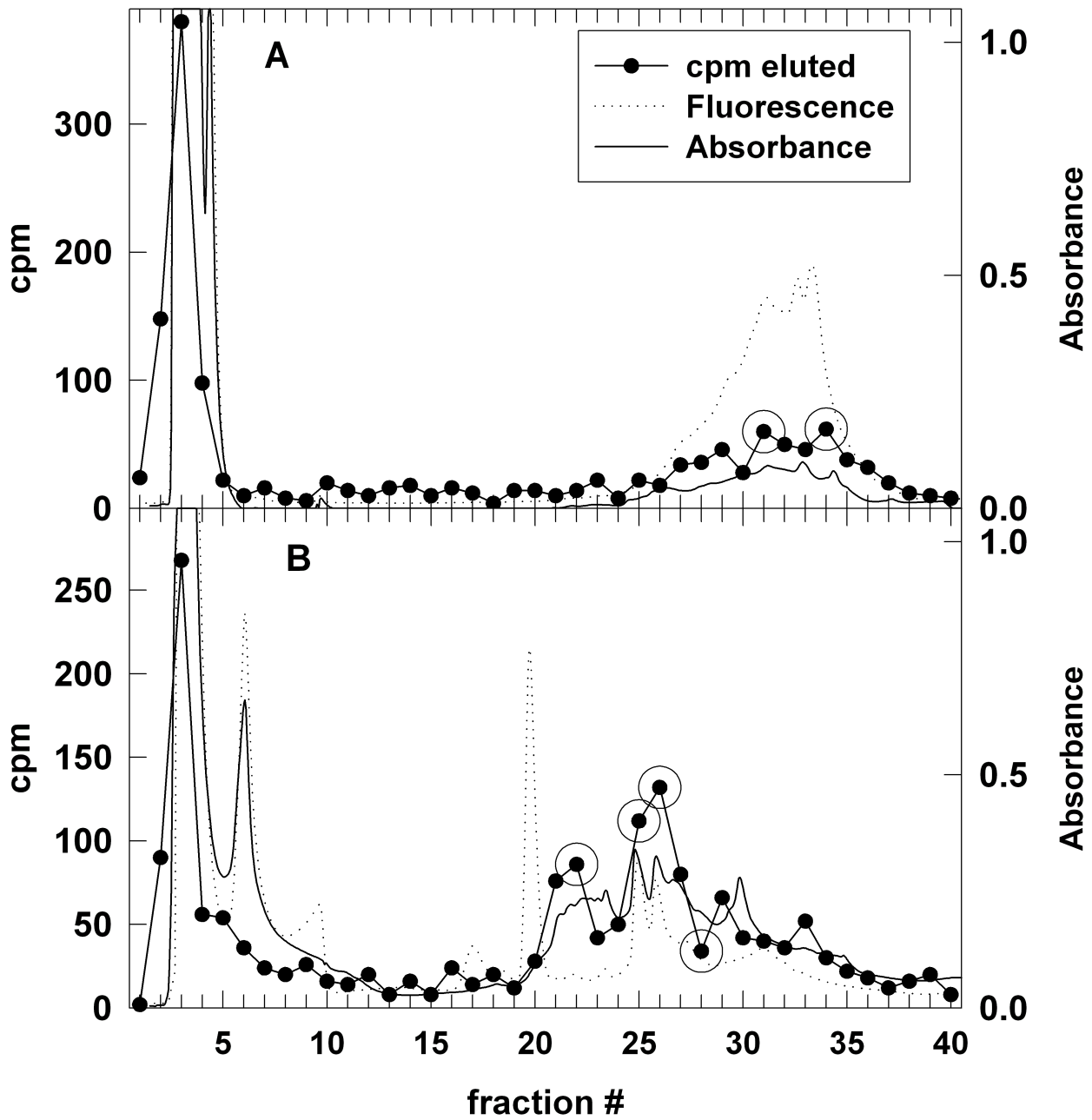


**Figure 4-5. HPLC purification of [<sup>3</sup>H]progesterone aryl azide labeled fragments from trypsin digest of  $\beta$ -subunit**

A, B. nAChR  $\beta$ -subunit isolated from nAChR-rich membranes photolabeled with [<sup>3</sup>H]progesterone aryl azide was digested with trypsin. The digest was initially fractionated by Tricine SDS-PAGE. Two bands containing <sup>3</sup>H (Band 2, 4-8 kD (A); Band 1, 2-4 kD (B)) were applied to a Brownlee Aquapore C4 column and fractionated by reverse-phase HPLC. <sup>3</sup>H elution profiles (●) are from scintillation counting of 10% of each fraction. Fluorescence (·····) and absorbance profiles (—) were measured as described in methods. For Band 2 (A), material in fractions 31 and 24 (circled) was sequenced, and for Band 1 (B), fractions 22, 25, 26, and 28 was sequence (see Table 4-1).

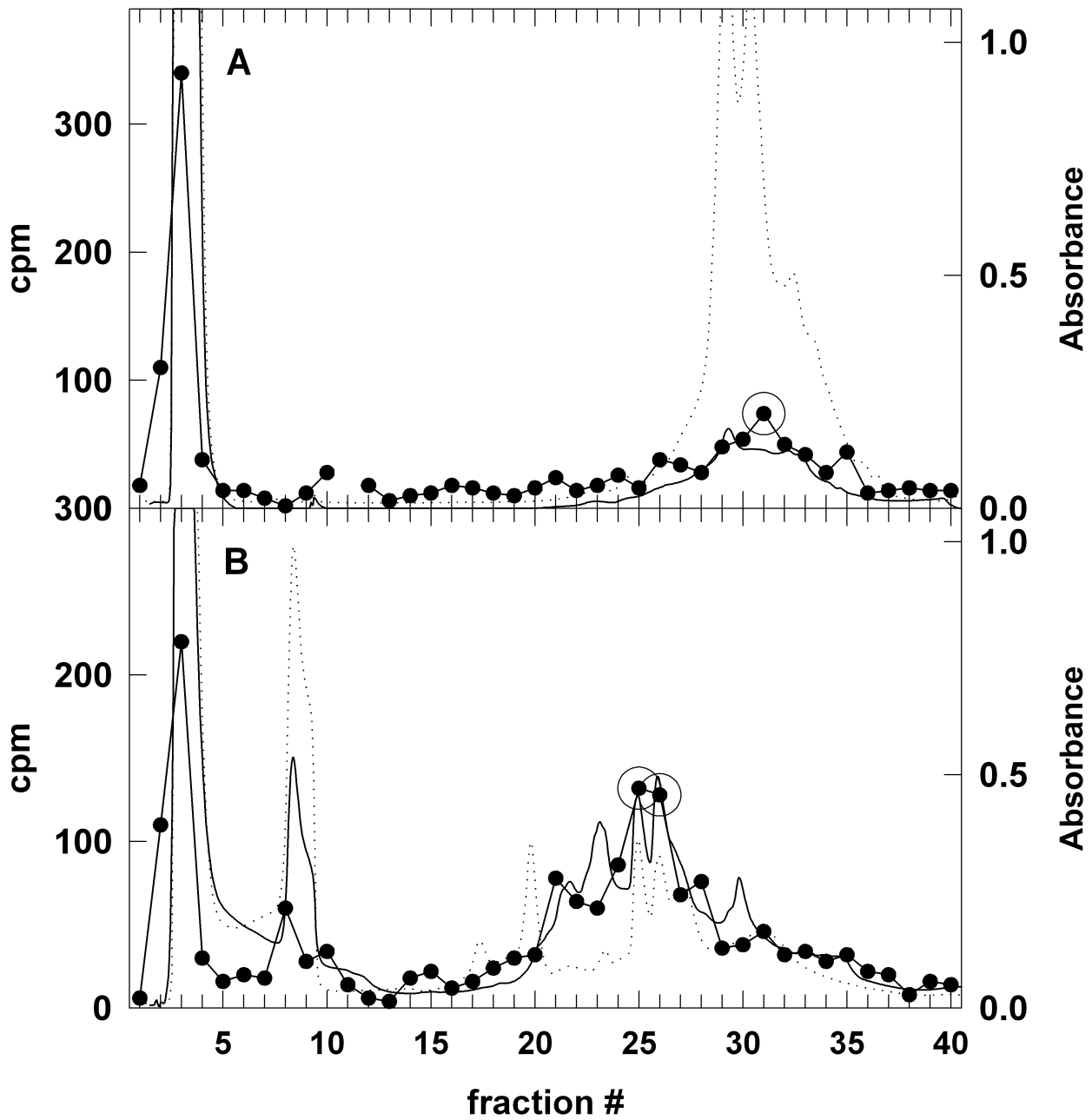


**Figure 4-6. HPLC purification of [<sup>3</sup>H]progesterin aryl azide labeled fragments from trypsin digest of  $\gamma$ -subunit**

A, B. nAChR  $\gamma$ -subunit isolated from nAChR-rich membranes photolabeled with [<sup>3</sup>H]progesterin aryl azide was digested with trypsin. The digest was initially fractionated by Tricine SDS-PAGE. Two bands containing <sup>3</sup>H (Band 2, 3-6 kD (A); Band 1, 1-3 kD (B)) were applied to a Brownlee Aquapore C4 column and fractionated by reverse-phase HPLC. <sup>3</sup>H elution profiles (●) are from scintillation counting of 10% of each fraction. Fluorescence (·····) and absorbance profiles (—) were measured as described in methods. For Band 2 (A), fraction 31 was sequenced, and for Band 1 (B) fractions 25 and 26 were sequenced (see Table 4-1).

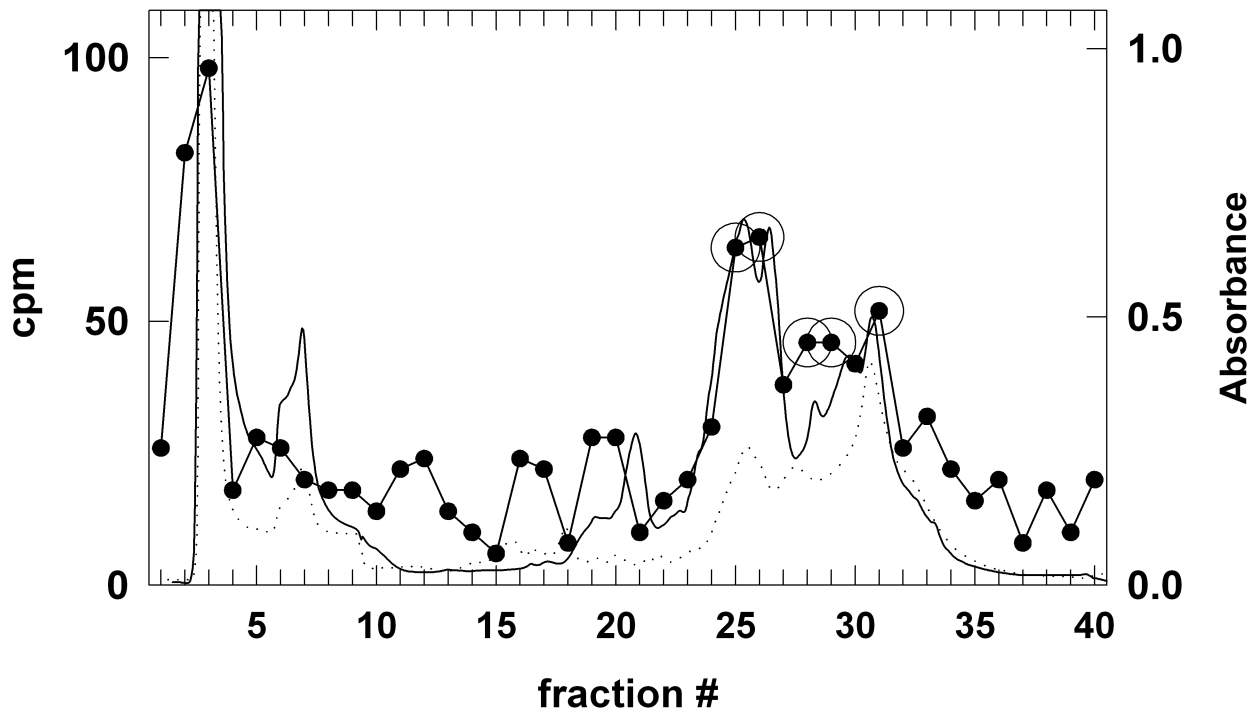


**Figure 4-7. HPLC purification of [<sup>3</sup>H]progesterin aryl azide labeled fragments from EndoLysC digest of  $\delta$ -subunit**

nAChR  $\delta$ -subunit isolated from nAChR-rich membranes photolabeled with [<sup>3</sup>H]progesterin aryl azide was digested with EndoLysC. The digest was initially fractionated by Tricine SDS-PAGE. One band containing <sup>3</sup>H (3-10 kD) was applied to a Brownlee Aquapore C4 column and fractionated by reverse-phase HPLC. <sup>3</sup>H elution profiles (●) are from scintillation counting of 10% of each fraction. Fluorescence (·····) and absorbance profiles (—) were measured as described in methods. Fractions 25, 26, 28, 29, and 31 (circled) were sequenced (see Table 4-1).

**Table 4-1 Sequence analysis of HPLC fractions of proteolytic fragments of  $\beta$ ,  $\gamma$ , and  $\delta$  subunits labeled with [ $^3\text{H}$ ]progesterone aryl azide.**

$\beta$  and  $\gamma$  subunits were digested with trypsin, and  $\delta$ -subunit was digested with EndoLysC. The digests were first fractionated by Tricine SDS-PAGE, and bands were excised based on fluorescence and molecular weight. The proteolytic fragments in these bands were further separated by reverse-phase HPLC (Figure 4-5, Figure 4-6, Figure 4-7). The indicated HPLC fractions were loaded directly onto sequencing filters and subjected to Edman degradation with initial and repetitive yields of each fragment present shown.

## β subunit

Tricine gel band	HPLC fraction	cpm loaded on filter	N-terminus	I <sub>0</sub>	R
<b>BAND 2</b> 4-8 kD, 9000 cpm total	f31	540 cpm	βLys-216 βAsp-427	15 pmol 7 pmol	92% 95%
	f34	560 cpm	βMet-249	18 pmol	89%
<b>BAND 1</b> 2-4 kD, 11200 cpm total	f22	770 cpm	Ile-183 (βATPase)	86 pmol	77%
	f25	1010 cpm	Asn-207 (trypsin)	30 pmol	85%
	f26	1190 cpm	δMet-257 Asn-207 (trypsin)	20 pmol	94%
	f28	310 cpm	βLys-216	12 pmol	87%

## γ subunit

<b>BAND 2</b> 3-6 kD, 10600 cpm total	f31	610 cpm	γVal-466 γLys-218	6 pmol 2 pmol	
<b>BAND 1</b> 1-3 kD, 15800 cpm total	f25	1200 cpm	Asn-207 (trypsin)	70 pmol	98%
	f26	1200 cpm	γVal-466 δMet-257 δArg-223	10 pmol 23 pmol 47 pmol	91% 92% 91%

## δ subunit

<b>BAND 2</b> 3-10 kD, 6900 cpm total	f25	580 cpm	δVal-1 βATPase Arg-147	26 pmol 40 pmol	90% 90%
	f26	600 cpm	δPhe-208 δAsn-200	88 pmol 102 pmol	91% 90%
	f28	410 cpm	δSer-421 δAsn-437	15 pmol 11 pmol	84% 97%
	f29	410 cpm	δAsn-437 δSer-421 δMet-257	33 pmol 15 pmol 10 pmol	94% 90% 90%
	f31	470 cpm	δMet-257	17 pmol	91%

- Fu DX and Sine S M (1994) Competitive Antagonists Bridge the  $\alpha$ - $\gamma$  Subunit Interface of the Acetylcholine Receptor Through Quaternary Ammonium- Aromatic Interactions. *J Biol Chem* **269**: pp 26152-26157.
- Gallagher MJ and Cohen J B (1999) Identification of Amino Acids of the Torpedo Nicotinic Acetylcholine Receptor Contributing to the Binding Site for the Noncompetitive Antagonist [ $^3$ H]Tetracaine. *Mol Pharmacol* **56**: pp 300-307.
- Galzi J-L, Devillers-Thiéry A, Hussy N, Bertrand S, Changeux J-P and Bertrand D (1992) Mutations in the Channel Domain of a Neuronal Nicotinic Receptor Convert Ion Selectivity From Cationic to Anionic. *Nature* **359**: pp 500-505.
- Galzi JL, Revah F, Black D, Goeldner M, Hirth C and Changeux J-P (1990) Identification of Novel Amino Acid  $\alpha$ -Tyrosine 93 Within the Cholinergic Ligands Binding Sites of the Acetylcholine Receptor by Photoaffinity Labeling. *J Biol Chem* **265**: pp 10430-10437.
- Giraudat J, Dennis M, Heidmann T, Chang J-Y and Changeux J-P (1986) Structure of the High-Affinity Binding Site for Noncompetitive Blockers of the Acetylcholine Receptor: Serine-262 of the  $\delta$  Subunit Is Labeled by [ $^3$ H]Chlorpromazine. *Proc Natl Acad Sci USA* **83**: pp 2719-2723.
- Giraudat J, Dennis M, Heidmann T, Haumont P-Y, Lederer F and Changeux J-P (1987) Structure of the High-Affinity Binding Site for Noncompetitive Blockers of the Acetylcholine Receptor: [ $^3$ H]Chlorpromazine Labels Homologous Residues in the  $\beta$  and  $\gamma$  Chains. *Biochemistry* **26**: pp 2410-2418.
- Giraudat J, Gali J-Z, Revah F, Changeux J-P, Haumont P-Y and Lederer F (1989) The Noncompetitive Blocker [ $^3$ H]Chlorpromazine Labels Segment M2 but Not Segment M1 of the Nicotinic Acetylcholine Receptor  $\alpha$ -Subunit. *FEBS Letts* **253**: pp 190-198.
- Gomez CM and Gammack J T (1995) A Leucine-to-Phenylalanine Substitution in the Acetylcholine Receptor Ion Channel in a Family With the Slow-Channel Syndrome. *Neurology* **45**: pp 982-985.
- Hager DA and Burgess R R (1980) Elution of Proteins From Sodium Dodecyl Sulfate-Polyacrylamide Gels, Removal of Sodium Dodecyl Sulfate, and Renaturation of Enzymatic Activity: Results With  $\sigma$  Subunit of *Escherichia Coli* RNA Polymerase, Wheat Germ DNA Topoisomerase, and Other Enzymes. *Anal Biochem* **109**: pp 76-86.
- Heidmann T, Oswald R E and Changeux J-P (1983) Multiple Sites of Action for Noncompetitive Blockers on Acetylcholine Receptor Rich Membrane Fragments From *Torpedo Marmorata*. *Biochemistry* **22**: pp 3112-3127.
- Herz JM, Johnson D A and Taylor P (1987) Interaction of Noncompetitive Inhibitors With the Acetylcholine Receptor. *J Biol Chem* **262**: pp 7238-7247.

- Herz JM, Johnson D A and Taylor P (1989) Distance Between the Agonist and Noncompetitive Inhibitor Binding Sites on the Nicotinic Acetylcholine Receptor. *J Biol Chem* **264**: pp 12439-12448.
- Horenstein J and Akabas M H (1998) Location of a High Affinity Zn<sup>2+</sup> Binding Site in the Channel of Alpha 1 Beta 1 Gamma-Aminobutyric Acid(A) Receptors. *Mol Pharmacol* **53**: pp 870-877.
- Hucho F, Oberthur W and Lottspeich F (1986) The Ion Channel of the Nicotinic Acetylcholine Receptor Is Formed by the Homologous Helices M II of the Receptor Subunits. *FEBS Letts* **205**: pp 137-142.
- Husain SS, Forman S A, Kloczewiak M A, Addona G H, Olsen R W, Pratt M B, Cohen J B and Miller K W (1999) Synthesis and Properties of 3-(2-Hydroxyethyl-3-*n*-Pentylidiazirine, a Photoactivatable General Anesthetic. *J Med Chem* **42**: pp 3300-3307.
- Imoto K, Busch C, Sakmann B, Mishina M, Konno T, Nakai J, Bujo H, Mori Y, Fukuda K and Numa S (1988) Rings of Negatively Charged Amino Acids Determine the Acetylcholine Receptor Channel Conductance. *Nature* **335**: pp 645-648.
- Imoto K, Konno T, Nakai J, Wang F, Mishina M and Numa S (1991) A Ring of Uncharged Polar Amino Acids As a Component of Channel Constriction in the Nicotinic Acetylcholine Receptor. *FEBS Letts* **289**: pp 193-200.
- Johnson DA and Nuss J M (1994) The Histronicotoxin-Sensitive Ethidium Binding Site Is Located Outside of the Transmembrane Domain of the Nicotinic Acetylcholine Receptor: A Fluorescence Study. *Biochemistry* **33**: pp 9070-9077.
- Kao P, Dwork A J, Kaldany R J, Silver M L, Wideman J, Stein S and Karlin A (1984) Identification of the  $\alpha$ -Subunit Half-Cystine Specifically Labeled by an Affinity Reagent for the Acetylcholine Receptor Binding Site. *J Biol Chem* **259**: pp 11662-11665.
- Karlin A (1991) Explorations of the Nicotinic Acetylcholine Receptor. *The Harvey Lectures* **85**: pp 71-107.
- Karlin A and Akabas M H (1995) Toward a Structural Basis for the Function of Nicotinic Acetylcholine Receptors and Their Cousins. *Neuron* **15**: pp 1231-1244.
- Katz B and Thesleff S (1957) A Study of the Desensitization Produced by Acetylcholine at the Motor End-Plate. *J Physiol* **138**: pp 63-80.
- Ke L and Lukas R J (1999) Effects of Steroid Exposure on Ligand Binding and Functional Activities of Diverse Nicotinic Acetylcholine Receptor Subtypes. *J Neurochem* **67**: pp 1100-1112.

- Korpi ER, Kleingoor C, Kettenmann H and Seeburg P H (1993) Benzodiazepine-Induced Motor Impairment Linked to Point Mutation in Cerebellar GABA<sub>A</sub> Receptor. *Nature* **261**: pp 356-359.
- Kotzyba-Hibert F, Kapfer I and Goeldner M (1995) Recent Trends in Photoaffinity Labeling. *Angew Chem Int Ed* **34**: pp 1296-1312.
- Krasowski MD, Koltchine V V, Rick C E, Ye Q, Finn S E and Harrison N L (1998) Propofol and Other Intravenous Anesthetics Have Sites of Action on the  $\gamma$ -Aminobutyric Acid Type A Receptor Distinct From That for Isoflurane. *Mol Pharmacol* **53**: pp 530-538.
- Kuner T, Wollmuth L P, Karlin A, Seeburg P and Sakmann B (1996) Structure of the NMDA Receptor Channel M2 Segment Inferred From the Accessibility of Substituted Cysteines. *Neuron* **17**: pp 343-352.
- Kym PR, Carlson K E and Katzenellenbogen J A (1993) Progestin 16 $\alpha$ ,17 $\alpha$ -Dioxolane Ketals As Molecular Probes for the Progesterone Receptor: Synthesis, Binding Affinity, and Photochemical Evaluation. *J Med Chem* **36**: pp 1111-1115.
- Kym PR, Carlson K E and Katzenellenbogen J A (1995) Evaluation of a Highly Efficient Aryl Azide Photoaffinity Labeling Reagent for the Progesterone Receptor. *Bioconjugate Chemistry* **6**: pp 115-122.
- Labarca C, Nowak M W, Zhang H Y, Tang L X, Deshpande P and Lester H A (1995) Channel Gating Governed Symmetrically by Conserved Leucine Residues in the M2 Domain of Nicotinic Receptors. *Nature* **376**: pp 514-516.
- Laemmli UK (1970) Cleavage of Structural Proteins During the Assembly of the Head of Bacteriophage T4. *Nature* **227**: pp 680-685.
- Lasalde JA, Tamamizu S, Butler D H, Vibat C R T, Hung B and McNamee M G (1996) Tryptophan Substitutions at the Lipid-Exposed Transmembrane Segment M4 of Torpedo Californica Acetylcholine Receptor Govern Channel Gating. *Biochemistry* **35**: pp 14139-14148.
- Laube B, Kuhse J and Betz H (1998) Evidence for a Tetrameric Structure of Recombinant NMDA Receptors. *J Neurosci* **18**: pp 2954-2961.
- Lee Y, Li L, Lasalde J, Rojas L, McNamee M, Ortiz-Miranda S I and Pappone P (1994) Mutations in the M4 Domain of Torpedo Californica Acetylcholine Receptor Dramatically Alter Ion Channel Function. *Biophys J* **66**: pp 646-653.
- Leonard RJ, Labarca C G, Charnet P, Davidson N and Lester H A (1988) Evidence That the M2 Membrane-Spanning Region Lines the Ion Channel Pore of the Nicotinic Receptor. *Sci* **242**: pp 1578-1581.

- Li L, Lee Y H, Pappone P, Palma A and McNamee M G (1992) Site-Specific Mutations of Nicotinic Acetylcholine Receptor at the Lipid-Protein Interface Dramatically Alter Ion Channel Gating. *Biophys J* **62**: pp 61-63.
- Liessem B, Glombitza G J, Knoll F, Lehmann J, Kellerman J, Lottspeich F and Sandhoff K (1995) Photoaffinity Labeling of Human Lysosomal B-Hexosaminidase B. *J Biol Chem* **270**: pp 23693-23699.
- Lo DC, Pinkham J L and Stevens C F (1991) Role of a Key Cysteine Residue in the Gating of the Acetylcholine Receptor. *Neuron* **6**: pp 31-40.
- Lurtz MM, Hareland M L and Pedersen S E (1997) Quinacrine and Ethidium Bromide Bind the Same Locus on the Nicotinic Acetylcholine Receptor From *Torpedo Californica*. *Biochemistry* **36**: pp 2068-2075.
- Mano I and Teichberg V (1998) A Tetrameric Subunit Stoichiometry for a Glutamate Receptor-Channel Complex. *NeuroReport* **9**: pp 327-331.
- Marsh D and Barrantes F J (1978) Immobilized Lipid in Acetylcholine Receptor-Rich Membranes From *Torpedo Marmorata*. *Proc Natl Acad Sci USA* **75**: pp 4329-4333.
- Marsh D, Watts A and Barrantes F J (1981) Phospholipid Chain Immobilization and Steroid Rotational Immobilization in Acetylcholine Receptor-Rich Membranes From *Torpedo Marmorata*. *Biochim Biophys Acta* **645**: pp 97-101.
- Martin MD and Karlin A (1997) Functional Effects on the Acetylcholine Receptor of Multiple Mutations of Gamma Asp174 and Delta Asp180. *Biochemistry* **36**: pp 10742-10750.
- McGurk KA, Pistis M, Belelli D, Hope A G and Lambert J J (1998) The Effect of a Transmembrane Amino Acid on Etomidate Sensitivity of an Invertebrate GABA Receptor. *Brit J Pharmacol* **124**: pp 13-20.
- McKernan RM and Whiting P J (1996) Which GABA<sub>A</sub>-Receptor Subtypes Really Occur in the Brain? *TINS* **19**: pp 139-143.
- Medynski, D. C. Histronicotoxin and aromatic amine interactions with nicotinic acetylcholine receptor from *Torpedo*: characterization of equilibrium binding and kinetic properties. Ph.D. Thesis, Harvard University. 1983.
- Mehta A and Ticku M (1999) An Update on GABA<sub>A</sub> Receptors. *Brain Res Rev* **29**: pp 196-217.
- Middleton RE and Cohen J B (1991) Mapping of the Acetylcholine Binding Site of the Nicotinic Acetylcholine Receptor: [<sup>3</sup>H]-Nicotine As an Agonist Photoaffinity Label. *Biochemistry* **30**: pp 6987-6997.

- Middleton RE, Strnad N P and Cohen J B (1999) Photoaffinity Labeling the Torpedo Nicotinic Acetylcholine Receptor With [3H]Tetracaine, a Nondesensitizing Noncompetitive Antagonist. *Mol Pharmacol* **56**: pp 290-299.
- Mihic SJ, Ye Q, Wick M J, Koltchines V V, Krasowski M D, Finn S E, Mascia M P, Valenzuela C F, Hanson K K, Greenblatt E P, Harris R A and Harrison N L (1997) Sites of Alcohol and Volatile Anaesthetic Action on GABA<sub>A</sub> and Glycine Receptors. *Nature* **389**: pp 385-389.
- Miyazawa A, Fujiyoshi Y, Stowell M and Unwin N (1999) Nicotinic Acetylcholine Receptor at 4.6 Angstrom Resolution: Transverse Tunnels in the Channel Wall. *J Mol Biol* **288**: pp 765-786.
- Moody EJ, Knauer C, Granja R, Strakhova M and Skolnick P (1997) Distinct Loci Mediate the Direct and Indirect Actions of the Anesthetic Etomidate at GABA<sub>A</sub> Receptors. *J Neurochem* **69**: pp 1310-1313.
- Moskovitz R, Haring R, Gershoni J, Kloog Y and Sokolovsky M (1987) Localization of Azidophencyclidine-Binding Site on the Nicotinic Acetylcholine Receptor  $\alpha$ -Subunit. *Biochem Biophys Res Commun* **145**: pp 810-816.
- Neher E (1983) The Charge Carried by Single-Channel Currents of Rat Cultured Muscle Cells in the Presence of Local Anaesthetics. *J Physiol* **339**: pp 663-678.
- Neubig RR and Cohen J B (1979) Equilibrium Binding of [<sup>3</sup>H]Tubocurarine and [<sup>3</sup>H] Acetylcholine by *Torpedo* Post-Synaptic Membranes: Stoichiometry and Ligand Interactions. *Biochemistry* **18**: pp 5464-5475.
- Newbolt A, Stoop R, Virginio C, Surprenant A, North R A, Buell G and Rassendren F (1998) Membrane Topology of an ATP-Gated Ion Channel (P2X Receptor). *J Biol Chem* **273**: pp 15177-15182.
- Nicke A, Bäumert H G, Rettinger J, Eichele A, Lambrecht G, Mutschler E and Scmalzing G (1998) P2X<sub>1</sub> and P2X<sub>3</sub> Receptors Form Stable Trimers: a Novel Structural Motif of Ligand-Gated Ion Channels. *EMBO J* **17**: pp 3016-3028.
- O'Leary ME, Filatov G N and White M M (1994) Characterization of *D*-Tubocurarine Binding Site of *Torpedo* Acetylcholine Receptor. *Am J Phys* **266**: pp C648-C653.
- Ohno K, Hutchinson D O, Milone M, Brengman J M, Bouzat C, Sine S M and Engel A G (1995) Congenital Myasthenic Syndrome Caused by Prolonged Acetylcholine Receptor Channel Openings Due to a Mutation in the M2 Domain of the Epsilon Subunit. *Proc Natl Acad Sci USA* **92**: pp 758-762.
- Ortiz-Miranda SI, Lasalde J A, Pappone P and McNamee M G (1997) Mutations in the M4 Domain of the *Torpedo Californica* Nicotinic Acetylcholine Receptor Alter Channel Opening and Closing. *J Membrane Biol* **158**: pp 17-30.

- Osaka H, Sugiyama N and Taylor P (1998) Distinctions in Agonist and Antagonist Specificity Conferred by Anionic Residues of the Nicotinic Acetylcholine Receptor. *J Biol Chem* **273**: pp 12758-12765.
- Paas Y (1998) The Macro- and Microarchitectures of the Ligand-Binding Domain of Glutamate Receptors. *TINS* **21**: pp 117-125.
- Pascual JM and Karlin A (1998) Delimiting the Binding Site for Quaternary Ammonium Lidocaine Derivatives in the Acetylcholine Receptor Channel. *J Gen Physiol* **112**: pp 611-621.
- Paul SM and Purdy R H (1992) Neuroactive Steroids. *FASEB* **6**: pp 2311-2322.
- Pedersen SE (1995) Site-Selective Photoaffinity Labeling of the *Torpedo Californica* Nicotinic Acetylcholine Receptor by Azide Derivatives of Ethidium Bromide. *Mol Pharmacol* **47**: pp 1-9.
- Pedersen SE and Cohen J B (1990) [<sup>3</sup>H]-Meproadifen Mustard Reacts With Glu-262 of the Nicotinic Receptor  $\alpha$ -Subunit. *Biophys J* **57**: pp 126A.
- Pedersen SE, Dreyer E B and Cohen J B (1986) Location of Ligand Binding Sites on the Nicotinic Acetylcholine Receptor  $\alpha$ -Subunit. *J Biol Chem* **261**: pp 13735-13743.
- Pedersen SE and Papineni R V L (1995) Interaction of *D*-Tubocurarine Analogs With *Torpedo* Nicotinic Acetylcholine Receptor. *J Biol Chem* **270**: pp 31141-31150.
- Pedersen SE, Sharp S D, Liu W-S and Cohen J B (1992) Structure of the Noncompetitive Antagonist Binding Site in the *Torpedo* Nicotinic Acetylcholine Receptor: [<sup>3</sup>H]Meproadifen Mustard Reacts Selectively With  $\alpha$ -Subunit Glu-262. *J Biol Chem* **267**: pp 10489-10499.
- Pribilla I, Takagi T, Langosch D, Bormann J and Betz H (1992) The Atypical M2 Segment of the  $\beta$  Subunit Confers Picrotoxinin Resistance to Inhibitory Glycine Receptor Channels. *EMBO J* **11**: pp 4305-4311.
- Prince RJ and Sine S M (1996) Molecular Dissection of Subunit Interfaces in the Acetylcholine Receptor - Identification of Residues That Determine Agonist Selectivity. *J Biol Chem* **271**: pp 25770-25777.
- Pritchett DB and Seeburg P H (1991)  $\Gamma$ -Aminobutyric Acid Type A Receptor Point Mutation Increases the Affinity of Compounds for the Benzodiazepine Site. *Proc Natl Acad Sci USA* **88**: pp 1421-1425.
- Rajendra S, Lynch J W and Schofield P R (1997) The Glycine Receptor. *Pharmacol Ther* **73**: pp 121-146.

- Rankin SE, Addona G H, Kloczewiak M A, Bugge B and Miller K W (1997) The Cholesterol Dependence of Activation and Fast Desensitization of the Nicotinic Acetylcholine Receptor. *Biophys J* **73**: pp 2446-2455.
- Rassendren F, Buell G, Newbolt A, North R A and Surprenant A (1997) Identification of Amino Acid Residues Contributing to the Pore of a P2X Receptor. *EMBO J* **16**: pp 3446-3454.
- Renard S, Olivier A, Granger P, Avenet P, Graham D, Sevrin M, George P and Besnard F (1999) Structural Elements of the Gamma-Aminobutyric Acid Type A Receptor Conferring Subtype Selectivity for Benzodiazepine Site Ligands. *J Biol Chem* **274**: pp 13370-13374.
- Revah F, Bertrand D, Galzi J L, Devillers-Thiery A, Mulle C, Hussy N, Bertrand S, Ballivet M and Changeux J P (1991) Mutations in the Channel Domain Alter Desensitization of a Neuronal Nicotinic Receptor. *Nature* **353**: pp 846-849.
- Revah F, Galzi J L, Giraudat J, Haumont P-Y, Lederer F and Changeux J-P (1990) The Noncompetitive Blocker [<sup>3</sup>H]Chlorpromazine Labels Three Amino Acids of the Acetylcholine Receptor  $\gamma$  Subunit: Implications for the  $\alpha$ -Helical Organization of Regions MII and for the Structure of the Ion Channel. *Proc Natl Acad Sci USA* **87**: pp 4675-4679.
- Rick CE, Ye Q, Finn S E and Harrison N L (1998) Neurosteroids Act on the GABA(A) Receptor at Sites on the N- Terminal Side of the Middle of TM2. *NeuroReport* **9**: pp 379-383.
- Role LW and Berg D K (1996) Nicotinic Receptors in the Development and Modulation of CNS Synapses. *Neuron* **16**: pp 1077-1085.
- Schagger H and von Jagow G (1987) Tricine-Sodium Dodecyl Sulfate-Polyacrylamide Gel Electrophoresis for the Separation of Proteins in the Range From 1 to 100 KDa. *Anal Biochem* **166**: pp 368-379.
- Schmeiden V, Kuhse J and Betz H (1993) Mutation of Glycine Receptor Subunit Creates B-Alanine Receptor Responsive to GABA. *Sci* **262**: pp 256-258.
- Schmider W, Fahr A, Voges R, Gerok W and Kurz G (1996) Irreversible Inhibition of Hepatic Fatty Acid Salt Uptake by Photoaffinity Labeling With 11, 11-Azistearate. *j lipid res* **37** : pp 739.
- Seyle H (1941) The Anesthetic Effect of Steroid Hormones. *Proc Soc Exp Biol Med* **46**: pp 116-121.
- Sine SM (1993) Molecular Dissection of Subunit Interfaces in the Acetylcholine Receptor: Identification of Residues That Determine Curare Selectivity. *Proc Natl Acad Sci USA* **90**: pp 9436-9440.

- Sine SM, Kreienkamp H J, Bren N, Maeda R and Taylor P (1995) Molecular Dissection of Subunit Interfaces in the Acetylcholine Receptor: Identification of Determinants of  $\alpha$ -Conotoxin M1 Selectivity. *Neuron* **15**: pp 205-211.
- Sine SM, Quiram P, Papanikolaou F, Kreienkamp H J and Taylor P (1994) Conserved Tyrosines in the Alpha Subunit of the Nicotinic Acetylcholine Receptor Stabilize Quaternary Ammonium Groups of Agonists and Curariform Antagonists. *J Biol Chem* **269**: pp 8808-8816.
- Sine SM and Taylor P (1982) Local Anesthetics and Histrionicotoxin Are Allosteric Inhibitors of the Acetylcholine Receptor. *J Biol Chem* **257**: pp 8106-8114.
- Smith GB and Olsen R W (1994) Identification of a [<sup>3</sup>H]Muscimol Photoaffinity Substrate in the Bovine  $\gamma$ -Aminobutyric Acid<sub>A</sub> Receptor  $\alpha$  Subunit. *J Biol Chem* **269**: pp 20380-20387.
- Sobel A, Weber M and Changeux J-P (1977) Large-Scale Purification of the Acetylcholine-Receptor Protein in Its Membrane-Bound and Detergent Extracted Forms From *Torpedo Marmorata* Electric Organ. *Eur J Biochem* **80**: pp 215-224.
- Tamamizu S, Todd A P and McNamee M G (1995) Mutations in the M1 Region of the Nicotinic Acetylcholine Receptor Alter the Sensitivity to Inhibition by Quinacrine. *Cell Mol Neurobiol* **15**: pp 427-438.
- Tobimatsu T, Fujita Y, Fukuda K, Tanaka K-I, Mori Y, Konno T, Mishina M and Numa S (1987) Effects of Substitution of Putative Transmembrane Segments on Nicotinic Acetylcholine Receptor Function. *FEBS Letts* **222**: pp 56-62.
- Tomaselli GF, McLaughlin J T, Jurman M E, Hawrot E and Yellen G (1991) Mutations Affecting Agonist Sensitivity of the Nicotinic Acetylcholine Receptor. *Biophys J* **60**: pp 721-727.
- Unwin N (1993) Nicotinic Acetylcholine Receptor at 9 Å Resolution. *J Mol Biol* **229**: pp 1101-1124.
- Unwin N (1998) The Nicotinic Acetylcholine Receptor of the Torpedo Electric Ray. *J Struct Biol* **121**: pp 181-190.
- Valenzuela CF, Weign P, Yguerabide J and Johnson D A (1994) Transverse Distance Between the Membrane and Agonist Binding Sites on the *Torpedo* Acetylcholine Receptor: A Fluorescence Study. *Biophys J* **66**: pp 674-682.
- Valera S, Ballivet M and Bertrand D (1992) Progesterone Modulates a Neuronal Nicotinic Acetylcholine Receptor. *Proc Natl Acad Sci USA* **89**: pp 9949-9953.

- Vandenberg RJ, French C R, Barry P H, Shine J and Schofield P R (1992) Antagonism of Ligand-Gated Ion Channel Receptors: Two Domains of the Glycine Receptor  $\alpha$  Subunit Form the Strychnine-Binding Site. *Proc Natl Acad Sci USA* **89**: pp 1765-1769.
- Villarroel A, Herlitz S, Koenen M and Sakmann B (1991) Location of a Threonine Residue in the  $\alpha$ -Subunit M2 Transmembrane Segment That Determines the Ion Flow Through the Acetylcholine Receptor Channel. *Proc Natl Acad Sci USA* **243**: pp 69-74.
- Westh-Hansen SE, Rasmussen P B, Hastrup S, Nabekura J, Naguchi K, Akaike N, Witt M-R and Nielsen M (1997) Decreased Agonist Sensitivity of Human GABA<sub>A</sub> Receptors by an Amino Acid Variant, Isoleucine to Valine, in the A<sub>1</sub> Subunit. *Euro J Pharmacol* **329**: pp 253-257.
- White BH and Cohen J B (1992) Agonist-Induced Changes in the Structure of the Acetylcholine Receptor M2 Regions Revealed by Photoincorporation of an Uncharged Nicotinic Non-Competitive Antagonist. *J Biol Chem* **267**: pp 15770-15783.
- White BH, Howard S, Cohen S G and Cohen J B (1991) The Hydrophobic Photoreagent 3-(Trifluoromethyl)-3-(m-[<sup>125</sup>I]Iodophenyl)Diazirine Is a Novel Noncompetitive Antagonist of the Nicotinic Acetylcholine Receptor. *J Biol Chem* **266**: pp 21595-21607.
- Wick MJ, Mihic S J, Ueno S, Mascia M P, Trudell J R, Brozowski S J, Ye Q, Harrison N L and Harris R A (1998) Mutations of Gamma-Aminobutyric Acid and Glycine Receptors Change Alcohol Cutoff: Evidence for an Alcohol Receptor? *Proc Natl Acad Sci USA* **95**: pp 6504-6509.
- Wieland HA, Luddens H and Seeburg P H (1992) A Single Histidine in GABA<sub>A</sub> Receptors Is Essential for Benzodiazepine Agonist Binding. *J Biol Chem* **267**:3: pp 1426-1429.
- Wieland HA and Lüddens H (1994) Four Amino Acid Exchanges Convert a Diazepam-Insensitive, Inverse Agonist-Preferring GABA<sub>A</sub> Receptor into a Diazepam-Preferring GABA<sub>A</sub> Receptor. *J Med Chem* **37**: pp 4576-4580.
- Wingrove PB, Thompson S A, Wafford K A and Whiting P J (1997) Key Amino Acids in the  $\gamma$  Subunit of the  $\Gamma$ -Aminobutyric Acid<sub>A</sub> Receptor That Determine Ligand Binding and Modulation at the Benzodiazepine Site. *Mol Pharmacol* **52**: pp 874-881.
- Wingrove PB, Wafford K A, Bain C and Whiting P J (1994) The Modulatory Action of Loreclezole at the G-Aminobutyric Acid Type A Receptor Is Determined by a Single Amino Acid in the B<sub>2</sub> and B<sub>3</sub> Subunit. *Proc Natl Acad Sci USA* **91**: pp 4569-4573.
- Witzemann V and Raftery M (1978) Ligand Binding Sites and Subunits Interactions of *Torpedo Californica* Acetylcholine Receptor. *Biochemistry* **17**: pp 3598-3604.

- Wood SC, Forman S A and Miller K W (1991) Short Chain and Long Chain Alkanols Have Different Sites of Action on Nicotinic Acetylcholine Receptor Channels From *Torpedo*. *Mol Pharmacol* **39**: pp 332-338.
- Wood SC, Hill W A and Miller K W (1993) Cycloalkanemethanols Discriminate Between Volume- and Length-Dependent Loss of Activity of Alkanols at the *Torpedo* Nicotinic Acetylcholine Receptor. *Mol Pharmacol* **44**: pp 1219-1226.
- Wood SC, Tonner P H, Dearmendi A J, Bugge B and Miller K W (1995) Channel Inhibition by Alkanols Occurs at a Binding Site on the Nicotinic Acetylcholine Receptor. *Mol Pharmacol* **47**: pp 121-130.
- Xu M and Akabas M H (1996) Identification of Channel-Lining Residues in the M2 Membrane-Spanning Segment of the GABA<sub>A</sub> Receptor A<sub>1</sub> Subunit. *Journal of General Physiology* **107**: pp 195-205.
- Xu M, Covey D F and Akabas M H (1995) Interaction of Picrotoxin With GABA<sub>A</sub> Receptor Channel-Lining Residues Probed in Cysteine Mutants. *Biophys J* **69**: pp 1858-1867.
- Yan D, Schulte M K, Bloom K E and White M M (1999) Structural Features of the Ligand-Binding Domain of the Serotonin 5HT<sub>3</sub> Receptor. *J Biol Chem* **274**: pp 5537-5541.
- Ye Q, Koltchine V V, Mihic S J, Mascia M P, Wick M J, Finn S E, Harrison N L and Harris R A (1998) Enhancement of Glycine Receptor Function by Ethanol Is Inversely Correlated With Molecular Volume at Position A267. *J Biol Chem* **273**: pp 3314-3319.
- Yu DH, Zhang L, Eisele J L, Bertrand D, Changeux J P and Weight F F (1996) Ethanol Inhibition of Nicotinic Acetylcholine Type Alpha 7 Receptors Involves the Amino-Terminal Domain of the Receptor. *Mol Pharmacol* **50**: pp 1010-1016.
- Zhang H and Karlin A (1997) Identification of Acetylcholine Receptor Channel-Lining Residues in the M1 Segment of the Beta-Subunit. *Biochemistry* **36**: pp 15856-15864.
- Zhang H and Karlin A (1998) Contribution of the Beta Subunit M2 Segment to the Ion-Conducting Pathway of the Acetylcholine Receptor. *Biochemistry* **37**: pp 7952-7964.
- Zhong WG, Gallivan J P, Zhang Y N, Li L T, Lester H A and Dougherty D A (1998) From Ab Initio Quantum Mechanics to Molecular Neurobiology: A Cation- Pi Binding Site in the Nicotinic Receptor. *Proc Natl Acad Sci USA* **95**: pp 12088-12093.